IONOSPHERIC VLF WAVES AND OPTICAL PHENOMENA

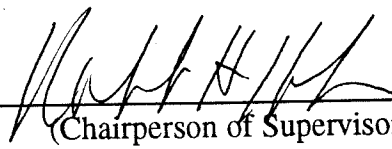**OVER ACTIVE THUNDERSTORMS**

by

Ya Qi Li

A dissertation submitted in partial fulfillment
of the requirements for the degree of

Doctor of Philosophy

University of Washington

1993

Approved by _____
(Chairperson of Supervisory Committee)

Program Authorized
to Offer Degree _____

Date _____

Doctoral Dissertation

In presenting this dissertation in partial fulfillment of the requirements for the Doctoral degree at the University of Washington, I agree that the library shall make its copies freely available for inspection. I further agree that extensive copying of this dissertation is allowable only for scholarly purposes, consistent with "fair use" as prescribed in the U. S. Copyright Law. Requests for copying or reproduction of this dissertation may be referred to University Microfilms, 1490 Eisenhower Place, P. O. Box 975, Ann Arbor, MI 48106, to whom the author has granted "the right to reproduce and sell (a) copies of the manuscript in microform and/or (b) printed copies of the manuscript made from microform."

Signature _____

Date ___ *May 7, 1993* ___

University of Washington

Abstract

**IONOSPHERIC VLF WAVES AND OPTICAL PHENOMENA
OVER ACTIVE THUNDERSTORMS**

by Ya Qi Li

Chairperson of the Supervisory Committee: Professor Robert H. Holzworth
Geophysics Program

In 1987 and 1988, two campaigns, the Wave Induced Particle Precipitation campaign and the Thunderstorm II campaign, were conducted to investigate lightning-generated effects in the upper atmosphere and ionosphere. Two rockets (apogees 420km and 330km) and 6 balloons (float altitudes 30km) were launched near thunderstorms in these campaigns. Optical and electric signals from hundreds of lightning strokes were recorded by both the rockets and balloons.

Using the data obtained in these two campaigns, we have been able to study some problems about lightning-generated VLF waves in the ionosphere which have not been well investigated previously. In this dissertation, we report the following: 1) The downward-looking optical detector on the rocket recorded some anomalous characteristic optical phenomena which had not been reported previously. Our study shows that they occurred above the balloon altitude (30km), and we interpreted the results in terms of discharges at high altitudes. 2) We studied the relation between the amplitude of lightning-generated VLF waves in the ionosphere and the lightning current recorded by the SUNYA lightning network. Our study shows that the amplitude of waves at frequencies below 5 kHz has linear response to the lightning current. Above 5 kHz, there is not a significant linear correlation between the wave amplitude and the lightning current. 3) We have been able to determine the propagation path of the lightning-generated VLF waves from the source to the rocket. The path is consistent with the leaky waveguide hypothesis in which waves travel in

the waveguide to the vicinity of the rockets, and then propagate vertically through the ionosphere. 4) We have found that the amplitude of lightning-generated VLF waves have maxima and minima at different altitudes, instead of being attenuated monotonically with altitude as expected. A theoretical model has been proposed which shows that the wave amplitude profiles are the result of interference between waves from an aperture area below the rocket. 5) We numerically calculated the absorption of VLF waves at the bottom of the ionosphere. The electron density gradient of the ionosphere was taken into account. The characteristics of the absorption, such as the frequency dependence, were investigated. Comparing the lightning spectrum received on the ground and by a rocket, we deduced that significant heating of the ionosphere is caused by lightning-generated VLF waves.

TABLE OF CONTENTS

LIST OF FIGURES

ACKNOWLEDGMENTS

CHAPTER 1
INTRODUCTION

1.1 LIGHTNING AND ITS ELECTROMAGNETIC RADIATION

Lightning is a transient, high-current electric discharge which originates in the electric charges separated in thunderstorm clouds. There are intracloud (IC) discharges, cloud-to-cloud (CC) discharges, cloud-to-air (CA) discharges and cloud-to-ground (CG) discharges. CC and CA discharges are relatively rare in comparison with other discharges. The most common discharges are IC discharges, which account for well over half of all lightning discharges (Uman, 1987). However, the discharge which has been most extensively studied is CG discharge.

CG discharges include positive CG discharges and negative CG discharges. Positive discharges are generally stronger than negative discharges, but are relatively uncommon. A negative CG discharge typically brings to earth tens of coulombs of negative charge. In such a process, a preliminary breakdown within the cloud initiates an ionized channel which is called stepped leader. This stepped leader propagates from cloud to ground in a series of discrete steps in about 20 ms. As the leader tip, which has an electric potential of magnitude in excess of 10^7V with respect to the ground, is close to ground, the electric field at certain points near sharp objects on the ground exceeds the breakdown value of air, and then one or more upward-moving discharges are initiated from those points. As the upward-moving discharge from the ground contacts the downward-moving stepped leader some tens of meters above the ground, the leader tip is connected to ground potential. Then a strong upward current flows along the previously ionized and charged leader path to the top of the leader channel. Such upward current, which typically has a peak intensity of tens of kiloamperes near ground, is called return-stroke (Magono,1980; Uman, 1987).

The current of return-strokes reaches its peak value in a few microseconds and falls to half of the peak value in about 50μs. Currents of the order of hundreds

amperes may continue to flow for times of a few milliseconds to several hundred milliseconds. After the first return-stroke, if additional charge becomes available at the top of the discharge channel, a continuous dart leader may propagate down the residual first-stroke channel and initiate another return stroke. A lightning flash may have only one return stroke or several return strokes. The time between successive return strokes in a flash is typically several tens of milliseconds. The currents of subsequent return-strokes are usually smaller than that of the first return-stroke (Uman,1987).

The three components of fields related to lightning discharges are electrostatic, inductive, and radiative components (Uman et al, 1975; Magono, 1980; Siefering, 1987). In this work, we will mostly consider the lightning radiation field, that is, electromagnetic waves generated by lightning. Lightning-generated waves cover a frequency range from several Hertz (Hz) to several hundred mega-Hertz (MHz). The radiation spectra of lightning flashes may differ considerably, due to the conditions and characteristics of lightning discharge channels (Newman, 1958; Kimpara, 1965). Typical spectra of CG lightning flashes measured on the ground have dominant energy between 1 kHz to 20 kHz in the Very-Low-Frequency (VLF) range. The typical amplitude spectra decreases by more than 50 dB from 20 kHz to 500 MHz (Kimpara,1965; Uman, 1987; Nanevicz et al., 1990).

The radiations below 20 kHz from lightning discharges are mainly generated by return-strokes. The radiated power of return-strokes remains significant up to 1-2 MHz, above which the contributions from the preliminary discharge processes and other parts of discharge processes become dominant. The radiations from IC lightning discharges are considerably smaller than that of CG discharges at frequencies below 20 kHz. Above 50 kHz, radiations from IC discharges tend to be comparable to those from CG discharges (Kimpara,1965; Pierce, 1977).

1.2 WHISTLERS AND LIGHTNING-ASSOCIATED PHENOMENA

A large fraction of the VLF power from lightning is confined in the waveguide

formed by the earth and the lower edge of the ionosphere. These waves, called atmospherics or sferics, can propagate in the earth-ionosphere waveguide for a large distance. They are broadband pulses and last typically less than 1ms when received by ground receivers (Taylor, 1965). Also, a small fraction of lightning-generated VLF wave power is coupled into whistler-mode waves at the base of the ionosphere and propagates into the ionosphere. The lightning-generated waves in the earth-ionosphere waveguide have been actively studied for decades. By comparison, less research has been done on lightning-generated waves in the ionosphere (Siefring, 1987).

These VLF waves launched into the ionosphere by lightning are subject to strong attenuation in the lower ionosphere due to collisions between electrons and neutral particles (Budden, 1985). Some of these waves may be guided approximately along the geomagnetic lines of force by field-aligned ionization irregularities, called whistler ducts, to the other hemisphere. These ducted waves are partially reflected at the top of the ionosphere in the other hemisphere and some of their energy can be transmitted into the atmosphere. Because of the dispersion, these waves which reenter the atmosphere, coupling back into EM waves, produce a whistling sound in the audio frequency range and are therefore called "whistlers". The partial reflection of waves may repeat several times to produce whistler echo trains in both hemispheres (Helliwell, 1965).

Classical whistler dispersion starts at high frequency and drops to a lower limit of about 1 kHz within one to three seconds. The amplitude of whistlers is usually greatest at a frequency near 5 kHz (Helliwell, 1965). The association between lightning spectra and occurrence of whistlers has been investigated in many studies. Observations indicate that almost any intense lightning discharge is likely to excite whistlers. There is also evidence that lightning discharges with peaks near 5 kHz are more likely to produce whistlers than those with peaks at higher frequencies (Helliwell et al., 1958; Norinder and Knudsen, 1959).

In the magnetosphere, lightning-generated VLF waves can interact with energetic particles in the radiation belt. During this interaction process, pitch angle scattering can occur in which waves gain energy from particles, so wave amplitudes are greatly increased (Kennel and Petschek, 1966; Etcheto et al., 1973). Evidence for such amplification effects can be found in a large fraction of whistlers (Helliwell, 1965). The other consequence of this wave-particle interaction is that the pitch angles of the particles are reduced. So some of these magnetospheric particles would be caused to penetrate to lower altitude in the ionosphere, and lose their energy by colliding with ionospheric particles. Such lightning-induced particle precipitation can produce enhanced ionospheric ionization and optical emissions in the upper atmosphere and ionosphere, as well as X-rays detectable down to about 30 km altitude (Rosenberg et al., 1971; Carpenter et al., 1982; Inan et al., 1987).

1.3 DIRECT UPWARD EFFECT OF LIGHTNING IN THE IONOSPHERE

The process of lightning-induced particle precipitation results in dumping of stored magnetospheric particle energy into the upper-atmosphere and the ionosphere. Thus lightning-generated waves play a role in the downward energy coupling between the magnetosphere and the atmosphere. For some time, particle precipitation was considered to be the only significant ionospheric effect of lightning. Since this effect relies on wave-particle interactions in the magnetosphere, it is basically an indirect effect.

In the last decade, more and more evidence has indicated that direct upward effects of lightning discharges on the ionosphere are much more significant than had been previously thought. In 1985, it was first reported that large transient electric field associated with lightning strokes was recorded by a rocket at altitudes above 140 km in the ionosphere (Kelley et al., 1985). A remarkable feature of this transient field was a significant electric field component parallel to the background magnetic field. Such parallel electric fields could drive electrons along the magnetic field line and generate

plasma instabilities in the local medium (Siefring, 1987). Similar transient electric fields from lightning were also observed by Goldberg et al. (1986). More recently, a strong non-dispersive transient electric pulse associated with lightning discharges has been recorded by a rocket in the direction parallel to the geomagnetic field (Kelley et al., 1990). Unlike the transients field reported earlier, this parallel signature was received at the rocket well-ahead of the typical lightning-generated whistler waves. The cause and effect of such a precursor pulse has not been well-understood. Lightning-generated VLF waves also give rise to certain processes in local media as they propagate in the ionosphere and the magnetosphere. For example, lower-hybrid waves excited by whistler waves in the ionosphere and the magnetosphere have been observed (Woodman and Kudeki, 1984; Kelley et al, 1990, Bell et al, 1991a, 1991b).

VLF transmitter signals have been used to detect lightning-induced particle precipitation events in the ionosphere for some years. When precipitating particles generate ionization in the lower ionosphere near the great circle path of the transmitter signal, the phase and amplitude of the received signal could have characteristic perturbations, called "trimpi" events (Helliwell et al., 1973; Lohrey and Kaiser, 1979; Carpenter et al., 1984). Normal trimpi events occur 0.3-1.5 seconds after the causative lightning, because the lightning-generated waves and the magnetospheric particles must travel a large distance before precipitation can occur. In the last decade, a new kind of "trimpi", called "fast (or early) trimpi", has been reported (Armstrong, 1983; Inan et al, 1988). Such fast trimpis occur almost instantaneously (< 50 ms) after the causative lightning. This new phenomenon indicate that the lower ionosphere is disturbed by lightning discharges by mechanisms other than the wave-induced particle precipitation. It has been suggested in recent years that direct heating of the lower ionosphere by lightning-generated VLF waves could be the cause of such phenomena (Inan, 1990; Inan et al, 1991). The direct coupling of lightning-generated energy to the middle atmosphere and ionosphere have also been used to explain other atmospheric electrical phenomena (Hale and Baginski, 1987; Hale, 1992).

All evidence suggests that lightning-generated electromagnetic energy has direct and significant effects on the ionospheric plasma. To understand these effects, it is necessary to understand the physics of lightning-generated electromagnetic energy in the ionosphere. Since the dominant energy radiated from lightning discharges is in the VLF range, lightning-generated VLF waves in the ionosphere are fundamental to the investigation of lightning effects in the ionosphere.

1.4 MAGNETO-IONIC THEORY

1.4.1 Appleton-Hartree Formula

Magneto-ionic theory is commonly used to describe the properties of electromagnetic waves in the ionosphere. This theory assumes: 1) the medium is electrically neutral and consists of neutral particles, electrons and ions; 2) the charged particles in the medium are "cold", so effects of their thermal motion can be ignored; 3) the medium is homogeneous, so the waves can be treated as plane waves; 4) the effects of electron collisions are instantaneous; and 5) the collision frequency is the same for all electrons. Based on these assumptions, a dispersion relation of waves in the medium can be derived from the motion equation of electrons (ions motion is usually ignored) and Maxwell's equations (Budden, 1985).This dispersion relation expressed as Appleton-Hartree formula for the index of refraction is

$$n^2 = 1 - \frac{X}{1 - iZ - \frac{1}{2}\frac{Y_t^2}{1 - X - iZ} \pm \frac{1}{1 - X - iZ}\left[\frac{1}{4}Y_t^2 + Y_l^2(1 - X - iZ)^2\right]^{1/2}} \qquad (1.1)$$

$$X = \left(\frac{f_p}{f}\right)^2,$$

$$Y_l = \frac{f_{ce}\cos\theta}{f},$$

$$Y_t = \frac{f_{ce}\sin\theta}{f},$$

$$Z = \frac{\nu}{f},$$

where, f is the frequency of the wave; f_p is the plasma frequency; f_{ce} is the gyro-frequency of electrons; ν is the effective collision frequency between electrons and neutral particles; and θ is the propagation angle of the wave, which is the angle between the wave normal and the background magnetic field.

The positive and negative sign in the denominator of the Appleton-Hartree formula represents the extraordinary wave mode and the ordinary wave mode, respectively, which are arisen from the anisotropy of the medium in a background magnetic field.

For some problems the approximation of a homogenous medium for use of the Appleton-Hartree formula can be ignored. When the change of the medium is not significant within a wavelength, the medium can be treated as slowly-varying. In such cases, the Appleton-Hartree equation can be applied using some approximations. In some other cases, however, when the medium is not slowly-varying, the equation cannot be applied. For example, the ionospheric electron density changes abruptly within a wavelength of VLF waves at the base of the ionosphere, so it may be inappropriate to use the Appleton-Hartree equation to deal with some problems of VLF waves in this region.

1.4.2 Quasi-Longitudinal Approximation

The properties of whistler waves propagating at an arbitrary angle to the background magnetic field are obtained by the Appleton-Hartree formula.When the wave propagation direction is sufficiently close to the magnetic field direction, the Appleton-Hartree formula can be simplified by using the quasi-longitudinal (QL) approximation (Ratcliffe, 1959; Budden, 1985). Specifically, the QL condition is

$$\frac{Y^2 \sin^4\theta}{4\cos^2\theta} \gg \left| (1 - X - iZ)^2 \right| ,\qquad (1.2)$$

where $Y = f_{ce}/f$. The simplified formula under the QL condition is

$$n^2 = 1 - \frac{X}{1 - iZ \pm |Yl|} . \qquad (1.3)$$

It should be noticed that the QL condition may still be valid for propagation at a large angle under certain circumstances. For example, considering the conditions at 120 km altitude in the ionosphere, let $f_{pe} = 200\,\text{kHz}$, $f_{ce} = 1000\,\text{kHz}$ and $\nu \approx 0$, the QL condition can still be valid for a 10 kHz wave propagating in an angle as large as 60 degrees.

1.4.3 Full Expression of Appleton Hartree Formula

In many cases, the QL approximation can not be applied. We will encounter such cases later when we investigate wave propagation in the lower ionosphere, where the plasma frequency is much lower than the electron gyrofrequency. So, a complete expression for the refractive index is needed. The full expression of the Appleton-Hartree formula we derived is the following.

$$n = n_r + i n_i;$$

$$n_r = \pm (C_1^2 + C_2^2)^{1/4} \cos\Theta_1 ,$$

$$n_i = \pm (C_1^2 + C_2^2)^{1/4} \sin\Theta_1 ;$$

$$\Theta_1 = \frac{1}{2} tg^{-1}\left(\frac{C_2}{C_1}\right),$$

$$C_1 = 1 - \frac{XB_1}{B_1^2 + B_2^2} ,$$

$$C_2 = \frac{XB_2}{B_1^2 + B_2^2} ,$$

$$B_1 = 1 - \frac{1}{2}\frac{Y_t^2(1-X)}{(1-X)^2 + Z^2} \pm \frac{(A_1^2 + A_2^2)^{1/4}}{(1-X)^2 + Z^2}\left[(1-X)\cos\Theta_2 - Z\sin\Theta_2 \right] ,$$

$$B_2 = -Z - \frac{1}{2}\frac{Y_t^2 Z}{(1-X)^2 + Z^2} \pm \frac{(A_1^2 + A_2^2)^{1/4}}{(1-X)^2 + Z^2}\left[(1-X)\sin\Theta_2 + Z\cos\Theta_2 \right] ;$$

$$A_1 = \frac{1}{4}Y_t^4 + Y_l^2(1-X)^2 - Y_l^2 Z^2 ,$$

$$A_2 = -2Y_l^2 Z(1-X) ,$$

$$\Theta_2 = \frac{1}{2} tg^{-1}\left(\frac{A_2}{A_1}\right).$$

Given the electron density, the background magnetic field intensity and the effective collision frequency, the wave refractive index can be calculated from these equations. In this thesis, the wave refractive index is generally calculated using these full equations.

1.4.4 Profiles of Ionospheric Electron Density and Effective Collision Frequency

As shown by the Appleton-Hartree formula, the wave refractive index is a function of the electron density n_e, intensity of the geomagnetic field (B) and effective collision frequency (ν) between electrons and neutral particles. To calculate the propagation of VLF waves in the ionosphere, the changes of n_e, B and ν with altitude have to be known.

In this thesis, we assume the geomagnetic field is a dipole field with intensity of 0.38 Gauss at the surface of the earth on the equator. The electron density profile used in our calculation is obtained by running an International Reference Ionospheric

(IRI) model (Rawer et al., 1978). The following parameters were chosen in running the IRI model:

Day:	212
Local time:	23:00
Geographic latitude/longitude:	37.8 N / 75.4W
Sunspot Number:	34.3
F2 Peak Intensity:	$1.03 \times 10^6 cm^{-3}$
F2 Peak Altitude:	350 km

The location was chosen to be Wallops Island, Virginia where WIPP and Thunderstorm II rockets (see next chapter) were launched. Local time and sunspot number were selected according to actual conditions when the WIPP rocket was
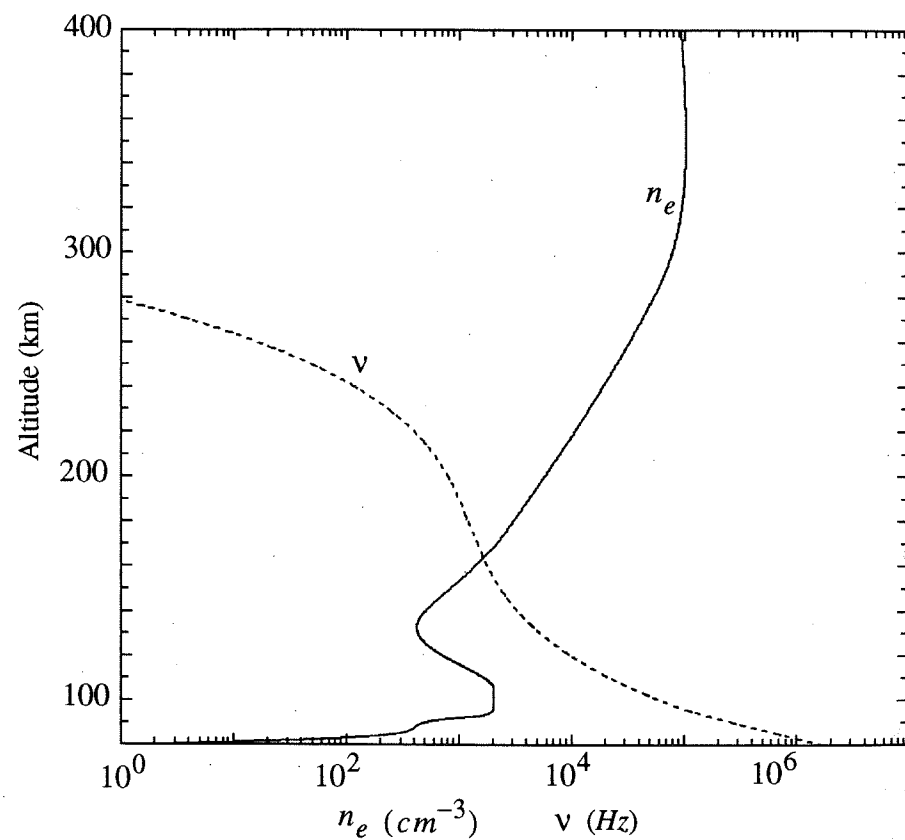
Figure 1.1:   Electron density and effective collision frequency profiles of the ionosphere used in this dissertation

launched. The electron density and altitude of the F2 peak were determined by in-situ electron density measurements conducted by another simultaneous rocket during the WIPP campaign.

The profile of effective collision frequency ν was given by Budden (1985), which has had very little changes for the last thirty years. The value of ν changes slightly with time of day and with seasons, and the profile of ν also depends on latitude. However, these changes are very small and usually can be ignored (Budden, 1985).

The profiles of electron density and the effective collision frequency used in our calculations are shown in Figure 1.1. Using these profiles and a dipole geomagnetic field, the wave refractive index at each altitude of the ionosphere can be calculated. Figure 1.2 shows an example of the calculated real refractive index for a
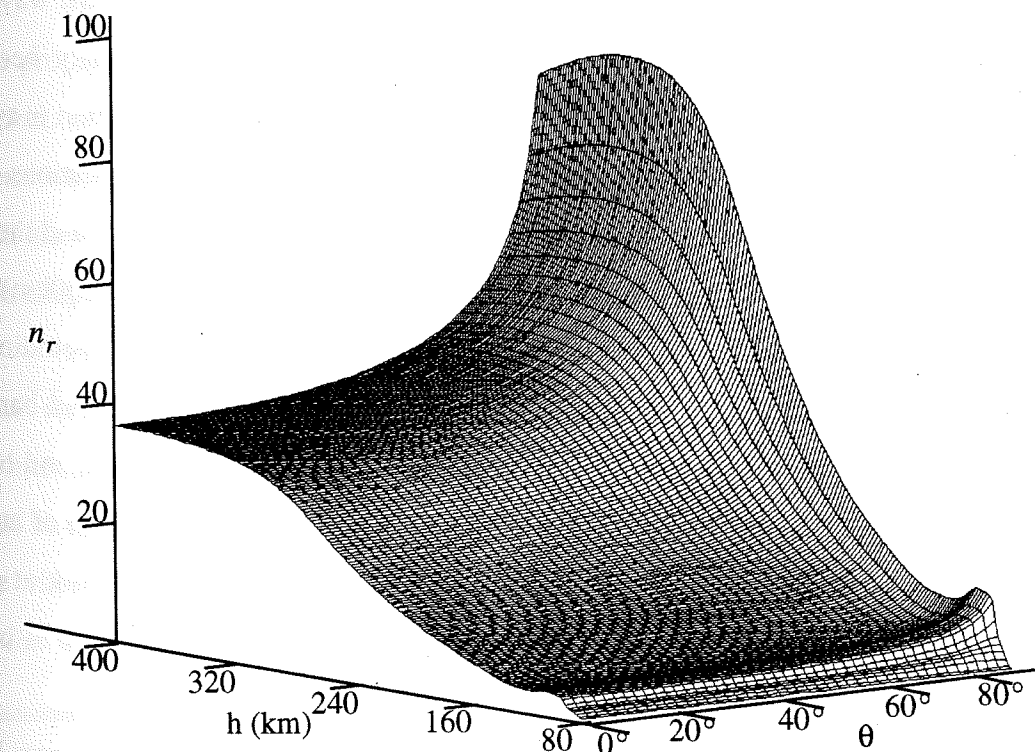
Figure 1.2:   Calculated refractive index of a 5 kHz wave using the profiles of the electron density and the effective collision frequency shown in Figure 1.1

5 kHz wave at altitudes from 80 km to 440 km in the ionosphere. At each altitude, the refractive index at different propagation angles (between wave normal and background magnetic field) was calculated.

1.5 ABOUT THIS DISSERTATION

Lightning-generated VLF waves play an important role in electrodynamic and plasma processes in the ionosphere, but there are still many gaps in our knowledge about the properties of these waves in the ionosphere. For examples, how does the amplitude of these waves change with altitude in the ionosphere? What is the relationship of the amplitude of these waves measured in the ionosphere to the lightning current measured on the ground? Where are these lightning-generated waves launched into the ionosphere? What are the characteristics of the wave absorption in the lower ionosphere? What is the effect of wave self-modulation on the wave spectrum in the ionosphere? These questions either have not previously been well answered or have never been addressed. The data from our participation in two collaborative campaigns provide us a chance to answer many of these questions

During the Wave Induced Particle Precipitation (WIPP, 1987) and the Thunderstorm II (1988) campaigns, two rockets (apogees 420km and 330km) and 6 balloons (float altitudes 30km) were launched near thunderstorms. A photodiode sensor for measuring the broad-band optical power of lightning and a broad-band VLF receiver for measuring electric field were included in both the rocket- and balloon-borne payloads. During the rocket flights, the optical and electric signals of hundreds of lightning strokes were located by the State University of New York at Albany (SUNYA) lightning network (Orville, et al., 1983, 1987) and recorded at both the rockets and balloons.

In the next chapter, we will describe the WIPP and Thunderstorm II campaigns and the instruments used on the rockets and balloons. Our emphasis will be on the optical lightning detector which we contributed. We will also give a general over-

view of the data we obtained from these two campaigns.

In Chapter 3, we will discuss an optical phenomenon recorded by our downward-looking optical lightning detector at the WIPP rocket. This phenomenon has some anomalous characteristics which have not been reported previously. Our study suggests that this phenomenon occurred above balloon altitude (30km) and may be evidence for discharges at high altitudes.

In Chapter 4, we will study the correlation between the amplitude of lightning-generated VLF in the ionosphere and the lightning current intensity measured by the SUNYA lightning network. Our results indicate that the wave components at lower frequencies, presumably below 4 kHz, have a fairly good linear correlation with the SUNYA current intensity. But wave amplitudes at higher frequencies normally do not have a positive linear response with the SUNYA current.

With the optical signal of lightning, we have been able to determine accurately the propagation time of the lightning-generated VLF waves from the source to the rocket. In Chapter 5, using the wave propagation time, we will investigate the locations where the lightning-generated waves were launched into the ionosphere. We will also discuss the relationship of our results to the wave generation mechanisms in this chapter.

From the rocket measurements, we have found that the lightning-generated VLF waves have maxima and minima in their intensity at different altitudes, instead of attenuating monotonically with altitude as normally predicted.This phenomenon will be reported and discussed in Chapter 6. Using a preliminary theoretical model, we will show that the wave amplitude profiles could be explained by the interference of the VLF waves.

The heating of the lower ionosphere by lightning-generated VLF waves has been of interest in recent years. Such heating originates from the absorption of VLF wave energy. The VLF wave absorption in the ionosphere has usually been evaluated using the Appleton-Hartree equation, which is not valid for VLF waves in the lower

ionosphere because of the sharp electron density gradient. In chapter 7, we numerically calculate the absorption of VLF waves at the bottom of the ionosphere. The electron density gradient of the ionosphere is taken into account. The characteristics of the absorption, such as the frequency dependence, are investigated. Comparing the lightning spectra received on the ground and by a rocket, we found possible evidence of large increase in the collision frequency between electrons and neutrals, which implies significant heating of the ionosphere from lightning-generated VLF waves.

In the last chapter, chapter 8, we will summarize the main results of this dissertation and discuss some problems for future studies.

CHAPTER 2

EXPERIMENTS, INSTRUMENTS AND DATA

2.1 THE WIPP AND THE THUNDERSTORM II CAMPAIGNS

During the summer of 1987 and 1988, the Wave Induced Particle Precipitation (WIPP) campaign (Kintner et al., 1987; Arnoldy and Kintner, 1989; Hu et al., 1989, Li et al., 1990) and the Thunderstorm II campaign (Kelley et al., 1988 and 1990) were conducted at the NASA Wallops Flight Facility (37.8 N, 75.4W). During these two campaigns, all together two rockets and six balloons were launched near thunderstorms to investigate thunderstorm related phenomena in the ionosphere and
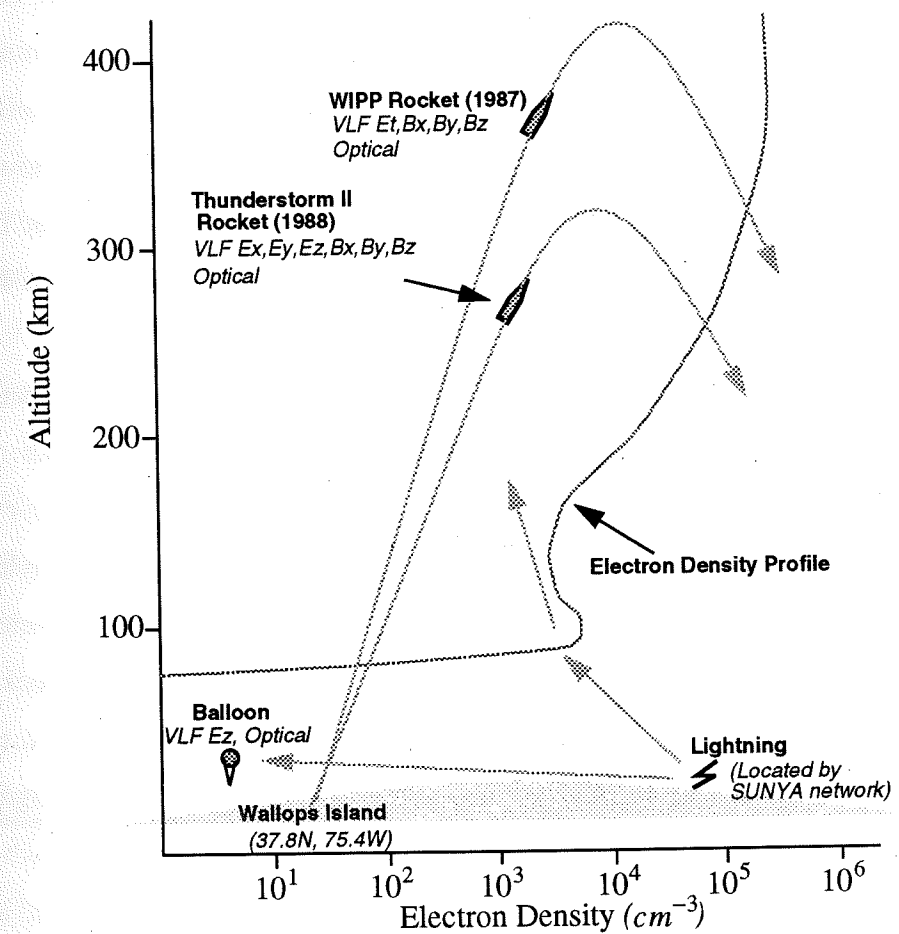
Figure 2.1:   Measurements conducted by the rockets and balloons in the WIPP and Thunderstorm II campaigns

atmosphere. Figure 2.1 is a diagram showing the measurements conducted by the rockets and balloons in the WIPP and the Thunderstorm II campaigns.

The WIPP rocket (Principal investigator: P. Kintner) was launched at about 3:53:49 UT on the night of July 31, 1987. It flew about 10 minutes and achieved an altitude of about 412 km. A down-looking optical lightning detector for measuring the broad-band optical power of lightning was included in the rocket payload. Besides the optical power of lightning, the broad-band VLF electric field in the direction perpendicular to the geomagnetic field and the broad-band VLF magnetic field vector were also measured by the rocket. Also included in the rocket payload were two photo-multiplier photometers and a Reticon imager. Even though its spatial resolution was relatively low, the imager was intended to provide a means for locating any important optical events observed. During the rocket flight, a balloon launched about two hours earlier was floating at an altitude of 31 km. An optical lightning detector was also mounted at the bottom of the balloon payload to make it down-looking. Other measurements conducted on the balloons included the quasi-static DC electric field vector and VLF electric field in the vertical direction (Hu et al, 1989; Li et al, 1990).

The Thunderstorm II rocket (Principal investigator: M. Kelley) was launched at about 5:47:22 UT on the night of July 27, 1988. The apogee of the rocket was about 333 km. The flight lasted about 8 minutes. A down-look lightning-detector which was identical to that used on the WIPP rocket was also included in the payload of this rocket. Besides the optical power of lightning, the broad-band VLF electric field vector and magnetic field vector were measured at the Thunderstorm II rocket as well.

The spin rate of both the WIPP and the Thunderstorm II rockets was about one cycle per second. The spin axes of the rockets were approximately in alignment with the earth's magnetic field line during the rocket flight. Telemetry from both the rocket and balloon payloads included both digital PCM (pulse-code modulation) and analog FM/FM downlinks.

In these two campaigns, the locations and discharge current intensities of cloud-to-ground lightning flashes which occurred within a horizontal range of a thousand kilometers from the rocket were detected by the State University of New York at Albany (SUNYA) lightning locating network (Orville, et al., 1983, 1987). Other ground-based data included broadband VLF magnetic measurement using a magnetic loop antenna at Wallops Island (Rodriquez et al, 1992).

2.2 INSTRUMENTS

In this dissertation the rocket data from the WIPP and the Thunderstorm II campaigns are used primarily, so, our emphasis here will be on the instruments used on the rockets. The instruments for measuring VLF electric and magnetic field at the rockets in the WIPP and Thunderstorm II campaigns were contributed by Cornell University (Kintner et al, 1987; Arnoldy and Kintner, 1989; Kelley et al, 1988 and 1990). The optical imager and photometers were provided by G. Parks of University of Washington (Massey et al., 1990). These instruments will only be briefly described. The optical lightning detector was fabricated by our group at the University of Washington and calibrated by the author.

2.2.1 Optical Lightning Detector

The broad-band optical lightning detector was used on two rockets and six balloons in the WIPP and the Thunderstorm II campaigns. This detector applied Hamamatsu photodiodes (PN: S1336-8BK) as optical sensors. One photodiode was used in each balloon detector while two photodiodes in parallel were used in the rocket-borne detector to provide redundancy and to double the amplitude of that signal. Otherwise, the balloon and rocket optical sensors and electronics were identical.

The detector ignores continuous optical signals of duration longer than approximately 1 sec by using a DC canceling circuit. Photodiode output is compressed into a 0 - 5 volt range by a square-root circuit before the voltage signal is

relayed to ground telemetry receivers. An electric circuit diagram of the detector is given in Appendix 1.

The photodiode bandwidth covered the visible wavelengths between 400 and 700 nm. For the balloon sensor with one photodiode, the minimum detectable input optical power was approximately 300 pW, which is equivalent to detecting a 5,000 kW optical source at a distance of 400 km. Saturation input power for a single photodiode was about 4 μW. Hence the dynamic range of the detector was about 40 dB in optical power. With two photodiodes, the sensitivity of the rocket detector was 150 pW.

The lightning detector has a wide field of view. A window of diameter 1.2 cm was used with either one or two photodiodes, and the overall sensor was uncollimated. The measured angular sensitivity function for a detector with one photodiode is
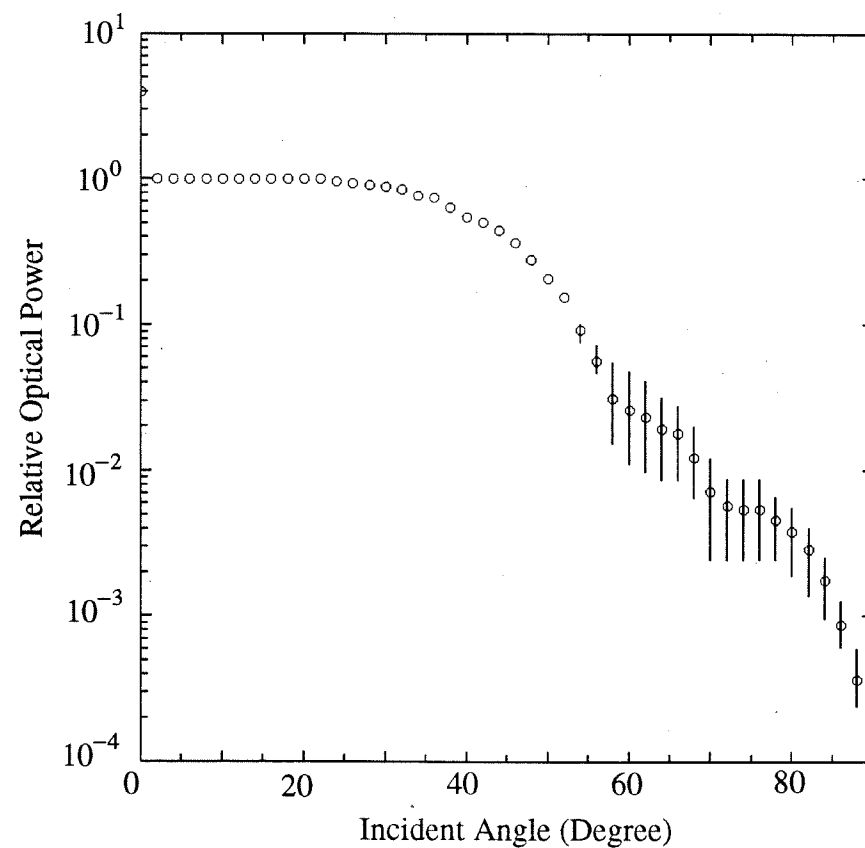
Figure 2.2:   Angular sensitivity of the lightning optical detector

shown in Figure 2.2. Circles plot the mean optical power values of the angular sensitivity found in three separate calibrations. Bars on the circles indicate the range of values. Ledges apparent in the plot near 60° and 70° are probably due to light reflected into the photodiode from the edge of the aperture. Apart from the small error of measurement, the range of values in different measurements (error bars) is due to rotation of the sensor about the axis normal to the aperture; note that reflection may not be uniform around the edge of the aperture. As the incident angle of the optical signal changes from 0° - 88° the normalized optical power sensitivity of the detector falls off by a factor of more than 2.3×10^{-4} .

The optical lightning detector was installed on the bottom of a balloon or rocket payload to make it down-looking in flight. Detectors at both the rockets and balloons have recorded a large number of optical pulses generated by lightning strokes.

Optical detectors of this type have been previously used on 8 balloons (Holzworth et al., 1986).

b. VLF electric field and magnetic field detector

The dipole electric field detectors employed spherical conductors mounted on the ends of a 3-m tip-to-tip boom pair extended perpendicular to the spin axis of the rocket. Since the spin axis of the rocket was maintained parallel to the geomagnetic field, the boom was approximately perpendicular to the geomagnetic field during the rocket flight.

The detector on the WIPP rocket had only one boom pair, so only the perpendicular electric field component was measured. The highest frequency response of this detector for the E-field component was 32 kHz (digitized at 64 kHz). The detector on the Thunderstorm II rocket measured the vector electric field by applying three pairs of booms (two 3-m pairs and one 1-m pair). The sample rates for the three components of electric field were 10 kHz, 20 kHz and 20 kHz respectively.

The quasi-static vector E field detector and the broadband VLF E field

detector used at the balloon consisted of six spherical conductors mounted on the ends of three pairs of orthogonal 1.5-m booms. Maximum frequency response of the balloon E field detector for vertical component was 50 kHz. Similar rocket and balloon E-field detectors have been used in previous flights and are described more completely by Kelley et al. (1985), Holzworth et al. (1985) and Sefering (1987). The vector magnetic field was measured at both rockets using three-axis search coils magnetometer furnished by Cornell University.

c. Optical imager and photometers

Besides the optical lightning detector, two photo-multiplier photometers (3914Å, 5577Å) and a Reticon imager were also mounted on the bottom of the WIPP rocket payload for detecting optical sources below it (Massey et al., 1990). Viewing angle of the photometers and imager were 35° and 45° full angular width, respectively. Photometer bandwidths were 30Å, and photons were counted during an integrating period of 1 msec for each point measured. With overlapping field of view, the 32×32 array of light-sensitive cells in the Reticon imager produced an image once every 54 msec. From these images, the approximate locations of observed optical sources can be determined.

2.3 DATA OVERVIEW

Both the WIPP and Thunderstorm II rockets recorded optical signals and VLF electric field responses of a large number of lightning strokes. Many of these lightning strokes were located by the State University of New York at Albany (SUNYA) lightning detecting network.

Examples of the data obtained by the optical lightning detector and the VLF electric field detector at the Thunderstorm II rocket, as well as the data from the SUNYA lightning network, are shown in Figure 2.3. The top panel (Opt-R) in this 100-msec figure is the optical measurement from the lightning optical detector. The second and third panels (V12 and V34) are broadband measurements of two

components of the VLF electric field perpendicular to the geomagnetic field. The fourth panel (V35) is the parallel component of the electric field. The bottom panel (SUNYA) are the data from the SUNYA lightning network, in which the location and the multiplicity of the lightning flashes are indicated.

As shown in Figure 2.3, a single-stroke lightning flash located at 37.1N, 71.6W occurred at 5:51:16.596 UT. Its optical signal was detected by the rocket at about 5:51:16.597 UT at an altitude of 314 km. The horizontal distance between the flash and the rocket was approximately 300 km. About 5 ms after receiving the optical signal, a VLF wave packet generated by this lightning stroke was detected.
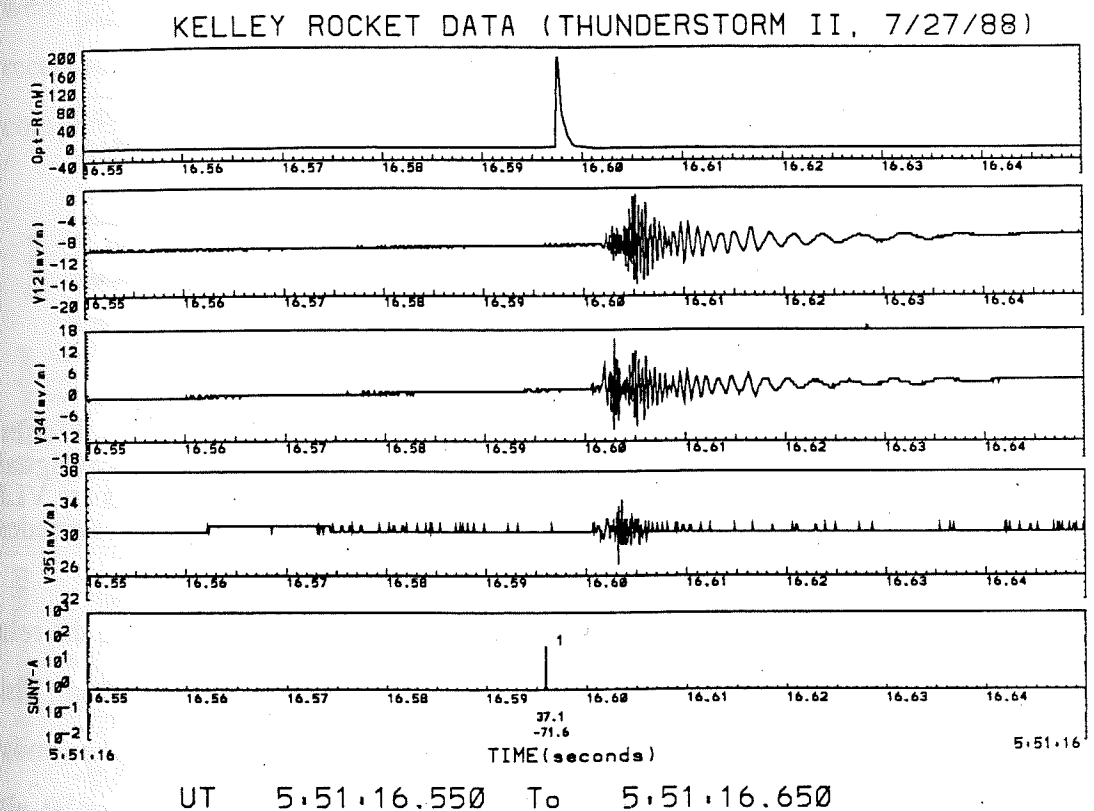
Figure 2.3: Lightning-generated optical signal and VLF waves received at the Thunderstorm II rocket. The top panel is the lightning optical signal recorded by the lightning optical detector. The second and third panels are two perpendicular components of the VLF electric field. The fourth panel is the VLF electric field in the direction parallel to the geomagnetic field. The bottom panel is the data from the SUNYA network. The location and the multiplicity of the lightning flash are also indicated in this panel.

Rocket Optical and VLF data (WIPP, 1987)
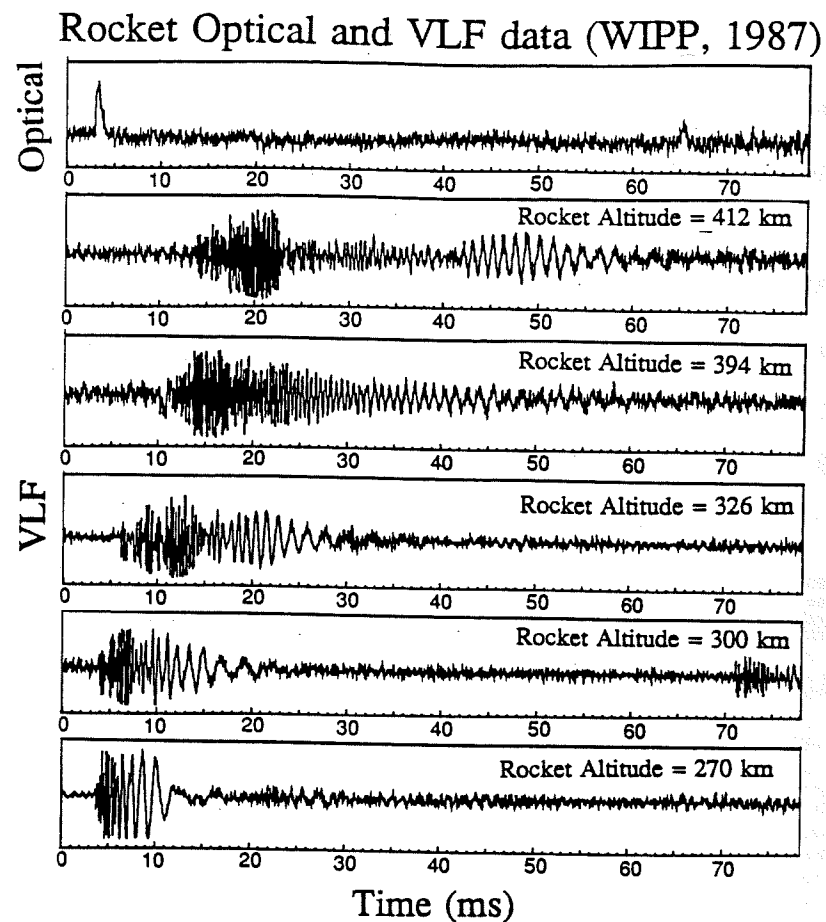
Figure 2.4: Typical lightning-generated VLF waves received at different altitudes in the ionosphere. The top panel is the lightning optical signal which serves as a timing of the lightning flash. The rest panels are VLF waves generated by different lightning strokes and received at altitudes from 270 km to 412 km.

The time delay of the VLF waves to the optical signal is due to the relatively slow speed of whistler-mode waves propagating in the ionosphere medium. This time delay becomes longer when waves propagate a longer distance in the ionosphere. Figure 2.4 shows several wave packets received by the WIPP rocket at altitudes between 270 km and 412 km. The first panel in this figure is the lightning optical signal. The rest five panels are the perpendicular component of VLF waves generated by different lightning strokes and received at different altitudes. It is seen that the time delay of VLF waves to the optical signal increases significantly with altitude. Besides

the relatively slow speed, these waves also have a dispersive feature. The wave packets last much longer when received at higher altitudes. The typical duration of the wave packets ranges from 15 ms at an altitude of 150 km to 50 ms at an altitude of 400 km. The dispersive feature of these waves can be better seen in Figure 2.5.

Figure 2.5 shows 100-msec optical and VLF data obtained by the WIPP rocket at an altitude of 393 km. The top panel in this figure is the lightning optical signal. The middle panel is the measurement of the perpendicular VLF electric field. The bottom panel is the spectra of the VLF electric field. The time resolution of the spectra is one msec. It is seen in this figure that the optical signals of four lightning strokes were detected by the rocket. The wave packets generated by these strokes were received by the rocket at 3:58:19.774, 792, 812 and 842. It is seen that the frequency components above 20 kHz in each wave packet arrive at the rocket almost

Kintner Rocket Data (WIPP, 7/31/87)

03:58:19.750 - 03:58:19.850 UT
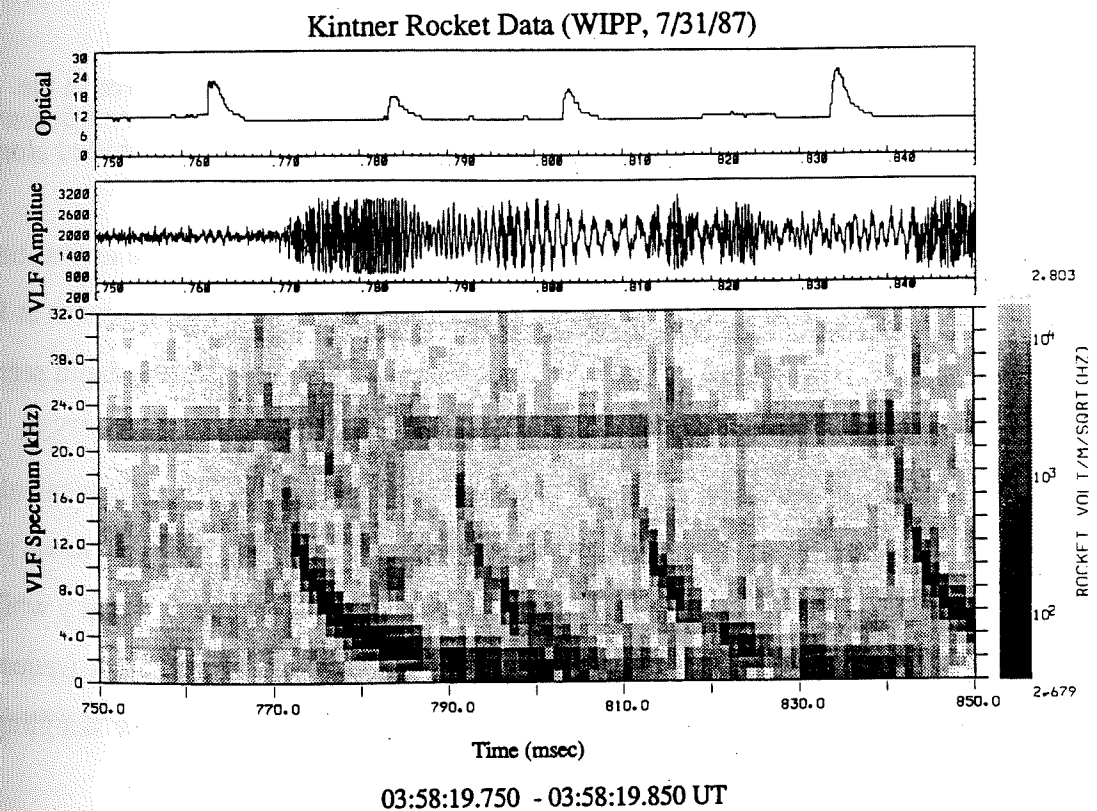
Figure 2.5: 100-msec spectra of the electric field recorded by the WIPP rocket at 393 km.

KELLEY ROCKET VLF (THUNDERSTORM II,7/27/88)

UT 5:53:24.455 To 5:53:24.485
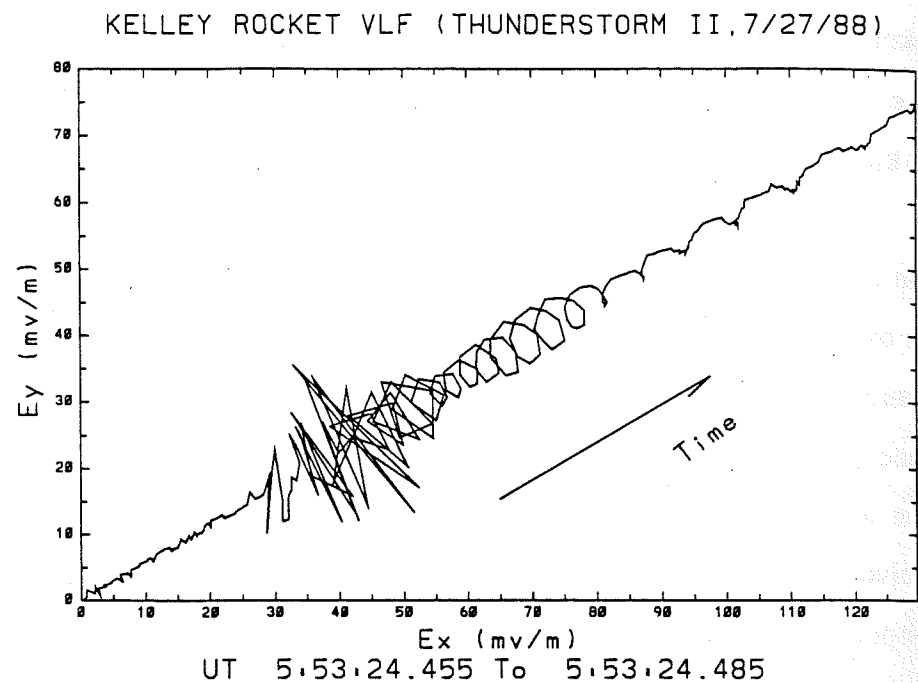
Figure 2.6: The polarization of lighting-generated VLF waves in the ionosphere. The two perpendicular (to geomagnetic field) components are plotted as x and y while the origin of the coordinate is shifted along he time.

simultaneously (within 1 msec). Below 20 kHz, the difference in the arrival time of different frequency components becomes significant. For example, the wave at 1 kHz arrived the rocket about 15 msec later than the wave at 20 kHz. The band seen at a frequency of 22 kHz in this figure is the signal from a VLF transmitter (NSS).

The circular polarization of these lightning-generated VLF waves can also be seen in the data. To show this, two perpendicular components of a wave packet received by the Thunderstorm II rocket are plotted in Figure 2.6 as x and y while the origin of coordinates is shifted with time. It is seen in the figure that at low frequencies the circular polarization is obvious, while at high frequencies the low sampling rate (10 kHz) prevents resolution of it.

The dispersion, polarization and propagation speed of lightning-generated waves in the ionosphere, shown in the above, have been measured by rockets in earlier

experiments (Maynard, 1970). It was shown that the measurements were consistent with the predictions by the magnetoionic theory for whistler-mode waves (Maynard, 1970).

CHAPTER 3
ANOMALOUS OPTICAL EVENTS DETECTED
BY THE LIGHTNING DETECTOR AT THE WIPP ROCKET

3.1 INTRODUCTION

During the Wave Induced Particle Precipitation (WIPP) campaign (Kintner et al., 1987; Arnoldy and Kintner, 1989), one rocket (apogee over 400 km) and four balloons (float altitudes over 30 km), were launched near thunderstorms. The optical lightning detectors were included in both the rocket and balloon-borne payloads.Two narrow-band photometers and a Reticon imager (Massey et al., 1990) were also mounted on the rocket.

During the 10 minute rocket flight, more than 500 events were detected by the lightning detectors on the rocket and balloon together. Many of these events were individually correlated with cloud-ground (CG) lightning flashes located by the State University of New York at Albany (SUNYA) lightning network. A number of other events not indicated in the SUNYA data can probably be attributed to intracloud (IC) lightning or to CG lightning missed by the network. In addition to all these lightning events, the rocket detected a third class of optical events which have anomalous signatures. These involve many more optical impulses and longer optical duration (about several hundred ms) than typical of lightning events. These anomalous optical events (AOEs) were always accompanied by characteristic radio signals detected primarily by the ground-based VLF receiver in the form of a strong clustering of VLF impulses embedded in mostly weaker, more continuous noise. At the rocket and balloon, the detected amplitude of these characteristic signals was generally less than that of the typical VLF radio impulses or "atmospherics" usually produced by the lightning.

None of the long-duration AOEs were detected by the WIPP balloon photo-diode sensor. This is true even though the data from the Reticon imager on the rocket indicated that some of them were from localized sources which should have been visible to the balloon sensor. By this we mean primarily that we have been able to localize some of the AOEs to regions from that the balloon did detect most of the SUNYA-located lightning flashes which were nearly simultaneous with some of the AOEs. In fact, no AOEs of the WIPP or any other type were ever seen by any of the six balloon payloads which were floated in similar situations (4 flights in 1987, 2 flights in 1988; see Hu et al., 1989). This suggests that the AOEs reported here for the WIPP rocket flight may have occurred above the balloon, that is at some altitude above 30 km.

Lightning discharges in the Earth's atmosphere typically occur below the tropopause at about 15 km altitude maximum. The few reports available indicate that lightning which sometimes goes upward to the clear air above 15 km is uncommon (Vaughan and Vonnegut, 1989). Other rare forms of upward discharges have been reported (Malan, 1937; Franz et al., 1990). In the mid-latitude atmosphere, some natural optical phenomena are also known to occur above 30 km, such as luminous meteors, light produced by precipitating electrons, ordinary (here, nighttime) air-glow and fast atmospheric light pulsations (Ögelman, 1970; Tümer, 1982). None of these sources have characteristics which resemble those of the AOEs detected during the WIPP rocket flight.

In this chapter we will present examples of anomalous optical events (AOEs) detected by the rocket and balloon on July 31, 1987. We will show that the AOEs have signatures which differ from those of well-known optical sources in the atmosphere.

3.2 DATA

As mentioned above, more than 500 lightning-related optical events were detected by the rocket and balloon payloads together during the 1987 WIPP rocket flight. For many of these impulsive events the SUNYA network located essentially simultaneous CG lightning flashes. Figure 3.1 shows those flashes located by SUNYA during the period when rocket data were being collected. Geographical positions of SUNYA-located flashes are plotted with symbols indicating whether a stroke was also detected by the rocket, the balloon, both or neither. As discussed below, most

data points are circles indicating simultaneous detection by both rocket- and balloon-borne sensors. Symbols for lightning flashes located at about the same geographical position have been offset as needed for clarity (see figure caption). Approximate projections of the rocket and balloon trajectories are also indicated.
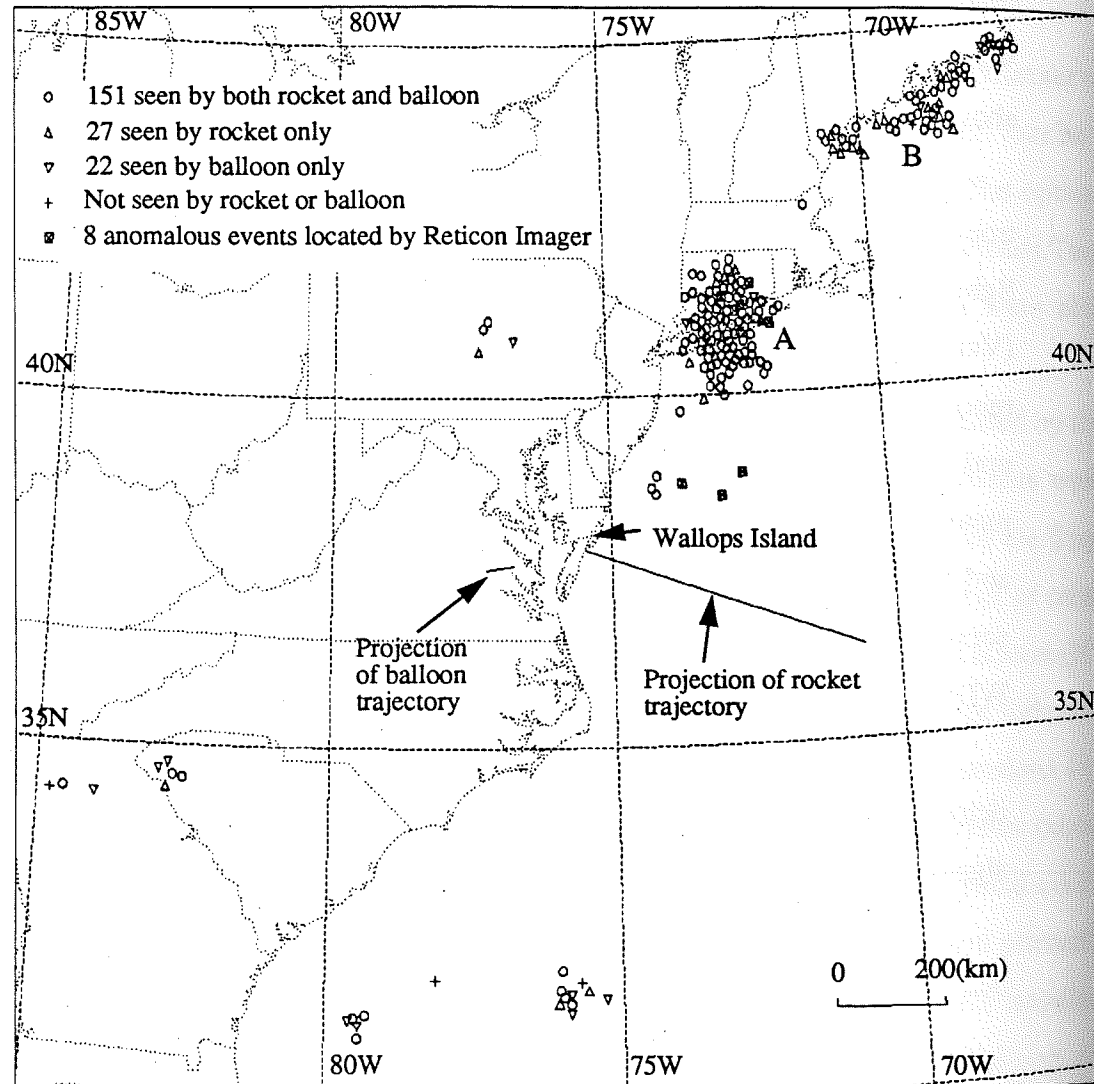
Figure 3.1:   Cloud-Ground lightning flashes located by the SUNYA network. Flash locations are plotted with different symbols indicating whether a flash was also detected by the rocket, the balloon, both or neither. Positions of the eight AOEs located by the Reticon array imager are plotted assuming the optical sources are at cloud altitude.

The total number of flashes in Figure 3.1 is 205. Of these, 87% were detected by the rocket, 84% by the balloon, and 74% by both rocket and balloon. Only 2% were

not detected by either the rocket or the balloon. The SUNYA lightning locations confirm the effective fields of view of the rocket and balloon optical photodiode sensors in an approximate way. It can be seen from the figure that both the rocket and balloon sensors detected nearly all SUNYA-located lightning flashes (more than 90%) within a range of approximately 500 km. In addition, many flashes beyond a range of 500
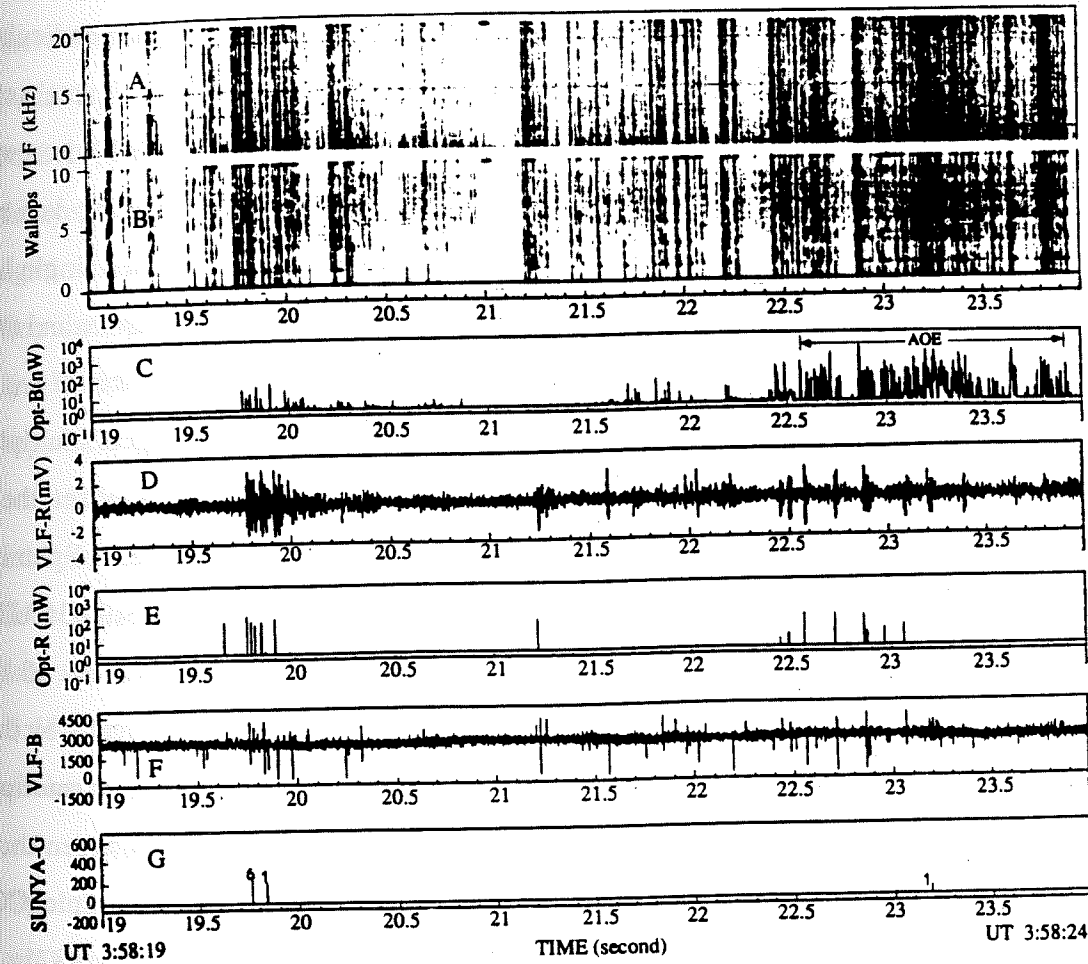
Figure 3.2:   Five seconds of data from the Wallops ground instruments, the WIPP rocket and balloon, and the SUNYA lightning network. Panels A and B show the 0-20 kHz VLF spectrum (Wallops VLF) recorded by a ground-based VLF receiver. Panel C shows the optical power (Opt-R) detected by the rocket photodiode sensor. Panel D shows the broad-band electric field (VLF-R) in a direction approximately perpendicular to the geomagnetic field at the rocket. Panels E and F show the optical photodiode power (Opt-B) and broad-band vertical electric field (VLF-B) detected at the balloon. The bottom panel (SUNYA-G) shows the SUNYA network lightning data, for which only the first stroke of a multistroke flash is plotted, with the multiplicity indicated by a number above it.

km were detected as well. (For reference, the line of rocket trajectory is about 500 km.)

Five seconds of data from the Wallops VLF receiver on the ground, the rocket, the balloon, and the SUNYA network are shown in Figure 3.2. Panels A and B (Wallops VLF) show the 0 - 20 kHz spectrum recorded by a ground-based VLF receiver with a magnetic (loop) antenna. The C and D panels show the optical power (Opt-R) and broad-band electric field (VLF-R), which is approximately perpendicular to the Earth's geomagnetic field, detected at the rocket (-R). The E and F panels show the optical power (Opt-B) and broad-band vertical electric field (VLF-B) detected at the balloon (-B). The bottom panel (SUNYA-G) is derived from lightning data recorded by the SUNYA network on the ground. For multiple flashes within a single lightning flash, the SUNYA data includes the time and intensity of the first stroke and the stroke multiplicity, which is indicated by a number written above the stroke.

Seen at approximately 3:58:19.8 UT in Figure 3.2 is a typical multiple stroke lightning event detected by the Wallops VLF ground receiver, the rocket, the balloon and the SUNYA network. For this event, the SUNYA data located a lightning flash with six strokes at 41.089N, 72.657W (3:58:19.762 UT). At 3:58:19.835 UT, 73 ms later, another individual flash was located at 40.702 N, 72.512W, about 45 km away from the first one. Both of these lightning events were detected optically by the rocket and balloon photodiode sensors. Three impulses due to the first or multiple event appear in the rocket and balloon optical data, the time interval between those three impulses is within the range expected for intervals between multiple CG return strokes in a typical multi-stroke flash (Thomson et al., 1984; Uman, 1987).

Besides CG lightning events such as these, the rocket and balloon detectors also registered many other impulsive optical events not indicated in the SUNYA data. Examples include the impulse just after 3:58:21.2 UT in the balloon data (panel E of Figure 3.2) and those impulses between 3:58:22.5 and 3:58:22.9 UT which occur in both the rocket (panel C) and balloon (panel E) data. Since these particular impulses are similar to others which were located by the SUNYA network, they are thought to

be most likely due either to IC or to CG lightning flashes missed by SUNYA. More than 500 such impulsive lightning responses were detected by the rocket and balloon sensors together, which is more than twice the number of CG flashes located by the SUNYA network during the same interval.

Along with most of the lightning responses either located as CG flashes by SUNYA or indicated as some other type of isolated optical impulse by a WIPP sensor, there is usually an active, burst response in the rocket and balloon VLF wave channels (VLF-R and VLF-B). This can be seen, for example, in the events occurring at 3:58:19.8 and 3:58:21.2 UT in Figure 3.2. Note that the burst of VLF signal is slightly delayed at the 390 km rocket altitude due to the low value of the whistler-mode propagation velocity. This will be seen more clearly in Figure 3.5 later. The stronger radio impulses (atmospherics) of some lightning strokes can also be resolved in panels A and B of Figure 3.2 where they appear as the more individual vertical lines in the Wallops VLF (ground) spectrum.

Up to this point we have been considering impulsive responses which we have attributed to the strokes in typical lightning flashes. In addition to these, the rocket sensor also detected some optical events which exhibited anomalous features not typical of any lightning. An example can be seen in Figure 3.2 starting perhaps at 3:58:22.41 UT, or more likely extending from 3:58:22.85 UT to 3:58:23.95 UT in the rocket optical data (panel C).

There are considerably more optical impulses in this event than typically in lightning events detected at the rocket, whether or not nearly simultaneous CG lightning flashes were located by the SUNYA network. Also, there are considerably more impulses than the typical number expected either for IC lightning flashes (Kitagawa and Kobayashi, 1958; Ogawa and Brook, 1964) or for CG flashes (Schonland, 1984; Thomson et al., 1984). Furthermore, the intervals between most of the impulses in this anomalous event were much smaller than intervals in the multi-stroke lighting we observed, for example in the flash at about 3:58:19.8 UT in Figure 3.2 and discussed above.

km were detected as well. (For reference, the line of rocket trajectory is about 500 km.)

Five seconds of data from the Wallops VLF receiver on the ground, the rocket, the balloon, and the SUNYA network are shown in Figure 3.2. Panels A and B (Wallops VLF) show the 0 - 20 kHz spectrum recorded by a ground-based VLF receiver with a magnetic (loop) antenna. The C and D panels show the optical power (Opt-R) and broad-band electric field (VLF-R), which is approximately perpendicular to the Earth's geomagnetic field, detected at the rocket (-R). The E and F panels show the optical power (Opt-B) and broad-band vertical electric field (VLF-B) detected at the balloon (-B). The bottom panel (SUNYA-G) is derived from lightning data recorded by the SUNYA network on the ground. For multiple flashes within a single lightning flash, the SUNYA data includes the time and intensity of the first stroke and the stroke multiplicity, which is indicated by a number written above the stroke.

Seen at approximately 3:58:19.8 UT in Figure 3.2 is a typical multiple stroke lightning event detected by the Wallops VLF ground receiver, the rocket, the balloon and the SUNYA network. For this event, the SUNYA data located a lightning flash with six strokes at 41.089N, 72.657W (3:58:19.762 UT). At 3:58:19.835 UT, 73 ms later, another individual flash was located at 40.702 N, 72.512W, about 45 km away from the first one. Both of these lightning events were detected optically by the rocket and balloon photodiode sensors. Three impulses due to the first or multiple event appear in the rocket and balloon optical data, the time interval between those three impulses is within the range expected for intervals between multiple CG return strokes in a typical multi-stroke flash (Thomson et al., 1984; Uman, 1987).

Besides CG lightning events such as these, the rocket and balloon detectors also registered many other impulsive optical events not indicated in the SUNYA data. Examples include the impulse just after 3:58:21.2 UT in the balloon data (panel E of Figure 3.2) and those impulses between 3:58:22.5 and 3:58:22.9 UT which occur in both the rocket (panel C) and balloon (panel E) data. Since these particular impulses are similar to others which were located by the SUNYA network, they are thought to

be most likely due either to IC or to CG lightning flashes missed by SUNYA. More than 500 such impulsive lightning responses were detected by the rocket and balloon sensors together, which is more than twice the number of CG flashes located by the SUNYA network during the same interval.

Along with most of the lightning responses either located as CG flashes by SUNYA or indicated as some other type of isolated optical impulse by a WIPP sensor, there is usually an active, burst response in the rocket and balloon VLF wave channels (VLF-R and VLF-B). This can be seen, for example, in the events occurring at 3:58:19.8 and 3:58:21.2 UT in Figure 3.2. Note that the burst of VLF signal is slightly delayed at the 390 km rocket altitude due to the low value of the whistler-mode propagation velocity. This will be seen more clearly in Figure 3.5 later. The stronger radio impulses (atmospherics) of some lightning strokes can also be resolved in panels A and B of Figure 3.2 where they appear as the more individual vertical lines in the Wallops VLF (ground) spectrum.

Up to this point we have been considering impulsive responses which we have attributed to the strokes in typical lightning flashes. In addition to these, the rocket sensor also detected some optical events which exhibited anomalous features not typical of any lightning. An example can be seen in Figure 3.2 starting perhaps at 3:58:22.41 UT, or more likely extending from 3:58:22.85 UT to 3:58:23.95 UT in the rocket optical data (panel C).

There are considerably more optical impulses in this event than typically in lightning events detected at the rocket, whether or not nearly simultaneous CG lightning flashes were located by the SUNYA network. Also, there are considerably more impulses than the typical number expected either for IC lightning flashes (Kitagawa and Kobayashi, 1958; Ogawa and Brook, 1964) or for CG flashes (Schonland, 1984; Thomson et al., 1984). Furthermore, the intervals between most of the impulses in this anomalous event were much smaller than intervals in the multi-stroke lighting we observed, for example in the flash at about 3:58:19.8 UT in Figure 3.2 and discussed above.

This particular anomalous optical event (AOE), which is one of about 23 similar events, lasted more than 1 sec (3:58:22.85 to 3:58:23.95 UT), a duration longer than that typical for multi-stroke lightning (Berger, 1977). As an additional distinguishing feature, nearly continuous optical output is apparent from about 3:58:23.2 to 3:58:23.4 UT. Although this AOE produced an enduring response with many relatively large-amplitude impulses at the rocket, correlated VLF signals received at both the rocket and balloon were relatively weak in comparison. The usual case of lightning detected at the rocket or balloon is quite different. Usually an individual lightning stroke can be identified as a strong, isolated optical impulse that is accompanied by an individual burst-like VLF response, also strong and isolated. This is also true to those lightning strokes which are not associated with SUNYA responses.For example, note that several detected impulses between 3:58:22.7 and 3:58:23.2 UT in the rocket and balloon optical data (panel C and E of Figure 3.2) have no corresponding SUNYA responses. Nevertheless these can be associated with individual bursts seen in the rocket and balloon VLF data. The distinction of the responses corresponding to the AOE and normal lightning on the rocket and balloon VLF panels will be seen more clearly later in Figures 3.5 and 3.6. Furthermore, although the rocket VLF signature of this anomalous source may be relatively weak (see also Figure 3.6 and its discussion), many impulses and much of the highly correlated, impulsive noise produced can be seen as clearly as lightning in the Wallops VLF ground spectrum (top two panels, A and B, of Figure 3.2)throughout the interval 3:58:22.4 to 3:58:23.9 UT.

Such anomalous VLF signatures recorded on the ground are characterized by an enhanced noise background which sometimes extends as much as 20 kHz above a cutoff that always seems to be present at approximately 3.2 kHz. (Decreasing sensitivity due to a low-pass filter in the Wallops receiver adds whiteness just below the top edge of panel B.) In addition there are bursts of impulsive noise with some components that last longer individually than the atmospherics normally attributed to individual CG lightning return strokes. With signals played through an audio amplifier and loudspeaker, the sound of an atmospheric is normally a short, sharp crack that

is quite different from the distinctive frying or sizzling sound (Burton and Boardman, 1933) produced along with the strongly clustered impulses in the VLF signature of this and the other AOEs. In spite of their long-enduring overall signatures, it is still likely that impulsive source discharges contribute to the AOEs.The impulsive noise in such anomalous VLF signatures has also been considered by Armstrong (1989) in terms of its spot-frequency radiation. He notes that this sort of impulsive noise may be a type which accompanies other phenomena in which lightning and ionospheric processes sometimes appear to be coupled under similar geophysical conditions.

The anomalous event now being discussed was also detected by the Reticon array imager on the rocket. Figure 3.3 consists of several superimposed images of this event taken in the rocket frame while the rocket was at about 395 km altitude and rotating at a rate of about 1 rev/sec. An image of the AOE was first acquired at 3:58:22.952 UT (image 1) just before it went out of the field of view. It was seen again from 3:58:23.061 to 3:58:23.387 UT (images 2 - 7) and then lost until 3:58:23.822 UT (image 9). Only part of images 1 and 9 are shown in Figure 3.3 because they occupy the same Reticon locations. This optical source produced Reticon data for about 1 sec, a duration substantially in agreement with the rocket optical photodiode data of Figure 3.2.The Reticon image of Figure 3.3 makes it apparent that this AOE was due to light from a localized source. Assuming that the source was at cloud level, further analysis indicates it was located at approximately 41.25N, 72.46W in the region labeled A in Figure 3.1.

Three seconds prior to this anomalous optical event (AOE), the SUNYA network located two lightning events in region A, as discussed above and shown in Figure 3.2 at 3:58:19.762 and 3:58:19.835 UT. Although the Reticon imager and SUNYA network independently show that both the source of the AOE and the source of the lightning signals might have been in the same region A, panel C of Figure 3.2 (note log scale) shows that at the rocket, the anomalous optical signal had an amplitude much larger than that of the lightning. As a matter of fact, the optical signal of this AOE is relatively strong in comparison with that of all the lightning strokes reg-

istered at the rocket. In spite of this, and even though more than 90% of the SUNYA-located lightning events in region A were detected by the balloon photodiode sensor, this AOE was not detected by the balloon photodiode sensor. This implies that the AOEs may not be produced by normal lightning.

Image (#)	Time (UT)	Relative maximum	Contour interval
1	3:58:22.952	20.1	2
2	3:58:23.061	25.9	2
3	3:58:23.115	86.0	10
4	3:58:23.169	141.0	10
5	3:58:23.224	232.2	15
6	3:58:23.278	97.6	10
7	3:58:23.333	97.0	10
8	3:58:23.387	83.0	5
9	3:58:23.822	81.0	5

(background subtracted out)
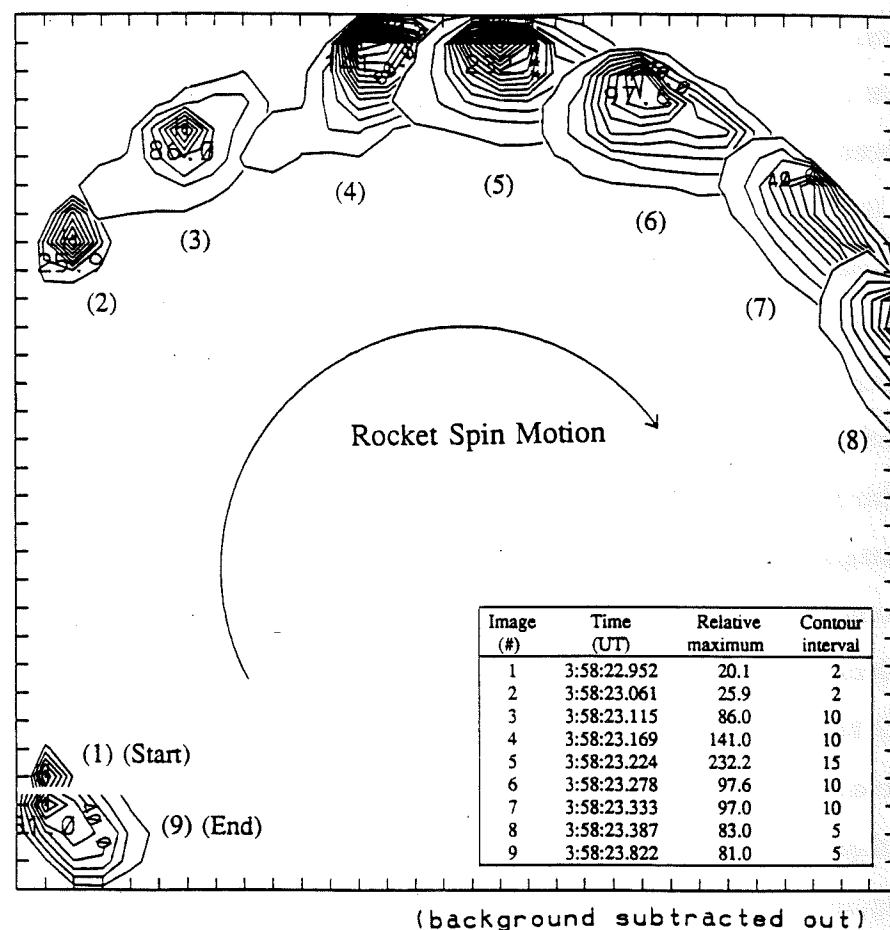
Figure 3.3: Relative amplitude contours derived from the Reticon array imager data are shown for the anomalous optical event (AOE) detected by the rocket optical photodiode sensor at about 3:58:23 UT in Figure 3.2. As the AOE evolved in time, nine images were taken between 3:58:22.952 (image 1) and 3:58:23.822 UT (image 9). The rocket was rotating about 1 rev/sec on an axis nearly parallel to the local geomagnetic field, and moved between altitudes of 395.15 and 395.68 km during this interval. Since images 1 and 9 are in the same location, only a part of each is shown. The maximum relative optical intensity and contour interval spacing are given in the table for each image. Intensity of the outermost contour is always normalized to the value 10.

Between 3:30 and 4:30 UT, an interval which included the rocket flight, a number of Trimpi amplitude-change events on the subionospheric VLF signal from the (45N, 67W) NAA 24.0 kHz transmitter were observed by the ground-based
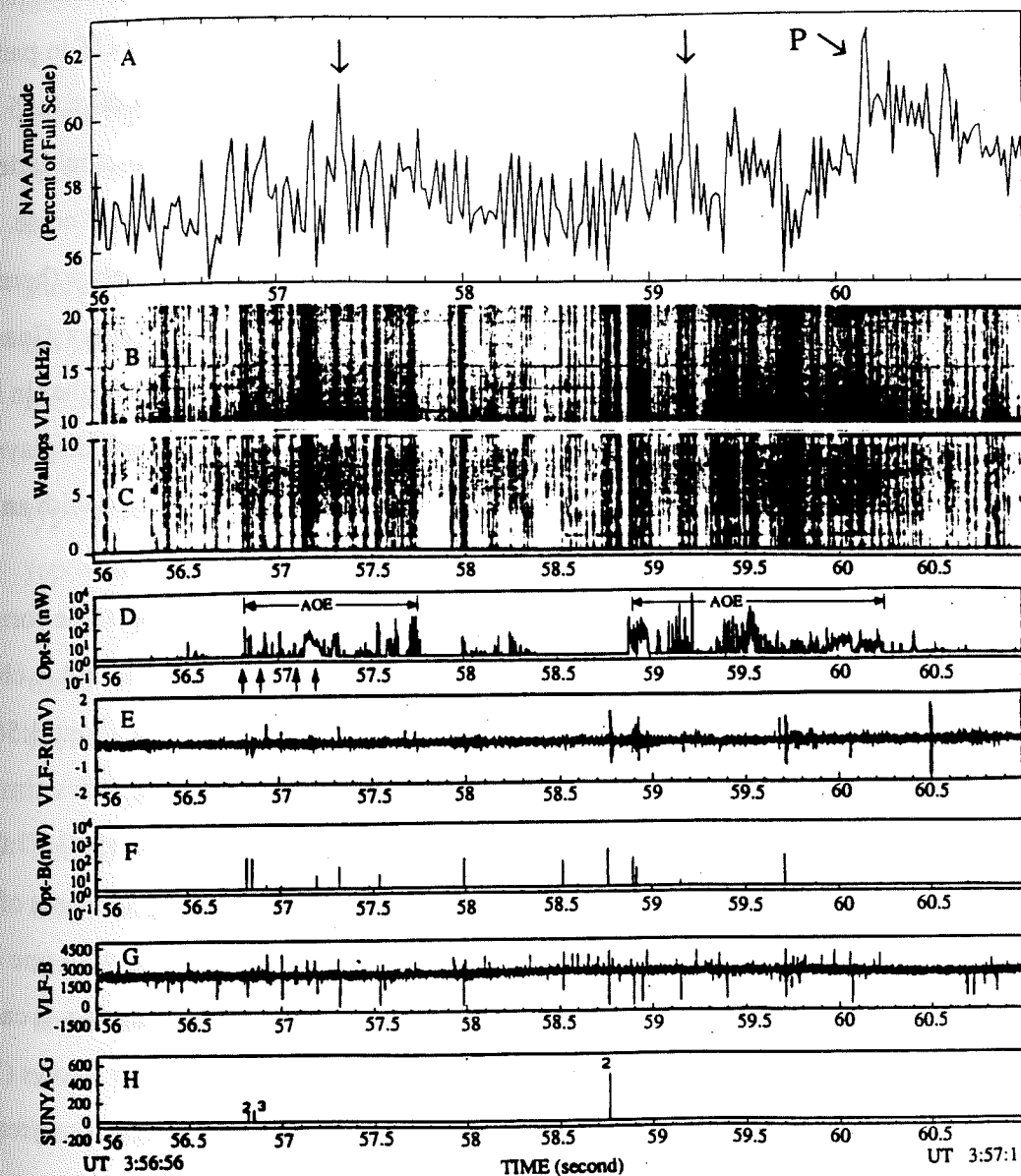
Figure 3.4: Five seconds of data from the Wallops VLF receiver on the ground, the rocket, the balloon, and the SUNYA network. Except for an additional panel A here showing the amplitude of the 24 kHz NAA channel on the ground at Wallops, this figure is identical to Figure 3.3. A subionospheric VLF signal perturbation (Trimpi event) occurs between about 3:56:59.8 and 3:56:60.2 UT in panel A while below it in panel D, an anomalous optical vent (AOE) is ending after a duration of about 1 sec. During the (Trimpi) perturbation, the average NAA signal strength increases from about 57% to 61%,exclusive of the peak (3) which is discussed in the text.

receiver at Wallops. Irregularly, each of these events was accompanied before and/or during the rise of the amplitude perturbation by a burst of impulsive VLF noise similar to that which accompanies the AOE between 3:58:23.2 and 3:58:23.4 UT in panels A and B of Figure 3.2. Furthermore, the NAA receiver channel (24.00 ± 0.15 kHz) exhibited a characteristic, new feature in the form of a sharp peak in amplitude, also near the onset of some of the Trimpi events, and in coincidence with such noise. Apart from this peak, the Trimpi events exhibit the rapid onset and slow decay (here typically about 0.5 and 30 sec respectively) of previously reported cases (Inan and Carpenter, 1987). The entire WIPP set of Trimpi events is discussed further in a separate paper by Rodriquez et al. (1992). Two Trimpi events which both displayed the sharp peak occurred during the rocket flight. Each is clearly associated with an AOE detected at the rocket, and one example is presented in Figure 3.4.

Except for the addition of a new panel A, Figure 3.4 has the same format of Figure 3.2. Panel A in Figure 3.4 shows an amplitude record of the NAA channel received on the ground at Wallops. Among others, the responses at about 3:56:57.2 and 3:56:59.5 UT in panels B, C and D of Figure 3.4 show characteristics similar to those discussed above for the AOE in Figure 3.2. At about 3:56:60.15 (3:57:00.15) UT in panel A, and indicated by arrow (3), is a peak distinguishing the onset of a 4% VLF Trimpi amplitude increase. This peak appears to be associated with one of the continuous optical components in an AOE in panel D. Upon examination, it can also be seen that other amplitude peaks in the NAA channel, as indicated by arrows (1) and (2) at about 3:56:57.3 and 3:56:59.2 UT in panel A, apparently occur preferentially during other AOEs in panel D.

As discussed previously, an anomalous optical event (AOE) consists of continued clusters of optical impulses and/or continuous optical emissions which correlate in great detail with characteristic impulsive noise, primarily in the Wallops VLF ground spectrum above a cutoff at about 2.3 kHz. We count clusters of impulses or continuous emissions as part of a single, continuing AOE as long as the intervals in between are less than 200 msec. This value is chosen somewhat arbitrarily based

on the WIPP data set itself. We have conducted a study of 23 such AOEs. Specifically, these events have the following notable characteristics:

(A) There are many more optical impulses in an AOE than in a typical multi-stroke lightning flash as seen by the WIPP rocket photodiode sensor and reported in previous research (Ogawa and Brook, 1964; Schonland, 1984: Thomson et al., 1984).

(B) The typical intervals between optical impulses in an AOE are usually shorter than the intervals typical between optical impulses which indicate the individual strokes of a multi-stroke lightning flash at the rocket. In many cases the AOEs include continuous optical emissions which last tens of msecs or longer.

(C) Most AOEs last for more than 1 sec overall, a duration longer than that typical for individual, multi-stroke lightning events as seen at the WIPP rocket and reported in previous research (Berger, 1977; Brook and Ogawa, 1977).

(D) The anomalous optical signals received at the rocket have large amplitudes which compare with or even exceed those of typical lightning strokes at the rocket.

(E) Even though the anomalous optical sources produce relatively stronger optical responses in the rocket data, and are accompanied by many impulses, the amplitude of the correlated radio activity in the rocket and balloon VLF channels is not relatively stronger in correspondence. Instead, relatively stronger background noise always appears in the Wallops VLF ground receiver, with a lower cutoff at about 3.2 kHz and highly correlated, characteristic bursts of impulsive noise or embedded clusters of VLF impulses that are relatively long-lasting individually.

(F) No AOEs of any kind were detected by an optical photodiode sensor on any balloon flight.

The WIPP rocket collected data for about 10 minutes over an altitude range of 150 km (up: 3:55:19 UT; down: 4:03:33 UT) to 412 km (3:59:26 UT), during which the balloon maintained an altitude of approximately 31 km. The first AOE was detected by the rocket photodiode sensor about 10 sec after data collection began, when the rocket altitude was approximately 170 km. Intervals between successive

occurrences of the AOEs are about randomly distributed between about 1 and 30 sec.

3.3 DISCUSSIONS

In this section we will discuss all the possible sources which may, within our knowledge, be responsible for the anomalous optical events (AOEs) detected by the photodiode sensor on the WIPP rocket. We will show that the AOEs are real atmospheric phenomena instead of effects due to spurious sources. We will also present reasons suggesting that these AOEs are neither normal lightning discharges nor some other well-known atmospheric phenomenon.

Since a great majority of the SUNYA-located lightning flashes were detected optically by the photodiode sensors on both the WIPP rocket and balloon, both sensors are believed to have functioned correctly. Such optical sensors have been used successfully on 14 balloon flights, and the data of this balloon flight are consistent with those recorded on other flights in similar situations. Even with smaller fields of view, the two photometers and the Reticon imager on the same (WIPP) rocket were able to detect some optical events that are well-correlated with photodiode AOE signatures. (A Reticon example shown in Figure 3.3 has the same duration and intensity evolution as the corresponding photodiode AOE response.) These concurrent observations of individual cases strongly imply that the AOEs being considered are not due to any sort of instrumental malfunction.

Components in all of the AOEs were correlated with significant clusters and individual VLF radio noise impulses that were strong in the Wallops ground spectrum. This implies the simultaneous generation of VLF radio emissions, and should rule out any possibility that a spurious effect in the local rocket environment, such as optical emissions by the rocket motor, is somehow responsible for producing the AOEs and/or the correlated radio noise.

It is not likely that the anomalous optical events (AOEs) were due solely to the cumulative effect of numerous lightning flashes occurring in a nearly simultaneous sequence over a vast area. Since there are so many optical impulses in each AOE, if

these were due to some cumulative effect of normal lightning flashes, a number of very active thunder-cloud cells would have to be involved. Collectively, these would probably have to transfer huge amounts of charge during the typical 1 sec course of an anomalous event. Also, however, the visual fields of the photometers and the Reticon imager were each just a few hundred km in lateral dimension on this flight, and weather records appear to show that they did not include many active thunder-cloud cells. Furthermore, those AOEs seen by the Reticon imager appeared quite clearly to be single, isolated and spatially continuous sources.

Continuing electric current in the channel of a CG lightning discharge sometimes can produce continuous low-level luminosity which lasts several hundred msec (Kitagawa et al., 1962). But the continuing current in CG lightning is not likely to be the source of these relatively bright AOEs. Most negative CG flashes include at least one short- (i.e. shorter than 40 msec) or long- (i.e. longer than 40 msec) continuing current component and roughly 50% of them have a long-continuing component (Uman, 1987). Therefore, many of the 178 lightning events located by SUNYA in Figure 3.1 and detected optically by the rocket should have had a component of continuing current. However, most SUNYA-located lightning detected optically at the rocket showed no evidence whatsoever of any apparently continuous optical feature. This could be an indication that the luminosity of a continuing lightning current is usually much weaker than that of a stroke, and is therefore too weak to be detected by the rocket photodiode sensor. On the other hand, the components of continuous optical emission in an AOE usually had an amplitude comparable to or even much greater than the typical amplitude of an optical impulse due to a SUNYA-located stroke. AOEs, therefore, do not seem to be caused by continuing currents in CG lightning.

Compared with CG lightning, IC (intracloud) discharges may have a relatively longer duration and may often include a continuing current component as well (Ishikawa and Kimpara, 1958; Brook and Ogawa, 1977). However, the AOEs we are discussing here have features unlike those of IC lightning. The reported duration of IC lightning discharges ranges between 350 and 550 msec most frequently (Ishikawa

and Kimpara, 1958; Ogawa and Brook, 1964; Mackerras, 1968), values which are about 50% of the typical duration of the AOEs. Also, the uniquely small and rapid K electric-field change detected for IC lightning reportedly corresponds directly to the optical impulse of the IC stroke (Kitagawa and Kobayashi, 1958), and many more optical impulses are detected during a typical AOE than there are K changes detected in an IC flash (Ogawa and Brook, 1964).

In connection with Figure s 3.2 and 3.4 we have shown that in comparison to the relatively stronger optical signal during an AOE, the rocket and balloon receivers

UT   3:56:56.800 To   3:56:56.900
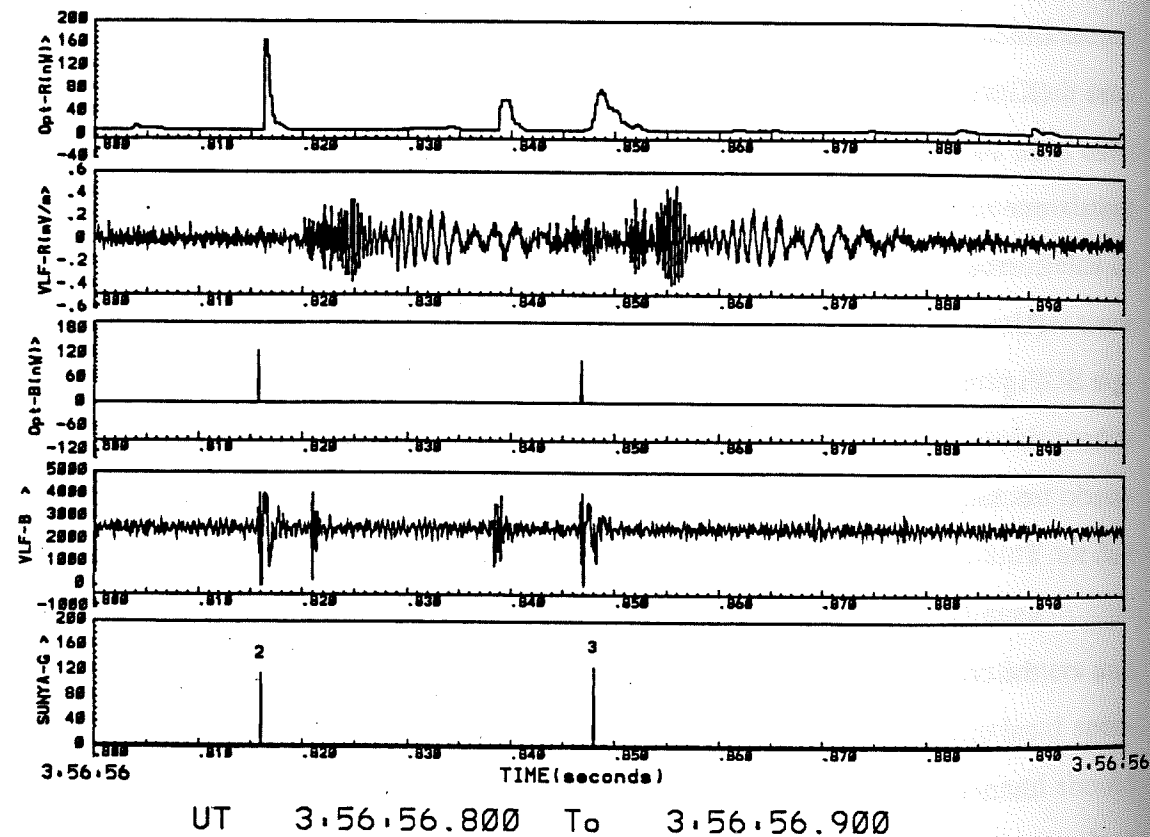
Figure 3.5:   An expanded, 100 msec view with five panels showing optical (Opt-R and Opt-B) and VLF data (VLF-R and VLF-B) from the rocket and balloon. VLF-R shows two of the delayed VLF signal bursts detected at the rocket in response to located strokes in the lightning data (SUNYA-G). Such VLF signatures and the frequency dispersion shown are characteristic of whistler-mode propagation and are expected high in the ionosphere. This same period is indicated by the two left-most arrows under panel D in Figure 5. When comparing previous figures, it is important to note the change to linear optical amplitude scales here and in Figure 3. 7. The time resolution of the Opt-R data is 1/4 msec, that of VLF-R, Opt-B and VLF-B is 1/16 msec. Reactive accuracy and resolution of the SUNY-G data are the same: 1 msec.

always detected VLF radio signals that were relatively weaker than those due to typical lightning strokes. In addition, the weaker, AOE-correlated VLF signals at the high-altitude rocket differ significantly from the temporal evolution and time of arrival of the characteristic VLF signal bursts typically due to a lightning stroke. We now pursue this aspect of the VLF radio observations.

UT   3:56:57.100 To   3:56:57.200
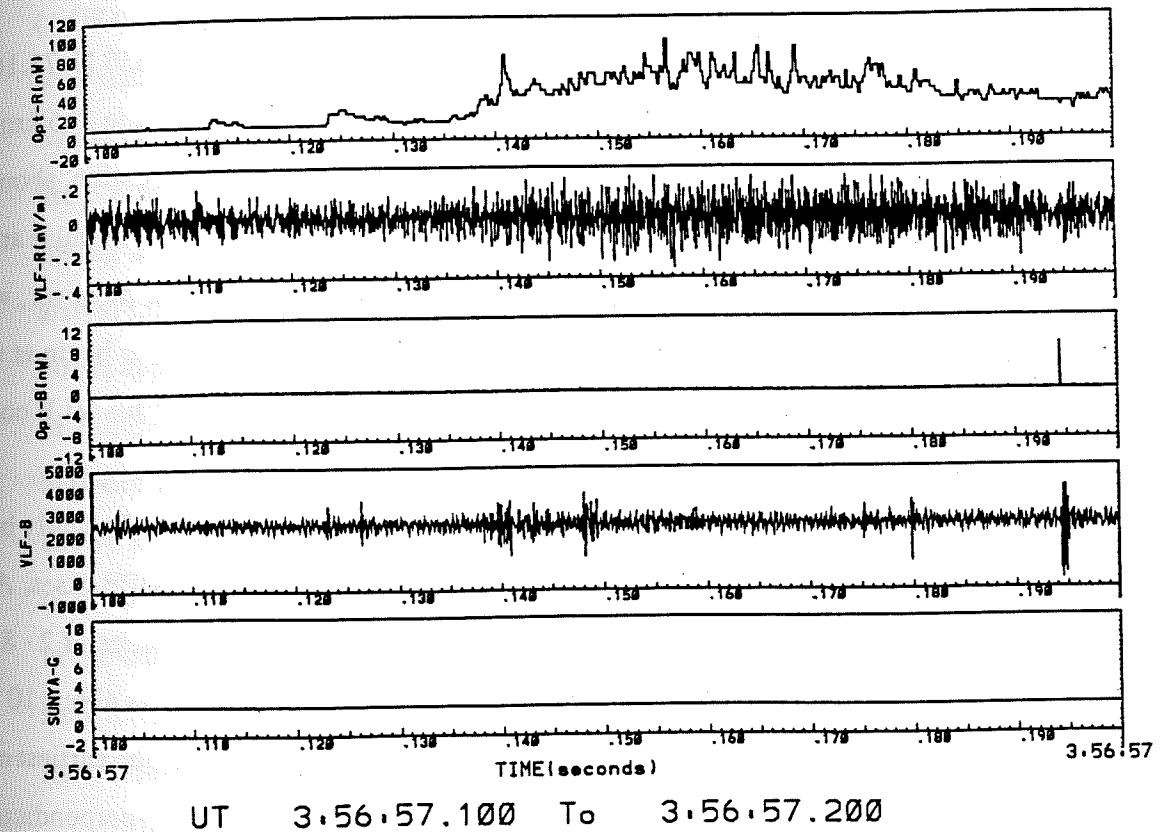
Figure 3.6:   An expanded, 100 msec partial view of an anomalous optical event (AOE) shown in Figure 3.5. All panels here are identical in format to those in Figure 3.5, but more amplitude sensitivity has generally been used to plot these data. Average rocket altitude was 318 km. This same interval is indicated by the two right-most arrows under panel D in Fig.3.5.

In response to most lightning strokes, including those which did not have SUNYA corresponding indications, the rocket detected uniformly delayed VLF signals having a dispersive feature. Such signatures are expected for whistler-mode propagation high in the ionosphere (Maynard et al., 1970). As examples, two

SUNYA-located lightning events which occurred between the two left-most arrows under panel D in Figure 3.4, are shown with high-resolution timing in the 100 msec interval 3:56:56.8 to 3:56:56.9 UT in Figure 3.5. From top to bottom, Figure 3.5 shows five panels with the optical and VLF data from the rocket (Opt-R and VLF-R) and the balloon (Opt-B and VLF-B), as well as the SUNYA lightning data on the ground (SUNYA-G). When comparing with previous figures, it is important to note a change to linear optical amplitude scales here and in Figure 3.6.

SUNYA located the first lightning event in Figure 3.5 at 42.636 N, 71.165 W and the second at 41.002 N, 72.749W. Distances to the rocket (altitude 315 km) and balloon (altitude 31 km) were approximately the same for the first location, about 650 km. Thus, after about 2.2 msec at a nominal 300 km/msec, the optical impulse arrived almost simultaneously at the rocket and the balloon. At the rocket, however, which was high in the ionosphere, the earliest VLF response is observed to begin at about 3:56:56.82 UT, almost 4 msec after the optical impulse. Evidently this VLF component propagated much more slowly at about 650/6.2 = 105 km/msec.

An individual, rocket VLF signal burst like those in Figure 3.5 usually begins with oscillations at a frequency as high as about 24 kHz in these WIPP cases. As the signal evolves, an amplitude peak with periodic oscillations in the range of 2 - 8 kHz, which is the typical range of maximum power density here, appears about 10 msec later, and after about 20 msec, oscillations at about 0.5 kHz appear (the earliest example in Figure 3.5). Since the rocket E-field antennas were maintained perpendicular to the local geomagnetic field line, this frequency dispersion can be taken as typical evidence of transverse whistler-mode signals (Maynard et al., 1970) propagating along a geomagnetic field line to the rocket. The time delay and dispersion of the whistler signal both become much larger as it continues along the geomagnetic field up to much higher altitudes. Other examples of such lightning-generated, dispersive whistler signals detected by rocket VLF receivers have been reported by Kelley et al (1988). Figure 3.5 shows a second case with the 3:56:56.847 UT starting time best defined by the balloon optical impulse, and deeper nulls in the envelope of the evolving VLF sig-

nal burst. Note that the second SUNYA impulse at 3:56:56.848 UT appears to be late by the maximum allowable timing error (1 msec) essentially because the WIPP and the network sample-accumulation time bases were not synchronized.

Dispersive VLF signal bursts were also received at the rocket for other SUNYA lightning located in more distant areas. In comparison with lightning, however, most impulses and continuing emissions in the anomalous optical events (AOEs) were not associated with such apparent whistler-mode signals in the rocket VLF data. As an example, the 3:56:57.1 to 3:56:57.2 UT portion of an AOE indicated by the two right-most arrows under panel D in Figure 3.4 is shown in Figure 3.6. Figure 3.6 has different amplitude scales, but otherwise uses the same high-resolution timing and overall format as Figure 3.5. No obvious component having the delayed arrival time and characteristic temporal evolution of the dispersive rocket VLF signal bursts appears in Figure 3.6. Spectral analysis of the rocket VLF data during the AOE of Figure 3.6 shows that it is only an enhanced band of apparently random noise between about 6 and 8 kHz, with no particularly coherent spectral forms like that shown by Maynard et al. (1970; their Figure 3.5) which indicate the typical whistler or other identifiable dispersion. This type of 6 - 8 kHz AOE noise is relatively weak in the balloon VLF data, perhaps because the balloon receiver had a lower effective sensitivity, or because the vertical alignment of the balloon antenna interacted with more complicated VLF mode or polarization effects (Turtle et al., 1989).

In some AOEs, the rocket occasionally received a few dispersive VLF signals. When there were not corresponding optical signals detected at the balloon or on the ground, it is impossible to tell whether these VLF waves were generated by the components of AOE or individual lightning flashes in other areas. Examples are the VLF bursts seen in the rocket and balloon wave panels (D and F) at 3:58:23.210 and 3:58:23.390 in Figure 3.2. However, it is significant that for many strong optical impulses occurring within an AOE, the rocket still did not detect any obviously dispersive signals. If the AOEs were due to normal lightning flashes, this would be very hard to explain. It also indicates that some relatively strong optical and electromag-

netic radio impulses must have originated independently of any identifiable lightning stroke.

Most SUNYA-located lightning flashes which produced optical impulses in the rocket data were detected optically by the balloon photodiode sensor as well. In the same rocket data, AOEs often appear with relatively larger optical amplitude than typical SUNYA-located and other lightning optical impulses. This means that an AOE source at cloud altitude would have to have an optical power comparable to or greater than that of normal lightning, and that the balloon would be expected to detect such AOE signals nearly as often as they appear with relatively larger amplitude at the rocket. It should be emphasized that in comparison with the rocket photodiode sensor, the photodiode sensor on the balloon showed no significant deficiency in its ability to detect distant lightning located by the SUNYA network, even though the balloon was at much lower altitude. Not only did the balloon payload detect most of the flashes which SUNYA located in regions A and B on the coastline to the northeast of Wallops (Figure 3.1), but also most of the SUNYA-located flashes scattered in other directions. Verification of this sort indicates that the balloon photodiode's normal capability for detecting weak optical impulses from distant lightning was usually or always available operationally, and was not dependent on any special viewing situations (for example, due to moving clouds) that may have been advantageous only occasionally.

This last point can be verified by considering the angular sensitivity function of the balloon sensor. From 31 km altitude, the effective horizon is about 600 km distant, and with the established observing angle of about 84.4° between the horizon and the axis of the aperture normal at the balloon sensor, we can see from Figure 2.1 that for an incident angle of 86°, the normalized sensitivity is about 8×10^{-4}. Based on a minimum detectable optical power of 300 pW, with 8×10^{-4} angular attenuation, the balloon sensor can still detect a source optical power of 4×10^7 kW at a distance of 1000 km. Since the optical power of lightning is often in the range of 10^6 - 10^8 kW or even larger (Christian et al., 1984; Turman, 1977; Turman and Edgar, 1982), the

balloon sensor has enough sensitivity to detect many lightning flashes at cloud altitude more than 600 km distant.

Optical impulses from lightning in region B of Figure 3.1 were apparently 'over the horizon' at the balloon, but were detected nevertheless. This may be explained by the following two facts: (1) lightning flashes can occur at least up to the altitude of cloud tops near the tropopause at 15 km, for which the source altitude effectively extends the true line-of-sight distance from the balloon to more than 1,000 km. (2) Since light from distant sources may be refracted by spatial changes in the atmospheric index, the effective line-of-sight could be extended beyond the horizon by refraction (McCartney, 1976). Nemzek and Winckler (1989) have detected some brief (about 2 msec), isolated optical impulses due to Rayleigh-scattered light, apparently from distant, radio-correlated lightning. Note that these isolated impulses are very different from the long-enduring anomalous optical events (AOEs) being discussed here.

As mentioned previously, the rocket and balloon photodiode sensors often detected lightning-like impulses with no corresponding indication by the SUNYA network. Some of these optical impulses might be due to IC lightning flashes, but without data to specifically distinguish IC flashes from those CG flashes which were missed by the network, it is impossible to establish the rocket and balloon sensors' efficiency for detecting IC flashes. This does not change the fact that the balloon sensor should have detected at least some optical sources in those regions where it detected most of the SUNYA-located CG flashes, provided only that the optical sources, whether IC flashes or not, all had optical power comparable to the average CG flash located by SUNYA.

Of the 23 anomalous optical events (AOEs) identified in our rocket optical photodiode data, 8 events were also detected by the Reticon array imager carried by the rocket. It is possible that the imager missed the other 15 events because its field of view was smaller and its sensitivity and time resolution lower than those of the photodiode sensor. Under the assumption that the anomalous sources occurred at cloud

altitude, locations for the 8 events have been determined from the Reticon data, and are plotted in Figure 3.1. Apparently 5 events occurred in region A and 3 others were still closer to the rocket and the balloon.

All these anomalous sources were within the region for which the balloon detected more than 90% of the SUNYA-located lightning. It should be re-emphasized here that the optical signals of AOEs were always at least as strong as those of typical SUNYA-located CG lightning flashes and other unlocated flashes, which include possible IC flashes, as detected at the rocket. Therefore if the AOEs were due to CG or IC lightning discharges, or any other strong sources within sight of the balloon, at least some of them should have been detected at the balloon. In actuality, however, even though the rocket photodiode sensor recorded about 23 AOEs during the 10 minute WIPP rocket flight, the balloon detected no such events during 5 hours of flight. Furthermore, no AOEs of the WIPP type, nor any similarly anomalous optical signature were ever detected by a balloon photodiode sensor on any of five other flights, each conducted under similar experimental conditions and typically 30 times longer than the WIPP rocket flight (two balloon flights in 1988 are included).

Although it cannot be ruled out completely, it is extremely unlikely that all of the balloon photodiode sensors somehow failed to detect all such anomalous optical sources occurring beneath them, even though such sources appeared to have strong optical power. Responses that are excluded so definitively from detection at the balloons suggest, most simply, the possibility that the anomalous optical sources were all located above the balloon sensors, that is, primarily above 30 km altitude.

There are several natural optical phenomena which occur at altitudes over 30 km in the mid-latitude atmosphere. Meteors, for example, can emit light in an altitude range of tens to hundreds of km. It is typical for an emission of meteor light to begin smoothly, increase to a maximum in about 1 sec, and then drop abruptly to zero (Jacchia, 1949). Although brief, explosive increases of light emission occur for some meteors, such flaring usually appears only occasionally during a meteor's fall. These are meteor optical features which do not resemble those of the WIPP rocket AOEs.

Moreover, the flaring of meteors always occurs below 100 km (Jacchia, 1949), and if we assume an anomalous source like the example in Figure 3.3 to be located at 100 km, then the altitude, viewing angle and image data of the Reticon imager give a source dimension on the order of tens of kilometers. This is much larger than the typical value of a few hundred meters for the luminous gas cloud of a meteor (Heide, 1957). Also, we are unaware of any evidence or mechanism suggesting that meteors could produce the clusters of impulses and other VLF radio noise correlated with significant components in all of the AOEs. We conclude, therefore, that the anomalous optical events do not seem to be due to meteors. Bursts of energetic electrons precipitating from the magnetosphere into the mid-latitude atmosphere can be a dominant ionization source at night in the altitude region near 80 km (Vampola and Gorney, 1983). Such particles can produce measurable amounts of light above balloon altitude. Optical power incident on the rocket photodiode from such a source can be calculated. Let us take 10^{-3}erg/cm^2 (Voss et al., 1984) as the energy flux of precipitating electrons, a factor of 10^{-3} as the efficiency of converting particle energy to optical wavelengths for an auroral case (Omholt, 1971), a deposition altitude of 80 km (Vampola and Gorney, 1983), and a target region of several tens of km as estimated from the Reticon imager data above. These values give an optical power due to a burst of precipitating electrons that is smaller by a few orders of magnitude than the optical power detected by the rocket sensor for an AOE component of duration equivalent to that of the burst. Particle precipitation therefore seems unable to account for the amplitude of the AOEs, and so precipitation does not seem to be a very likely source.

It is also important to note that the observed properties of the WIPP anomalous optical events (AOEs) do not resemble those of night-time airglow (Hargreaves, 1979) or those of fast atmospheric light pulsations (Ögelman,1973; Tümer, 1982).

The mean value of the albedo for clouds of various types and thickness is 0.50 - 0.55 (Robinson, 1966).For very bright optical sources at high altitude above the balloon, one could imagine that the balloon detectors might have detected some reflections from the cloud tops. Since no such signature of the AOEs has been identi-

fied in the balloon data, it may be that the AOEs are actually weak optical sources even though they appear to be strong in comparison with normal lightning in the rocket data. If AOEs are due to the high altitude sources, the apparent intensity at the rocket could be relatively stronger while, in fact, the optical power was weaker than that of the normal lightning near the ground. This is consistent with there having been no ground based observations which have the signature and characteristics of AOEs.

Their unique optical signatures and the highly-correlated VLF radio signatures all suggest that the anomalous events we are concerned with here may be related to some kind of discharge process. Our observations show that this proposed discharge process apparently is one that is not often associated with whistler-mode VLF signal bursts like those which propagate up a geomagnetic field line to the rocket in association with normal lightning. Since there is the possibility of a correlation between some of the subionospheric VLF signal amplitude changes (Trimpi events) seen on the ground at Wallops and some of the AOEs, some of the latter are perhaps accompanied by simultaneous perturbations of the in situ electron concentration or distribution at high altitudes in the atmosphere or lower ionosphere. This could also suggest a discharge.

Several writers have mentioned the possible existence of high-altitude discharges, that is, long discharges sometimes reaching upward from the top of the troposphere toward the bottom of the ionosphere (Wilson, 1925; Boys, 1926; Chalmers, 1949). Some evidence which may indicate this type of discharge process has been reported by Rumi(1957) in the form of numerous, unusually sudden and otherwise anomalous VHF radar echoes. More recently, Armstrong (1987, 1988) has found reason to suggest that such upward or high-altitude discharges may play a role in triggering the source discharges of some whistlers that are observed to be synchronized. In this context, the anomalous optical events (AOEs) observed by the WIPP rocket photodiode sensor, which have signatures very different from those of other optical sources reported previously, might be further evidence for high-altitude discharges.

3.4 CONCLUSIONS

1. Twenty three anomalous optical events (AOEs) were detected by a rocket-borne optical photodiode sensor in the WIPP campaign. These events have optical and radio signatures which imply that they might not be due to normal lightning, or to some other previously reported optical phenomenon in the atmosphere.

2. The AOEs were not detected by any balloon-borne optical photodiode sensor, a fact which is consistent with their occurrence above balloon altitude (30 km).

3. The AOEs were caused by localized sources and are always associated with characteristic, broad-band VLF noise and other impulsive signals. If amplified, these 'atmospherics' produce abnormal sizzling sounds in audio system. Their apparently anomalous optical power and the form of their temporal evolution suggest that the AOEs might be related to a discharge process.No apparent whistler-mode VLF bursts were detected at the rocket in association with most optical impulses in the AOEs, unlike the case of lightning strokes which normally did produce the characteristic whistler-mode bursts.

4. Since an AOE sometimes seems to have an association with a subionospheric VLF signal perturbation (Trimpi event), AOEs might sometimes be linked to a disturbance of the electron concentration in the high-altitude atmosphere or lower ionosphere.

While AOEs of this type are difficult to locate at any specific altitude, we conclude that they provide consistent evidence that high-altitude discharges occur much more frequently than previous research has suggested.

CHAPTER 4

THE CORRELATION BETWEEN THE AMPLITUDE OF LIGHTNING-GENERATED VLF WAVES IN THE IONOSPHERE AND THE SUNYA LIGHTNING CURRENT INTENSITY

4.1 INTRODUCTION

Lightning-radiated fields in the earth-ionosphere waveguide have been actively studied for decades (Kimpara, 1963; Pierce, 1977; Nanevicz et al., 1990; Boulch and Weidman, 1990). In the fields radiated from cloud-to-ground lightning flashes, the principal energy in the very-low-frequency (VLF) range is produced by the lightning return strokes (Kimpara, 1963). Generally, return strokes dominate the lightning-radiated fields up to a frequency at 300 kHz (Pierce, 1977). A small fraction of the VLF energy generated by lightning strokes can couple into the whistler-mode waves at the lower boundary of the ionosphere and propagate through the ionosphere. These whistler-mode waves can grow in amplitude through interaction with magnetospheric particles and return to the atmosphere as whistlers (Kennel and Petschek, 1966; Etcheto et al., 1973; Helliwell, 1967).

Strong cloud-to-ground lightning strokes usually bring a large amount of electric charges to earth and have strong electric current intensity in their return strokes (Uman, 1987). In the early studies of lightning-associated phenomena, the relative strength of lightning flashes was normally determined by the peak electric field in the atmospherics generated by the flashes (Norinder and Knudsen, 1959; Helliwell et al., 1958). In the last decade, a lightning detection network, SUNYA network, was developed in the eastern United States (Orville et al., 1983, 1987). Lightning-generated signals are received by crossed loop antennas of this network and processed to give information on the first stroke peak magnetic field, multiplicity of strokes within the flash, and flash location (Orville et al., 1983). A peak current for the first return stroke of each lightning flash is then calculated from the measurements

of the magnetic field (Orville et al., 1987). This lightning current intensity determined by the SUNYA network was in good agreement with that determined by other direct peak current measurements (Henderson et al., 1988).

The relations between lightning and whistlers have been studied by some workers. It was found that the lightning strokes with relatively higher energy content were more likely to be whistler sources (Norinder and Knudsen, 1959; Helliwell et al., 1958). In a case study, a linear relation was found between whistler amplitude in the 4 to 6 kHz range and the amplitude of lightning radiated field in the same frequency interval (Weidman et al., 1983). A linear relation between lightning intensity and the two-hop whistler amplitude over part of the whistler frequency range was also found by Carpenter and Orville (1989). These observations implied that stronger lightning strokes would inject stronger VLF waves into the ionosphere. However, in comparison with lightning-generated VLF waves in the earth-ionosphere waveguide (i.e. spherics), much less studies have been conducted on the lightning-generated VLF wave in the ionosphere. Thus far there have been no reports on the relation between the lightning current intensity and the amplitude of lightning-generated VLF waves in the ionosphere.

In the WIPP and Thunderstorm II campaigns, the amplitudes of VLF waves generated by hundreds of cloud-to-ground lightning flashes were measured in the ionosphere by rockets (see Chapter 2). The current intensities of these lightning flashes were also measured by the SUNYA lightning network. These measurements provide us with a good opportunity to investigate the relation between lightning current and the amplitude of lightning-injected VLF waves in the ionosphere.

In this chapter, we performed a Fast Fourier Transformation (FFT) on the VLF wave packets received by the WIPP and Thunderstorm II rockets and obtained some spectra of lightning-generated VLF waves in the ionosphere. With these spectra, we investigated the linear correlations between the SUNYA lightning current and the wave amplitude at each frequency. Our goal in this chapter is to answer the

following questions.

1) Do lightning flashes with stronger current measured on the ground always produce stronger VLF waves in the ionosphere? What frequency components of lightning-generated VLF waves in the ionosphere have most significant response to the lightning current? These questions have not been previously answered.

2) Can the lightning current measured by the SUNYA network be used to normalize the amplitude of lightning-generated VLF waves in the ionosphere? In some of our other studies, we need to organize the data to eliminate the effect of source strength on the amplitude of waves in the ionosphere. The SUNYA current was the only available measurement of the strength of lighting flashes, so it is important for us to know how effectively the SUNYA current can be used to normalize the wave amplitude.

4.2 DATA ANALYSIS

To study the frequency spectrum of lightning-generated VLF waves in the ionosphere, a Fast Fourier Transformation (FFT) was performed on more than one hundred lightning-generated VLF wave packets received at the WIPP and Thunderstorm II rockets. In many cases, the wave packets received by the rockets from different strokes were overlapping. It is not convenient to separate the wave spectra contributed by different sources. Therefore, we selected only those "clean" wave packets which did not have obvious overlap with others.

So that all the spectra have the same frequency resolution, an identical data sequence length should be used to perform the FFT for all the wave packets. For the WIPP data, this would require the data sequence to be as long as 60 ms, which was about the length of VLF wave packets received at the rocket apogee. However, using a fixed data sequence length would exclude some clean wave packets received at lower altitudes. This is because in many cases clean wave packets were so close to other waves that a fixed data sequence length would include other unwanted waves.

To select as many clean wave packets as possible, we took the data sequence length to be the length of each wave packet, then padded the data sequence with constants to a standard length before performing the FFT. The standard sequence lengths for the WIPP and Thunderstorm II data were chosen to be 60 ms (3840 points) and 20 ms (400 points) respectively.

The addition of padding constants affects the spectrum amplitude from the FFT. To compare different spectra, an amplitude compensation factor, which is related to the length of the padded sequence, must be applied to the FFT output. Normally, the amplitude compensation factor is $(N+M)/N$, where N and M are the lengths of the data sequence and the padded sequence respectively (Brault et. al, 1971). When a numerical window is applied in the FFT, however, the compensation factor may be different from $(N+M)/N$ (see Appendix B). In our case, we performed the FFT on simulated data sequences with different padded lengths. Comparing the input and output from the FFT, the compensation factors for different padded lengths were calculated. These calculated compensation factors were then applied to the spectrum of each wave packet. The calculated compensation factors are given in Appendix B.

The frequency spectra of 153 and 227 VLF wave packets received by the WIPP and Thunderstorm II rockets, respectively, were obtained. From these spectra, we can investigate the effect of the lightning current intensity on the amplitude of the waves at each frequency. To see this effect, other factors which could also affect the wave amplitude measured by the rockets must be considered.

The waves generated by lightning usually have propagated in the earth-ionosphere waveguide over a certain distance before entering the ionosphere (Helliwell,1965).The wave amplitude in the ionosphere is related to wave propagation in the earth-ionosphere waveguide. This effect depends on the orientation of the path, the earth surface topography, the ionospheric boundary conditions and other waveguide conditions (Alpert, 1967; Wait, 1986).To reduce the differences in

these waveguide propagation effects, we divided the wave packets into groups according to their geographic locations. We assumed that the waveguide effect was identical for the waves from a localized area which had a scale size much smaller than the wave propagation distance. Three groups of waves from three localized areas (one from WIPP and two from Thunderstorm II respectively) were then studied individually.

The VLF waves are subjected to attenuation in the ionosphere due to the collisions between the electrons and neutral particles. This attenuation is strongest at altitudes below 120 km, where there is a large population of neutral particles and the collision frequencies are higher (see Chapter 7). Above 200 km, the wave attenuation is not significant and can be ignored. The amplitude of waves received by the rockets is also related to the refractive index in the local ionospheric medium. The refractive index of VLF waves changes greatly with altitude in the ionosphere. Because the selected wave packets were received at different altitudes, the effect of the change in refractive index on wave amplitude has to be taken into account.

The average Poynting flux of a harmonic electromagnetic wave is (Jackson, 1962)

$$S = \frac{1}{2\mu} E \times B^*,$$ (4.1)

where E is the amplitude of the wave's electric field, B^* is the conjugate of the wave's magnetic field, S is the Poynting flux of the wave, μ is the magnetic permeability. In a medium with a refractive index n, we have

$$B = nE/c ,$$ (4.2)

where c is the speed of light. For parallel propagation, equations (4.1) and (4.2) give

$$E = (\frac{2\mu c S}{n})^{1/2} .$$ (4.3)

The wave refractive index can be approximately calculated using the Appleton-

Hartree formula in the magnetoionic theory (Budden, 1985). Under a quasi-longitudinal condition, which is usually valid for VLF waves at altitudes above 150 km (Helliwell, 1965), the refractive index can be approximated as

$$n(z) = \omega_{pe}(z) \, (\omega_{ce}(z) \, \omega)^{-1/2} ,$$ (4.4)

where ω_{ce} is the electron cyclotron-frequency, ω_{pe} is the plasma frequency, ω is the wave frequency and z is the altitude. Using equations (4.3) and (4.4), we get

$$E(z) = (\frac{A\omega B(z)}{n_e(z)})^{1/4} ,$$ (4.5)

where n_e is the electron density, B is the geomagnetic field and $A = (\mu^2 S^2 c)/\pi$. Assuming there is no wave energy loss in the ionosphere, A can be considered approximately constant with altitude.

In order to account the effect of refractive index changes, we have used equation (4.5) and an ionospheric electron density profile to normalize the amplitude of waves received at different altitudes. The electron density profile used was calculated from an International Reference Ionospheric model, which, shown in Figure 1.1, was very close to the electron density profile measured by a companion rocket during the WIPP campaign.

4.3 RESULTS

The sampling rate of the wave data from the Thunderstorm II rocket was 10 kHz, so that frequency components of the waves from 0 to 5 kHz could be investigated. During the Thunderstorm II rocket flight, two active lightning cells were located by the SUNYA network within a range of several hundred kilometers from the rocket. Figure 4.1 shows the source location of these waves received by the rocket at altitudes between 200 km and 333 km. Twenty two wave packets generated by lightning in the area labeled B in the figure were selected in our study. From this wave group, we calculated the linear correlation coefficients between the lightning current

intensity recorded by the SUNYA network and the wave amplitude for 100 frequency components from 0 to 5 kHz. The result is shown in Figure 4.2.

The two dashed lines in Figure 4.2 represent the 99% and 95% confidence levels. It is seen in this figure that the correlation coefficients at frequencies from 0.2 to 2.5 kHz are mostly higher than the 99% confidence level. From 2.5 to 5 kHz, the correlation between the wave amplitude and the SUNYA current appears to be relatively weaker, but are still significant at most of the frequencies. For this lightning group, the wave amplitude in the ionosphere apparently has a significant linear responses to the SUNYA lightning current at most of the frequencies from 0 to 5 kHz.

The positive correlation between the lightning current intensity and the wave
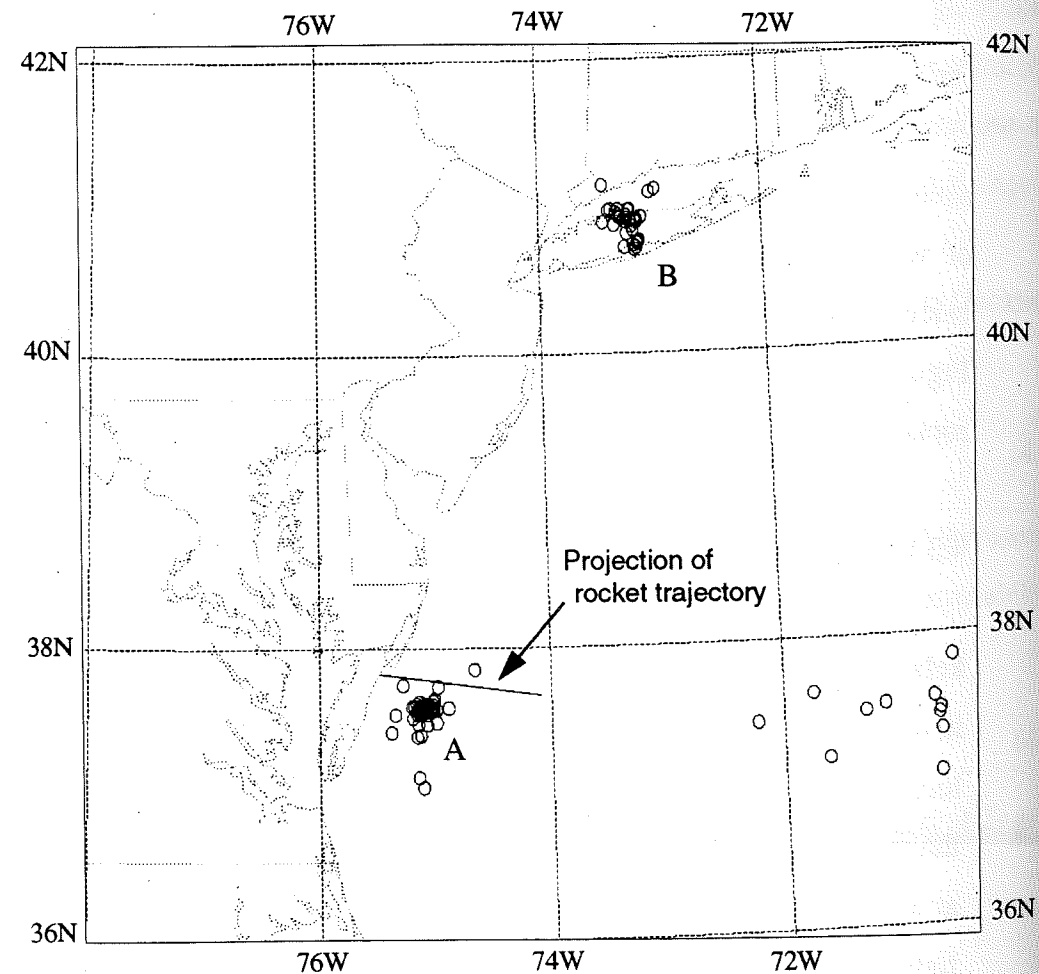

Figure 4.1: The source location of VLF waves received by the Thunderstorm II rocket at altitudes between 200 km and 333 km
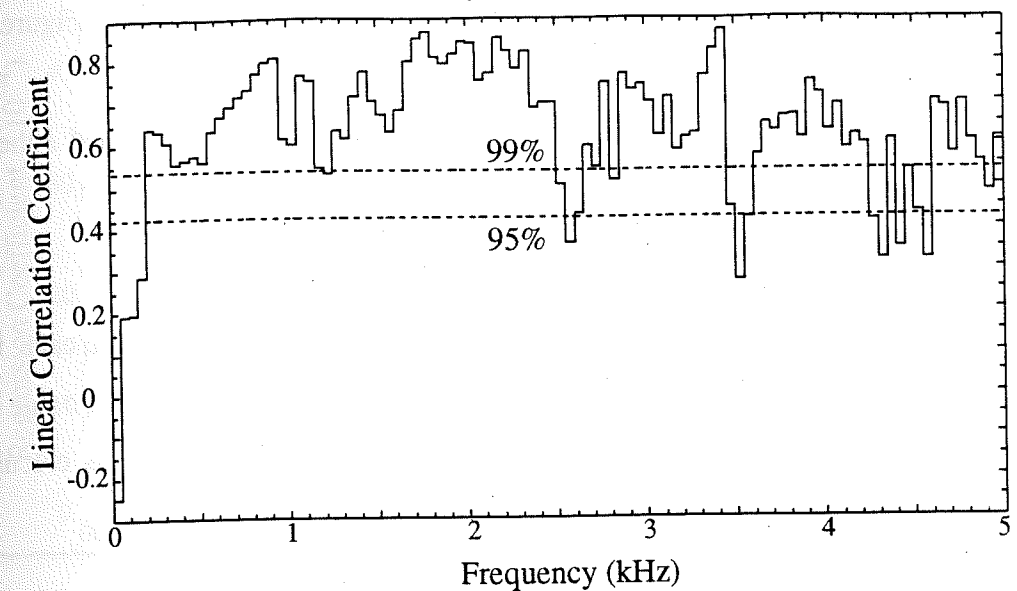
Figure 4.2: Linear correlation coefficients between the amplitude of lightning-generated VLF waves and the lightning current intensity measured by the SUNYA network. 22 lightning events in area B (see Figure 4.1) were selected in the calculation. The two dash lines indicate the 99% and 95% confidence levels.

amplitude can be directly seen from the data. As examples, in Figure 4.3, we plot the SUNYA lightning current intensities versus the amplitude of waves at four frequencies (1.0, 2.0, 3.4, and 4.6 kHz). Each point in this figure represents the wave amplitude recorded by the rocket from a single lightning event as a function of the lightning current intensity recorded by the SUNYA network. The electromagnetic radiations from lightning strokes are not only related to the strength of the strokes, but also the characteristics of the discharge channels (Newman, 1958). This, in addition to other possible wave propagation effects, might have caused the divergence of the data points in Figure 4.3. Nevertheless, a positive linear relation between the wave amplitude and the SUNYA lightning current intensity can still be clearly seen in the figure.

For this lightning group, the linear correlation between the wave amplitude and the SUNYA lightning current intensity is generally above the 99% confidence level at frequencies from 0 to 5 kHz (figure 4.1). It is therefore possible to fit the graph

of wave amplitude versus SUNYA current intensity (as shown in Figure 4.2) to a straight line by the least-squares method.

Let E_k be the amplitude of the kth frequency component and I the SUNYA lightning current intensity. The equation of the straight line fit is

$$E_k = a_k + b_k I \,,$$

where a_k and b_k are determined by the least-square method for each frequency component. The regression coefficient b_k in the equation indicates the rate of change of the wave amplitude with the lightning current intensity. We calculated this

Figure 4.4: Regression coefficient of the amplitude of VLF waves in the ionosphere and the SUNYA current intensity. 100 frequency components from 0 to 5 kHz are calculated. The result shown has been smoothed by using a 7-point running average along the frequency
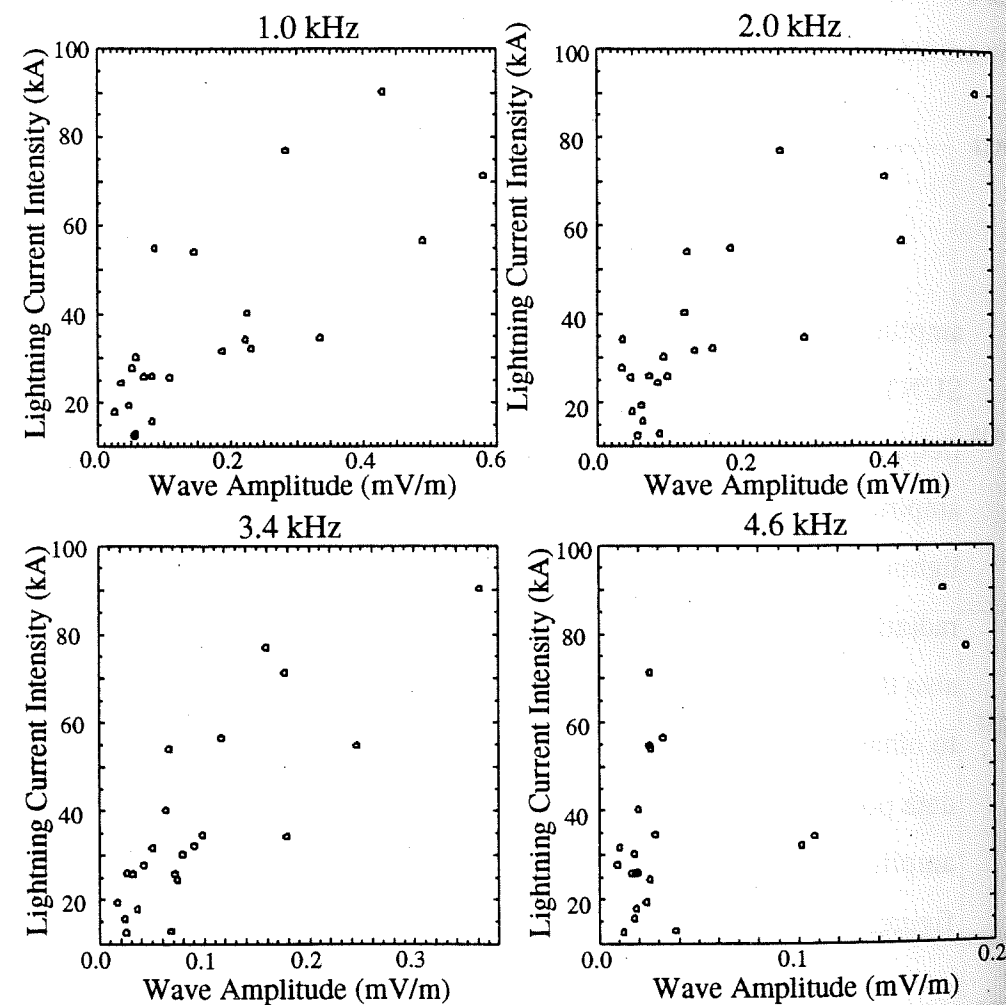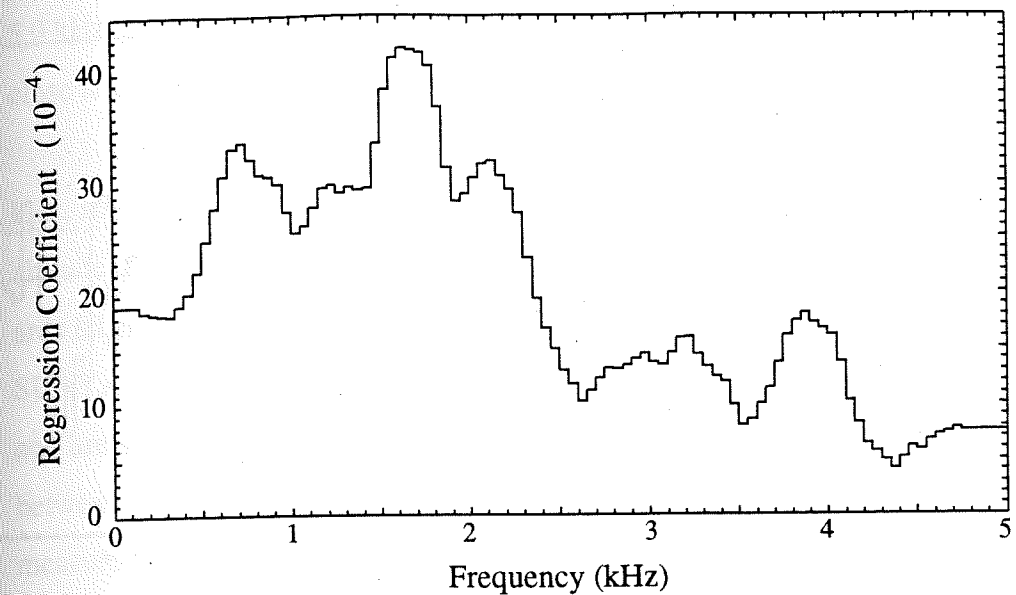

Figure 4.3: The relation between the amplitude of lightning-generated VLF waves in the ionosphere and the intensity of lightning current intensity detected by the SUNYA network. Four frequency components at 1.0, 2.0 3.4 and 4.6 kHz are shown

regression coefficient for 100 frequency components between 0 to 5 kHz. The result, which has been smoothed by conducting a 7-point running average along the frequency, is shown in Figure 4.4. It is seen from the figure that the rate of change of VLF wave amplitude with lightning current intensity peaked at a frequency between 1.5 kHz and 2.0 kHz. The rate of change at frequencies below 2.5 kHz is higher than that at higher frequencies. This indicates that frequency components below 2.5 kHz of lightning-generated waves in the ionosphere have more significant response to the lightning current measured by the SUNYA network.

With the same configuration as that of Figure 4.2, Figure 4.5 shows the linear correlation coefficients calculated from another wave group. This group includes 36 wave packets generated by lightning strokes located almost directly below the Thunderstorm II rocket (area A in Figure 4.1). These waves were also received at altitudes from 200 km to 333 km. For this group of lightning, the linear correlation between the wave amplitude and the SUNYA current intensity is above the 99% confidence level at most of the frequencies between 0.2 to 2.5 kHz. From 2.5 kHz to
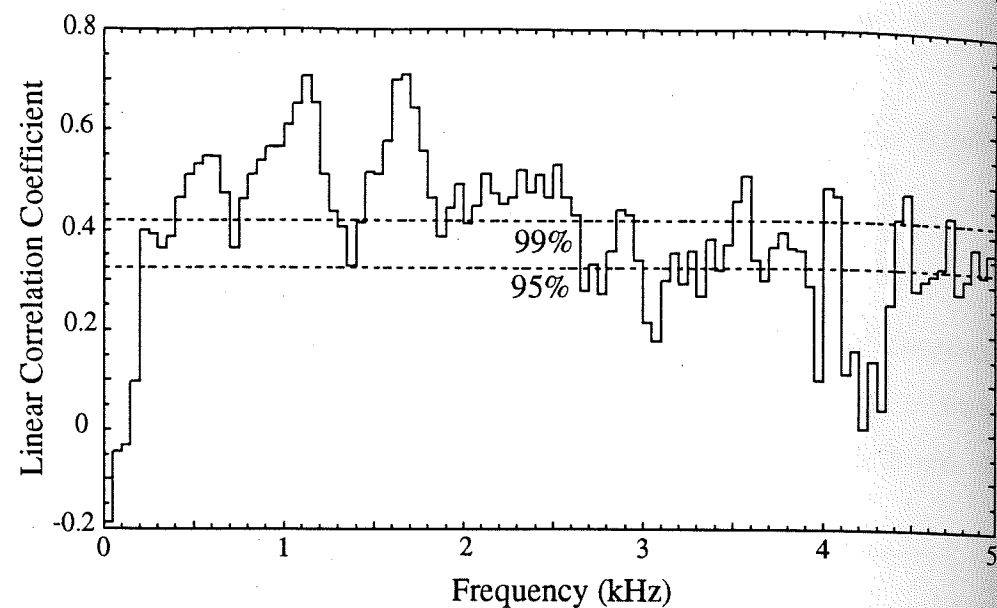
Figure 4.5   Linear correlation coefficients between the amplitude of VLF waves and the lightning current intensity measured by the SUNYA network. 36 lightning events in area A (see Figure 4.1) were selected in the calculation. The dash lines indicate the 99% and 95% confidence levels
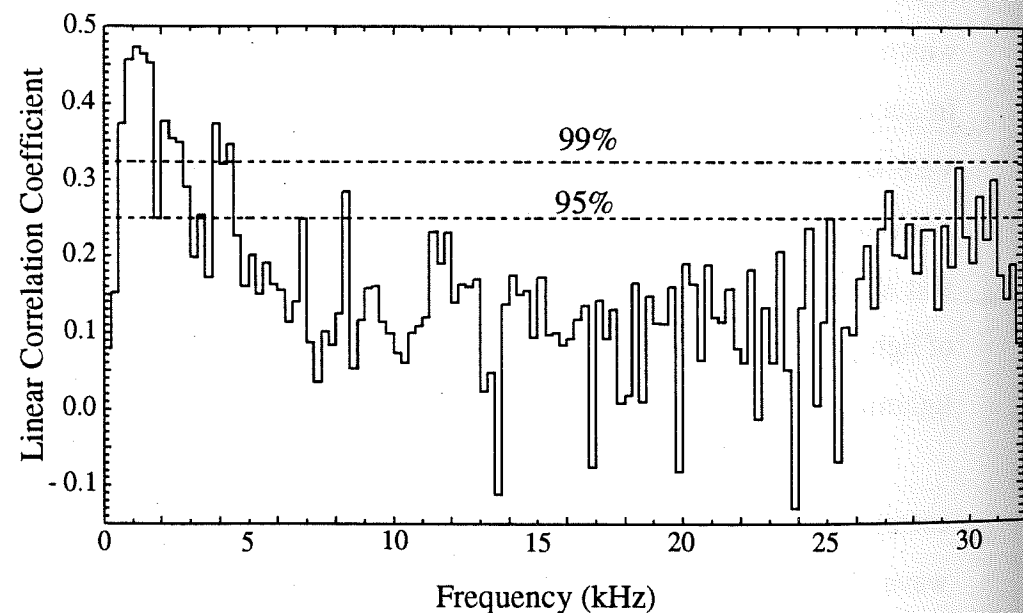

Figure 4.6   Linear correlation coefficients between the amplitude of lightning-generated VLF waves in the ionosphere and the intensity of lightning discharge current detected by SUNYA network. 128 frequency components from 0 to 32 kHz are calculated. The dash lines indicate the 99% and 95% confidence levels.

5.0 kHz, the correlation becomes relatively weaker but are still mostly higher than or close to the 95% level.

The sampling rate of the VLF measurements from the WIPP rocket was 64 kHz, so the wave amplitude at frequencies from 0 to 32 kHz were investigated. At altitudes from 200 km to 430 km, the WIPP rocket received 63 wave packets from the area labeled A in Figure 3.1 (Chapter 3). The linear correlation coefficients between SUNYA current and wave amplitude for 128 frequency components were calculated and are shown in Figure 4.6. From Figure 4.6, it is seen that the linear correlation between the SUNYA lightning current intensity and the VLF wave amplitude measured in the ionosphere is most significant in the frequency region from 0 to 2.5 kHz. In this frequency range, the correlation coefficients are higher than the 99% confidence level at most frequencies. From 2.5 to 5.0 kHz, the correlation becomes relatively weaker but is still mostly higher than or close to the 95% confidence level. These results are basically consistent with the results obtained from the Thunderstorm II rocket. Above 5 kHz, the correlation became significantly weaker, much lower than the 95% confidence level at most of the frequencies. This indicated that there was not a significant linear relation between the lightning current and wave amplitude at frequencies above 5 kHz.

4.4 DISCUSSION

Our statistical study shows that at frequencies below 2.5 kHz the amplitude of lightning-generated VLF waves in the ionosphere is linearly related to the lightning current intensity measured by the SUNYA network. The significance of this linear relation tends to decrease with frequency. At frequencies from 2.5 kHz to 5.0 kHz, the linear relation between the wave amplitude and the lightning current becomes relatively weaker, but is still significant (higher than or close to the 95% confidence level). At frequencies above 5 kHz, the amplitude of lightning-generated waves does not have a significant linear relation with the lightning current. In this frequency

range, the lightning c[...]tion for the strength of lightning radiated fields in the ionosphere.

It is known that the radiation from a lightning stroke is not only related to the strength of the discharge current but also to the characteristics of the discharge channel (Newman, 1958). Because the lightning discharge channel is generally unique for each lightning stroke, strokes with the same current intensity may produce different frequency spectra. For all the three lightning groups we studied, the linear correlation between the lightning current and the wave components below 2.5 kHz are all higher than the 99% confidence level. This may suggest that the characteristics of lightning discharge channels have little effect on lightning radiations at frequencies below 2.5 kHz.

As seen from Figure 4.2 and 4.5, the linear correlation coefficients we calculated from the two wave groups received by the Thunderstorm II rocket during the same time period are different. The amplitude of waves from a more distant area has a better linear relations to the SUNYA current in comparison with these waves from a area directly below the rocket. This is especially true at frequencies from 2.5 to 5.0 kHz. The difference between the results from the two lightning groups may be caused by different discharge conditions in the two thunderstorm areas. It may, however, also be caused by the heating of the ionosphere by lightning-generated VLF waves.

Lightning-generated VLF waves are subject to strong absorption in the lower ionosphere due to collisions between electrons and neutral particles. This absorption increases with the wave frequency. In Chapter 7, we will show that the frequency-dependence of VLF wave absorptions becomes more significant when the collision frequency between the electrons and neutral particles increases. The increase in collision frequency, however, will occur when the ionospheric media is heated by absorbing wave energy. When VLF waves propagate in the ionospheric medium, a fraction of wave energy would be absorbed by the medium. This absorbed energy

would increase the collision frequency in the local medium, which, in turn, would enhance the absorption in the region. This non-linear effect increases with the frequency and amplitude of the waves. This means that stronger waves are subject to more energy losses at higher frequencies in the lower ionosphere (see Chapter 7).

The different linear correlation between the wave amplitude and the lightning current calculated from the two lightning groups may be explained as follows. These VLF waves from the area directly below the rocket are generally stronger and would heat the lower ionosphere more significantly. Therefore, the amplitude of these waves would be affected more greatly by the non-linear effect of wave absorption in comparison with these wave from the distant area.

4.5 CONCLUSION

The correlation between the amplitude of lightning-generated VLF waves in the ionosphere and the lightning current intensity measured by SUNYA network has been investigated. We have obtained the following conclusions.

1) At frequencies lower than 5 kHz, the amplitude of lightning-generated waves in the ionosphere has a linear positive correlation with the lightning current intensity measured by SUNYA network. This means that a cloud-to-ground lightning with stronger SUNYA current usually launches stronger VLF waves into the ionosphere at frequencies lower than 5 kHz. In this frequency range, the SUNYA current intensity can be used to linearly normalize the amplitude of lighting-generated waves in the ionosphere.

2) At frequencies higher than 5 kHz, the lightning-generated waves in the ionosphere do not have significant linear responses with the SUNYA lightning current. In this frequency range, the SUNYA current intensity is not a good indication of the amplitude of VLF waves in the ionosphere.

3) For all the three lightning groups we studied, the linear correlation between the SUNYA current and the wave amplitude are higher than the 99% confidence level

at frequencies below 2.5 kHz. This suggests that lightning generated waves at frequencies below 2.5 kHz may be mainly determined by lightning current and essentially independent of detailed characteristics of the lightning discharge channels.

4) The correlations between the SUNYA lightning current and the wave amplitude calculated from waves from a more distant area has a better linear relation to the SUNYA current in comparison with these waves from a area directly below the rocket. This may suggest a significant heating of the ionosphere by these waves from the area directly below the rocket.

5) The frequency components between 1.5 kHz and 2.5 kHz in lightning-generated VLF waves in the ionosphere have most significant response to the lighting current measured by the SUNYA network.

CHAPTER 5

THE PROPAGATION PATH AND THE GENERATION MECHANISM OF THE VLF WAVES RECEIVED IN THE IONOSPHERE

5.1 INTRODUCTION

The electric and magnetic fields produced by lightning strokes have three components: electrostatic, inductive and radiative. The electrostatic field is caused by the change of the net electric charge in thunder clouds during the process of lightning discharges. This field roughly varies with r^{-3}, where r is the distance from the source. The inductive field is produced directly by the current in the lightning discharge channel. The change of this field with horizontal range is roughly proportional to r^{-2}. Normally, both the electrostatic field and the inductive field are called the near field of lightning discharges. The radiative field of lightning is generated by the time differential of the current (dI/dt) in the discharge channel. With a geometric factor proportional to r^{-1}, the radiative field can propagate over much greater distances than the other two fields (Lin et al., 1979, 1980, Master et al.,1981).

As we mentioned earlier, the radiative field of lightning can propagate in the earth-ionosphere waveguide with different modes. In the standard whistler generation mechanism, generally called the "leaky waveguide" mechanism, a small fraction of the wave energy in the waveguide can leak into the ionosphere and couple into whistler-mode waves at the base of the ionosphere. The refractive index increases with altitude in the ionosphere, the wave normal of these waves injected into the ionosphere will quickly change to the vertical direction (Helliwell, 1965). It is predicted, therefore, that the VLF waves will propagate nearly vertically and will be confined in small regions in the ionosphere. However, thus far there have not been any direct in situ measurements of the propagation path of VLF waves from a source to a receiver in the ionosphere.

The radiative field of lightning has been usually considered as the only source

of lightning-generated whistler waves in the ionosphere. In 1985, another whistler generation mechanism was proposed after strong transient electric fields were observed in the ionosphere (Kelley et al., 1985). In this mechanism, the area of the ionosphere above an active thunderstorm is regarded as an "aperture antenna", with the spatial and temporal variations in electric fields (or current) prescribed by the penetrating transient fields from a lightning discharge. This aperture antenna generates whistler-mode waves at a variety of wave normal angles in the ionosphere (Kelley et al, 1985, Siefering, 1987). Studies have shown that the large transient electric field in the ionosphere is caused by the electrostatic fields generated by lightning (Siefering, 1987). In the aperture antenna mechanism, lightning produces whistler-mode waves in the ionosphere by its near fields instead of by its propagating radiative fields.

The propagation paths of VLF waves from sources to rockets in the two whistler-generation mechanisms generally represent two extreme paths. In the "leaky waveguide" mechanism, the waves propagate in the earth-ionosphere waveguide and couple into whistler-mode waves from below the rocket. In the "aperture antenna" mechanism, the whistler-mode waves are generated in an area of the ionosphere over the lightning discharge and propagate to the rocket through the ionospheric media. The actual path of VLF waves may be between these two extreme paths. Since waves travel much faster in the earth-ionosphere waveguide than in the ionosphere, the propagation time along the two different paths can be significantly different. One can therefore distinguish the propagation paths of waves by their propagation time.

During the WIPP and Thunderstorm II campaigns, both the optical signals and VLF waves generated by lightning strokes were measured by the rockets. Knowing the time of the optical signals and the location of the source, we were able to determine the propagation time of the waves received by the rockets. In this chapter, using the propagation time of the VLF waves received by the rocket, we will show that these waves were injected into the ionosphere in a local area almost directly below the rocket. This is the first direct evidence from the in situ measurement that

the typical lightning-generated whistler waves received by the rocket were generated by the leaky waveguide mechanism. The possible paths of the VLF waves generated in the aperture antenna mechanism will also be investigated in this chapter.

5.2 DETERMINATION OF WAVE PROPAGATION TIMES

The lightning-generated VLF wave packets received by the rockets are made up of different frequency components which are received at different times due to dispersion. Therefore, the propagation time of waves is related to their individual frequency components. To determine the propagation time of waves at a particular frequency, it is necessary to determine the received time of the particular frequency in the VLF wave packet. However, in this study we only need the characteristic received time for each wave packet in order to compare the propagation times of waves from different sources. As long as the characteristic receiving time for each wave packet is determined using the same identical method, we will not need to know the particular frequency corresponding to the arrival time being determined.

To determine an arrival time for the waves received by the WIPP rocket, we took an FFT every msec in the data sequence for each wave packet. The sampling rate of the WIPP VLF electric field data was 64 kHz. The spectra obtained gave the amplitude of 32 frequency components from 1 kHz to 32 kHz. The arrival times of these frequency components were taken to be when their amplitudes were at a maximum in the spectrum. The resolution of the arrival times of waves determined by this method was 1 ms.

The arrival time of waves received by the thunderstorm II rocket was determined using a different method. A five point running average of the data was taken. Each of the 5 points was considered as positive or negative depending on whether its value was greater or smaller than the average value. The characteristic arrival time of a wave was determined as the earliest time when five data points had opposite signs in the 5-point sequence. A diagram of this method is shown in Figure 5.1. The sampling rate of the wave data from the Thunderstorm II rocket was 10 kHz.
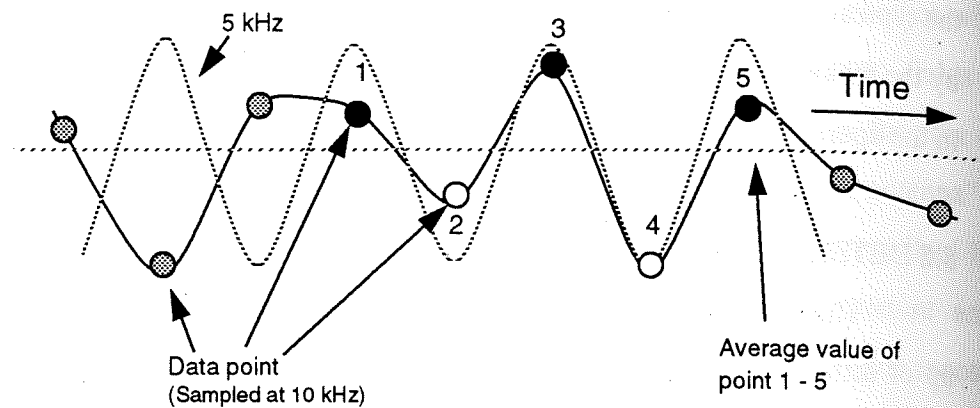
Figure 5.1:   Method of determining the arrival time of the wave packets

When five data points had opposite signs in sequence, the dominant frequency would be 5 kHz or an aliased frequency (i.e., 10 kHz, 20 kHz,... etc.).The earliest time when this data feature appears corresponds to the arrival time of 20 kHz or higher aliased frequencies. For the whistler waves received by the rockets, the arrival times of frequencies above 20 kHz do not have significant differences, and we simply refer to the time determined by this method as the arrival time of the waves at 20 kHz.

The arrival times of lightning optical signals were determined from the signal maxima.From the arrival times of optical and VLF signals, the time delays of VLF waves relative to their corresponding lightning optical signals were determined. In the following, the "time delay of the waves" will refer specifically the time delay of lightning-generated VLF waves to the lightning optical signals received by the rockets.

5.3 TIME DELAY OF VLF WAVES RELATIVE TO OPTICAL SIGNALS

From both the WIPP data and the Thunderstorm II data, we selected wave packets which were generated by lightning at different locations and received by the rockets at different altitudes. The time delays of each wave packet was compared to the horizontal distance of the various sources from the rocket and to the altitude of the rocket, respectively.

In Figure 5.2 the time delays at 24 kHz of 31 wave packets are shown with the

horizontal ranges of the wave sources from the rocket. These waves were received by the WIPP rocket at altitudes between 200 km to 412 km. Each "+" in the figure represents the time delay of an individual wave packet. Because the wave arrival times were determined using a 1-msec time resolution, time delays less than 1 msec were taken as 0 msec. It is seen in Figure 5.2 that most of the waves start at horizontal distances of 400 km from the rocket. These waves were from the thunder cell A, shown in Figure 3.1. Since they were all from the same area, the differences in their time delays, between   0 msec and 10 msec, were caused mainly by the change in rocket altitude. Several other wave packets generated by lightning with horizontal distances from 500 to 1200 km are also seen in Figure 5.2. The time delays of these waves also varies from less than 1 msec to about 10 msec. It is seen that the data points in this figure are widely dispersed. No relation between the time delays of VLF
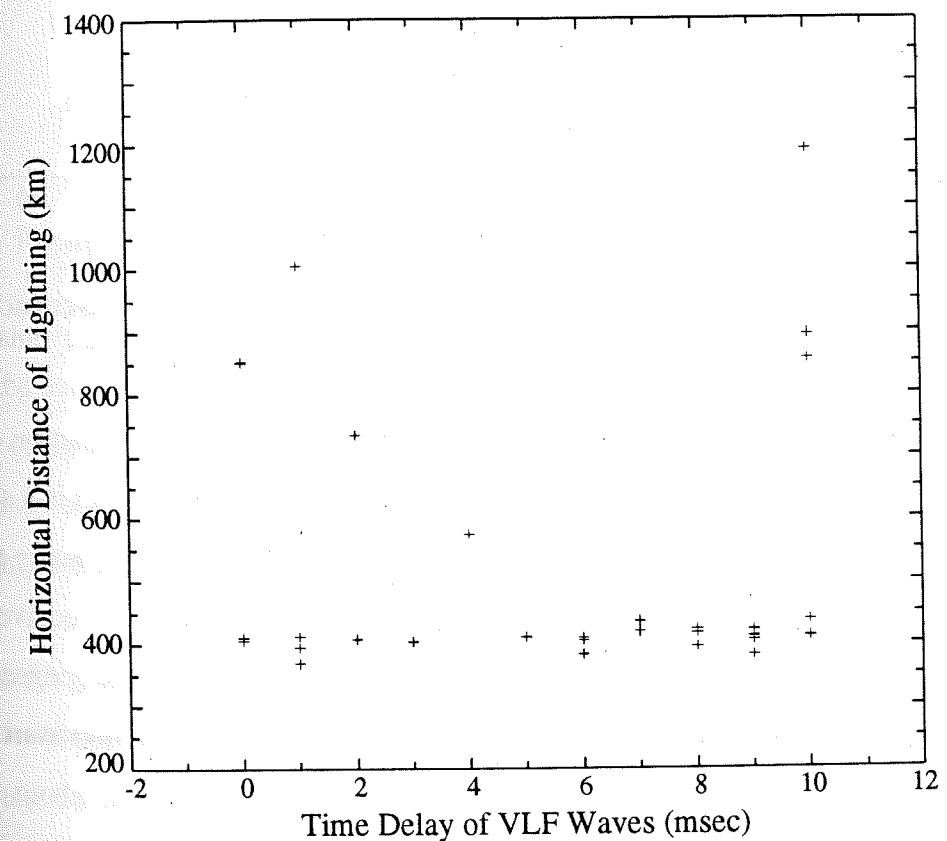

Figure 5.2:   Relation between the time delay of 24 kHz waves and the horizontal distance of lightning strokes from the rocket. Each "+" represents an individual lightning event.   Shown are 31 events recorded by the WIPP rocket.

waves in the ionosphere to the horizontal distance of the lightning sources is observed.
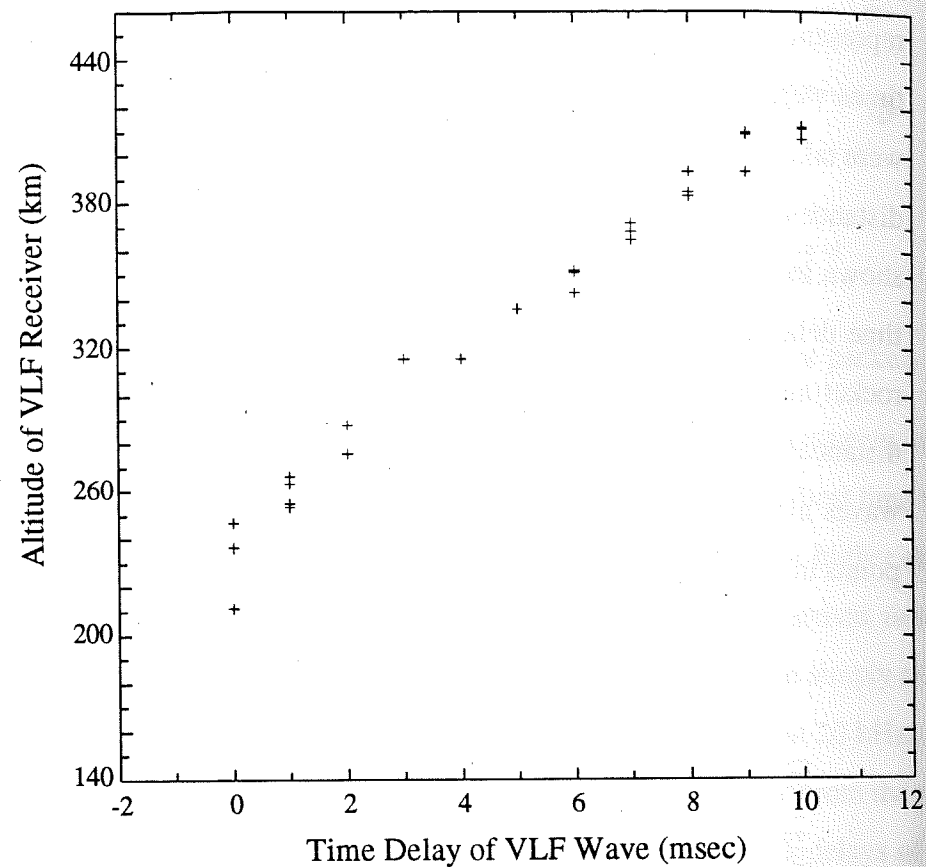

Figure 5.3:   Relation between the time delay of 24 kHz waves and the altitude of the rocket.   Lightning events in this figure are the same events shown in Figure 5.2.

The time delays of these same waves are plotted   as a function of the altitude of the rocket in Figure5.3. In this figure, all of the data points fall in a straight line. It can be seen that waves from sources with varying ranges have nearly the same time delay relative to their lightning optical signals when they were received at the same altitude. For example, the five wave packets received near the apogee of the rocket (only three can be seen in Figure 5.3 because of overlapping) start at horizontal distances from 500 km to 1200 km, but their time delays are all about 10 msec.

The time delays measured at 20 kHz for 47 VLF wave packets received by the Thunderstorm II rocket were plotted as a function of the horizontal distance between the lightning sources and the rocket, and are shown in Figure 5.4. Similar to Figure
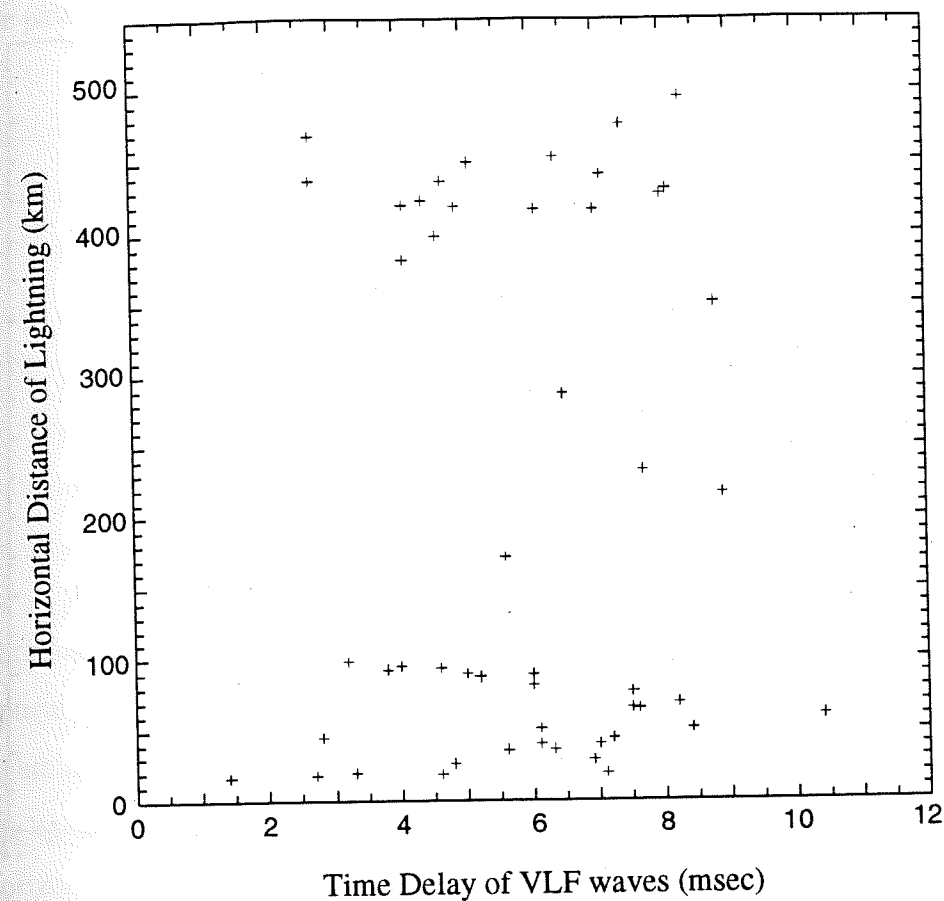
Figure 5.4:   Relation between the time delay of 20 kHz waves and the horizontal distance of the lightning strokes from the rocket. 50 lightning events recorded by the Thunderstorm II rocket are shown.

5.2, the data points in this figure are also dispersed and have no relations between the time delay and horizontal distance. However, when the time delay is plotted as a function of the altitude of the rocket, shown in Figure 5.5, all of the data points roughly fall along a straight line, consistent with the WIPP rocket data.

5.3 WAVE PATHS INDICATED BY THE DATA

In the above, we have shown that the delay of lightning-generated VLF waves are related to the altitude of the receiver but not the horizontal distance of the lightning from the receiver. This suggests that the VLF waves received by rockets were injected into the ionosphere in a localized area beneath the rocket.
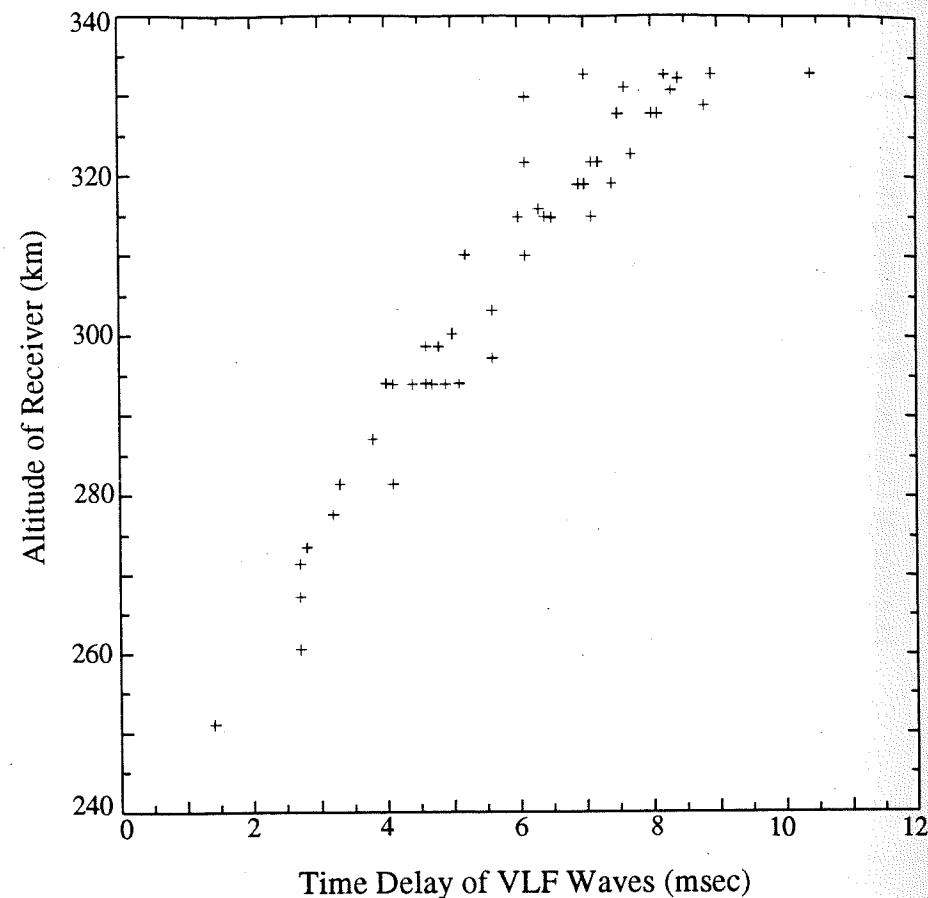
Figure 5.5:   Relation between the time delay of 20 kHz waves and the altitude of the rocket. Events in this figure are the same events shown in Figure 5.4.

Figure 5.6 is a diagram showing the possible wave paths from the lightning sources to the rocket. From a lightning source located at S1 up to the rocket, there are two extreme propagation paths for VLF waves. As shown in the figure, in Path 1 waves propagate in the earth-ionosphere waveguide from S_1 to the base of the ionosphere beneath the rocket ($S_0{}'$), these then propagate from $S_0{}'$ to the rocket. Path 2 waves are generated in the ionosphere above the lightning discharge ($S_0{}'$) and propagate from $S_1{}'$ to the rocket in the ionosphere. The actual paths of lightning-generated VLF waves will be between these two extreme paths. The high level of coherency of the waves received by the rocket (see Figure 2.3 - 2.5) suggests that only
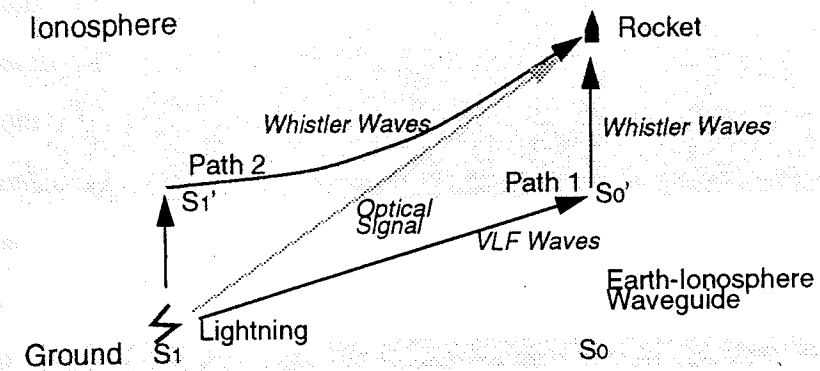
one path is taken by each wave.

Figure5.6: Possible paths of lightning-generated VLF waves in the ionosphere

For Path 1, waves generated by distant lightning have to propagate over a long horizontal distance in the ionosphere. Since VLF waves propagate more slowly than optical signals in the ionosphere, the time delay of these waves relative to the lightning optical signals must be greatly affected by the horizontal distance between the lightning and the rocket. However, the measurements by the rockets show that the horizontal distance from the lightning sources does not have a significant effect on the time delay of the VLF waves. It is therefore clear that these waves received by the rocket do not propagate along any of the paths close to Path 2.

Path 1 waves generated by distant lightning propagate mainly in the earth-ionosphere waveguide at the speed of light. For lightning with a horizontal range of several hundred kilometers, the times for the lightning optical signal to travel from S_1 to the rocket and for the waveguide waves from S_1 to $S_o{}'$ have typically less than 1 msec in difference. The time delays of the waves propagating along Path 1 are caused mainly by the propagation of waves from $S_0{}'$ to the rocket, and not related to the horizontal distance of the sources. This is exactly what was observed by both the WIPP and the Thunderstorm II rockets. The actual wave paths from lightning to rockets therefore should be closest to Path 1.

The contrasting wave propagation paths can indicate whether the waves are generated by the leaky waveguide or the aperture antenna mechanisms. When the

horizontal distance between the lightning and VLF receivers is small, Path 1 and Path 2 can hardly be distinguished and the generation mechanism of the waves cannot be determined by our method. Nevertheless, our study shows that the VLF wave packets received in the ionosphere at horizontal distances greater than several hundred kilometers from the lightning sources are very likely generated by the leaky waveguide mechanism, and not by the aperture antenna mechanism.

5.5 CALCULATION OF VLF WAVE PATHS IN THE IONOSPHERE

In the last section, we have assumed that the time delay of the VLF waves generated by the leaky waveguide will change significantly with horizontal range because VLF waves propagate much less rapidly than optical signals in the ionosphere. This assumption needs to be quantitatively verified. It is known that the refractive index of VLF waves changes greatly with altitude in the ionosphere. The wave normal will quickly change toward the vertical direction because of increasing refraction as the waves propagate upward in the ionosphere. It seems likely that the waves generated by the aperture antenna mechanism in the ionosphere will not be able to propagate over a large horizontal distance. This assumption also needs to be examined in detail. For these reasons, a further investigation of the VLF wave paths in the ionosphere is necessary. In this section, we will calculate the propagation paths of VLF waves in the ionosphere in order to examine the paths of the waves generated by the two whistler wave generation mechanisms.

Assuming that the ionosphere is horizontally stratified, we divide the ionosphere into horizontal layers. At the boundary of each layer, by Snell's law, the incident and transmitted waves must have refractive indexes whose projections on the boundary are equal. For waves which are injected into the ionosphere at an altitude h_0 with an incident angle θ_0, Snell's law gives

$$n_r(\theta, h) \sin\theta = n_r(\theta_0, h_o) \sin\theta_0 , \qquad (5.1)$$

where θ in the incident angle at the altitude of h, n_r is the real part of the refractive

index of the waves. For any incident angle θ_0 at the base of the ionosphere, θ at each layer in the ionosphere can be calculated using equation (5.1). However, because the wave refractive index is also a function of the incident angle, equation (5.1) is generally difficult to solve. In this study, the equation (5.1) was solved numerically.

In our calculation, the thickness of each layer was 1 km. The profiles of the electron density and the effective collision frequency in the ionosphere shown in the first chapter were used. For simplicity, the geomagnetic field was assumed to be in the vertical direction. The n_r were calculated using the full expression of the Appleton-Hartree equation (see Section 1.4.3). Although the conditions for applying the Appleton-Hartree equation may not be satisfied for VLF waves near the base of the ionosphere, it is expected that this calculation can still serve as a zeroth order approximation.

In the leaky-waveguide mechanism, lightning-generated waves in the waveguide are coupled into whistler-mode waves at the base of the ionosphere. Assuming that the coupling altitude is 80 km, we calculated the propagation paths of waves with different incident angles at this altitude. Figure 5.6 shows the paths of 5 kHz waves with incident angles of 10°, 25°, 40°, 55°, 70° and 85° at 80 km. Since the geomagnetic field is in the vertical direction, the calculated paths are axially symmetric. It is seen in Figure 5.7 that waves injected into the ionosphere are confined to an area with very small horizontal dimensions. For example, a wave injected with an incident angle of 85° can only propagate to a horizontal distance of 40 km when it reaches an altitude of 350 km. This indicates that waves generated by the leaky-waveguide mechanism and received in the ionosphere should be from a small area located underneath the receiver. This result is normally expected and is consistent with the observations made by the rockets.

In the aperture antenna model, waves are generated in the ionosphere at a variety of wave normal directions. Assuming that 5 kHz waves are generated by an isotropic source at an altitude of 80 km in the upper half space, Figure 5.7 shows that more than 90% of the wave energy would pass upward through a local area of the

ionosphere with horizontal dimensions less than 80 km. In other words, whistler waves generated at the base of the ionosphere cannot propagate over large horizontal distances.
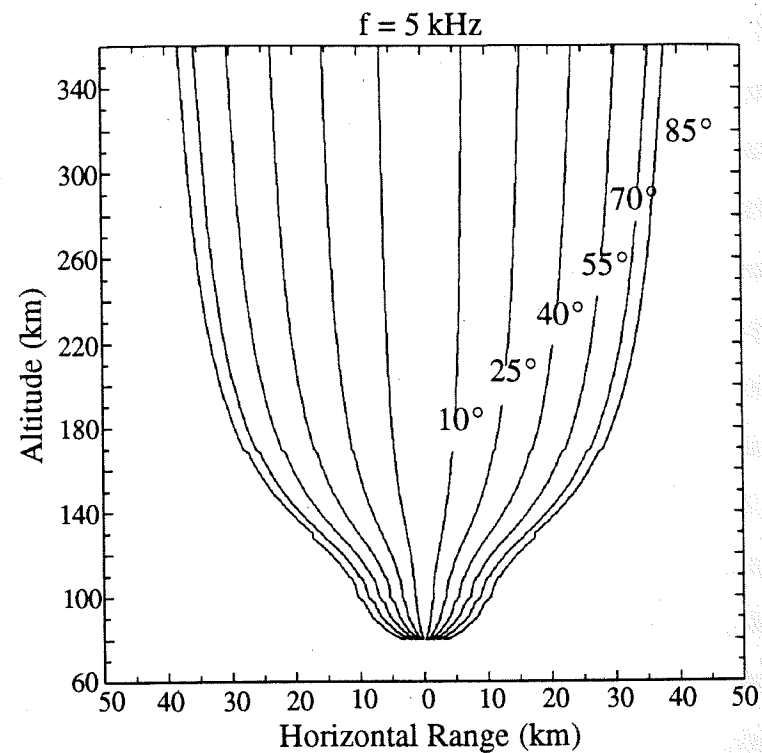
f = 5 kHz

Figure 5.7: The propagation paths of VLF waves injected into the base of the ionosphere. Paths of waves with 6 different incident angles at the base of the ionosphere are calculated. The geomagnetic field was assumed to be in the vertical direction, so the wave paths are axially symmetric

In Figure 5.8, waves with different normal angles were generated by an "antenna" with an altitude of 85 km. In comparison with Figure 5.7, it is seen that this antenna at a higher altitude generated waves which propagate over larger horizontal area. For example, waves with an incident angle of 85° can propagate to a horizontal range of 200 km, which is much larger than the case shown in Figure 5.7. In Figure 5.9, the altitude of the source has been increased to 130 km. For this case, waves with an 85° incident angle reach horizontal distances of 500 km. It appears that about 10% of the wave energy generated from an isotropic source at an altitude of 130 km could

propagate farther than 600 km in horizontal range. It can be shown that waves at higher frequencies or generated by sources at higher altitudes may propagate over significantly greater horizontal distances. It can also be seen that the propagation paths of waves generated at different altitudes have different features. These features are basically caused by the particular electron density profile used.
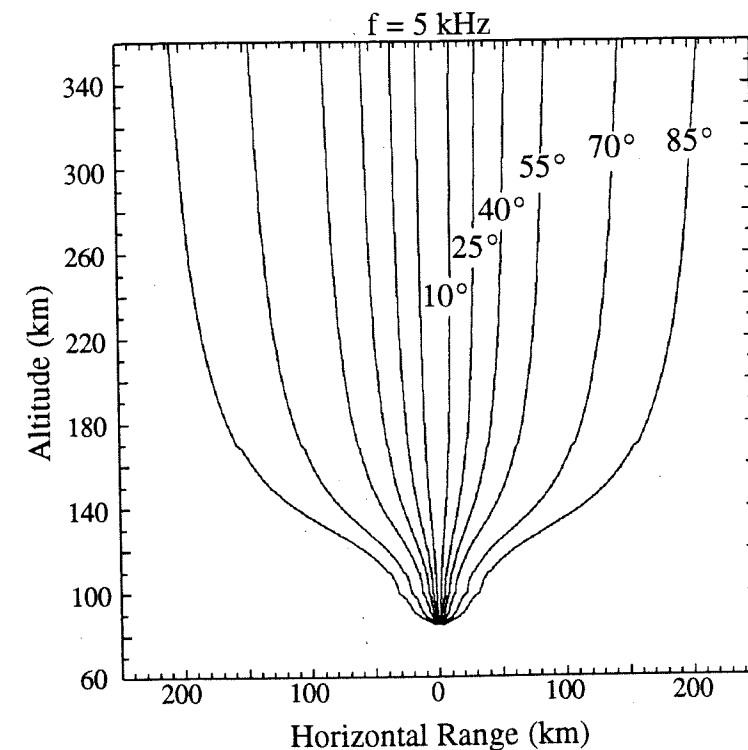
f = 5 kHz

Figure 5.8: The propagation paths of VLF waves generated by a source with an altitude of 85 km in the ionosphere. The labeled angles are the angle between the wave normal and the vertical when waves are generated.

The propagation times of a 5 kHz wave from the source to an altitude of 360 km along these paths shown in Figure 5.8 and 5.9 were calculated and are shown in Figure 5.9. In this figure, the calculated travel times are plotted for the horizontal ranges of the waves at an altitude of 360 km. It is seen that the propagation times increase significantly with the horizontal range. When the wave source is at an altitude of 85 km, there is about 3 msec difference in the propagation time of waves

received at the same altitude (360 km) but at different horizontal ranges from 0 - 200 km. When the source is at an altitude of 130 km, it would take an additional 20 msecs for waves to propagate to a horizontal range of 600 km.
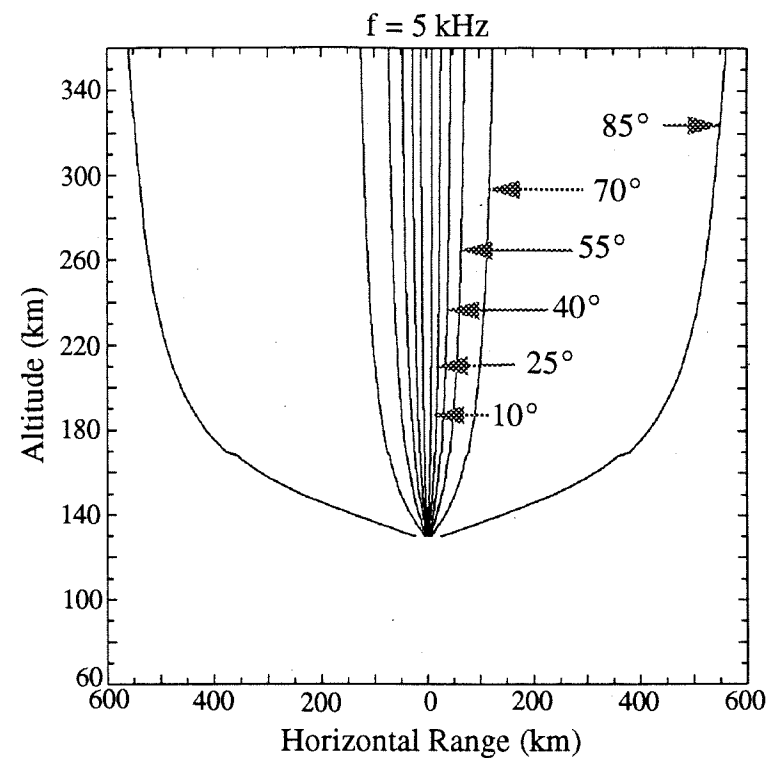

Figure 5.9: The propagation paths of waves generated by a source with an altitude of 130 km.

From the above calculations, we conclude that waves generated by the leaky waveguide mechanism would propagate almost vertically in the ionosphere. Waves generated in the aperture antenna mechanism may propagate to a large horizontal distance, depending on the altitude of the antenna, but the propagation times of these waves increases significantly with increasing horizontal range. These calculations show that if an aperture antenna can generate VLF waves as predicted, a receiver in the ionosphere would receive two waves at a horizontal distance of several hundred kilometers from each lightning stroke. The first wave would be a typical wave packet, which is generated by the leaky waveguide mechanism. Some msecs after receiving this first wave, the second wave would be received, having been generated by the aperture antenna mechanism. This second wave would be very weak and not phase
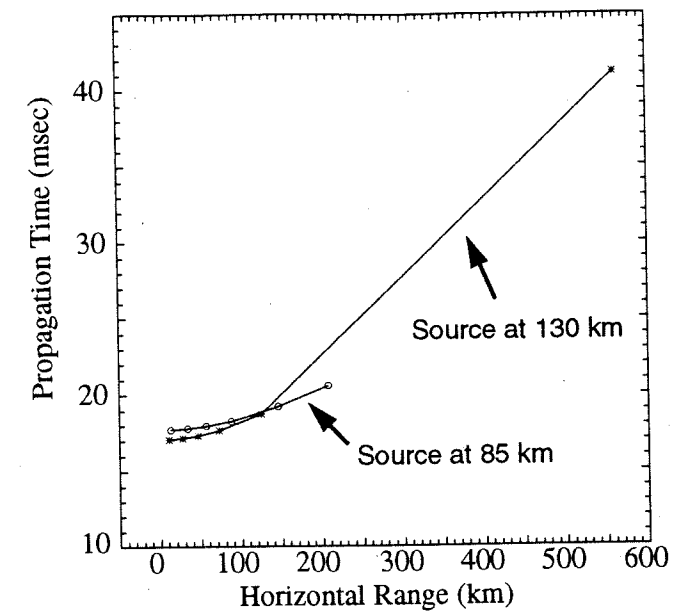
Figure 5.10: The relation of propagation time and the horizontal range calculated from waves (f = 5kHz) generated in the ionosphere

coherent, and as a result it may not be observed.

When the lightning sources are within a small horizontal range from the rocket, it can be expected that the waves generated by the aperture antenna mechanism may be received earlier than waves generated by the leaky waveguide mechanism. The difference in the receiving times depends on the altitude of the aperture antenna and the horizontal range of the sources.

5.6 SUMMARY

The time delay between reception of lightning-generated VLF waves and optical signals in the ionosphere depends on the altitude of the receivers, but very little on the horizontal distance between the lightning and the receiver. This indicates that the lightning-generated VLF wave packets received at rockets are all from a local area nearly below the rocket. Waves generated by sources with horizontal ranges from the rocket of several hundred kilometers are therefore more likely to have been generated by the leaky waveguide mechanism, not by the aperture antenna mechanism.

Calculation shows that VLF waves injected at the base of the ionosphere are confined in the ionosphere to an area with limited horizontal dimensions. For waves at 5 kHz, this dimension is typically around 100 km. This is consistent with the observations made by the WIPP and Thunderstorm II rockets.

Waves generated by sources in the ionosphere, such as the aperture antenna mechanism, may propagate in the ionosphere over large horizontal distances. However, for isotropic sources, only a small fraction of the generated wave energy could propagate to horizontal ranges greater than several hundred kilometers. If significant VLF wave energy can be generated by the aperture antenna mechanism, it would be expected that a receiver in the ionosphere would receive two waves from each lightning stroke over a horizontal distance of several hundred kilometers. The first wave would be the well-known VLF wave packet which is generated by the leaky waveguide mechanism. The second wave would be generated by the aperture antenna mechanism. This wave would be much weaker and would arrive several msecs after the first wave, but it was not detected in this study.

CHAPTER 6

AMPLITUDE VARIATION OF LIGHTNING-GENERATED VLF WAVES IN THE IONOSPHERE

6.1 INTRODUCTION

It is well known that lightning-generated VLF waves can produce whistlers, particle precipitation and other phenomena in the earth's atmosphere and ionosphere (Rosenberg et al., 1971; Carpenter et al., 1982; Inan et al.,1987). These VLF waves also give rise to certain processes in the local media as they propagate in the ionosphere and the magnetosphere. Lower-hybrid waves excited by lightning-generated whistler waves in the ionosphere and the magnetosphere have been observed (Kelley et al., 1990, Bell et al., 1991a, 1991b). These waves have been suggested to be a significant source of direct heating in the lower ionosphere. This heating could enhance the ionization in a local area and affect the sub-ionospheric propagation of VLF transmitter signals (Inan at al., 1991).To study the processes associated with lightning-generated VLF waves in the ionospheric media, it is important to know the amplitude of these waves at different altitudes in the ionosphere. The amplitude change of these waves with altitude is also of interest because it provides information about VLF wave propagation and attenuation, as well as the characteristics of the ionospheric media.

The properties of lightning-generated VLF waves in the ionosphere, such as dispersion, velocity, polarization and frequency spectrum, have been previously investigated by some researchers (Maynard et al., 1970; Kelley et al., 1988). In the experiments done by these researchers, the variation of wave amplitude with altitude in the ionosphere was not studied. The amplitude change of VLF transmitter signals in the ionosphere, however, has been reported by others in several studies. For example, the signal from a 3.85 kHz transmitter directly over Siple Station, Antarctica was measured from a rocket at altitudes from 65 km to 130 km. A gradual amplitude change of the VLF signal, with a change in the wave polarization, was

observed (Kintner, 1983). In another experiment, signals from two transmitters (17.8 and 21.4 kHz) were recorded by a rocket at altitudes below 155 km. It was found that these signals formed a standing wave pattern below an altitude of 106 km, due to wave reflections from the sporadic E layer (Siefering and Kelley, 1991). In these experiments, the apogees of the rockets were less than 160 km, so the amplitude changes of the VLF waves above this altitude were not measured.

One of the advantages of studying the signals from VLF transmitters is that their sources are constant, so they can be measured continuously by the rockets with altitude. Lightning-generated VLF waves, however, are very short wave packets which cover a broad frequency range. Clearly, some of the features observed in lightning-generated waves, such as wave dispersion, cannot be studied using continuous transmitter signals. And also, the dominant radiation energy from lightning is at frequencies below 10 kHz. The frequencies of most VLF transmitters in operation on the world are above 10 kHz. Therefore, there are limitations of using VLF transmitter's signals to study lightning -generated VLF waves.

In comparison with that of VLF signals from a controlled transmitter, the amplitude variation in lightning-generated VLF waves with altitude is more complicated and difficult to study. Lightning-generated waves received by rockets are normally produced by random lightning strokes over different areas. The amplitude variation of these waves can only be investigated statistically, provided that a large number of waves are received by the rocket with altitude and that the sources of the waves can be located.

During the WIPP and the Thunderstorm II campaigns, VLF waves generated by a large number of lightning strokes were measured on rockets at different altitudes. Many of these lightning strokes were recorded by the State University of New York at Albany (SUNYA)lightning network (now part of the National Lightning Network). Therefore the sources of many of the received wave packets can be identified and located. These data thus provide us with a good opportunity to investigate the amplitude change of lightning-generated VLF waves in the ionosphere with altitude.

It could be expected that the VLF electric field generated by lightning would gradually decrease with altitude above 150 km in the ionosphere, because of wave attenuation and changes in the refractive index. However, our analysis of the wave spectra received by the WIPP and the Thunderstorm II rockets revealed that the amplitude of typical lightning-generated VLF waves did not monotonically decrease with altitude. Instead, the amplitude of theses waves had significant peaks and troughs at altitudes above 150 km. This spatial variation of VLF wave amplitude with altitude, which has not been previously reported, cannot be explained using standing wave mechanisms or by changes in the wave refractive index. In this chapter, we will present data which shows the amplitude variation of lightning-generated waves with altitude observed by the WIPP and the Thunderstorm II rockets. We will also show how this variation might be caused by the interference of waves injected into the ionosphere from a local area located below the rocket.

6.2 DATA

In order to investigate the change of wave amplitude with altitude, other factors which could also affect the wave amplitude need to be considered.

The lightning-generated VLF waves received by rockets usually have propagated in the earth-ionosphere waveguide over considerable distances. The amplitude of the received waves are affected by the propagation distances and waveguide conditions, such as the path orientation, the earth's surface topography and the ionospheric conditions along the path (Wait, 1962; Alpert, 1967). To constrain these propagation effects in this study, we selected only waves which started from small localized areas. The geographic locations of the sources of the selected wave packets are shown in Figure 6.1. Of events received by the WIPP rocket, 75 wave packets were selected for study. These were wave packets generated by lightning flashes from the small area labeled A in Figure 6.1. The horizontal distances from these lightning flashes to the rocket were all about 450 km. Since the extent of this source area is much less than the propagation distance of the waves, we
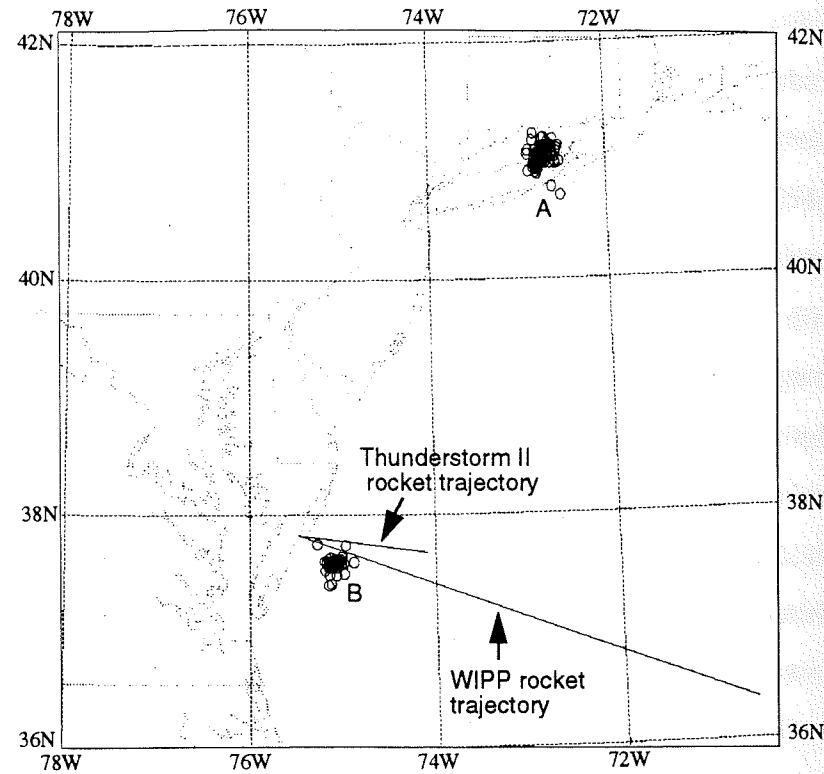
Figure 6.1: The location of selected lightning flashes. 75 flashes in the area labeled A occurred during the WIPP rocket flight, and 49 flashes in area B occurred during the Thunderstorm II rocket flight.

can assume that waveguide effects were approximately the same for all of the waves from this area. Also shown are sources of 49 wave packets received by the Thunderstorm II rocket from area B in Figure 6.1. Area B was located almost directly below the rocket. Because these waves only propagated in the earth-ionosphere waveguide over a very short distance, they should not have been strongly affected by the waveguide propagation conditions.

The electromagnetic radiation from lightning strokes are related to the characteristics of the strokes, such as the strength of the discharge current and the features of the discharge channels (Newman, 1958). The amplitude of waves received by the rockets included such source effects. These source effects, which differ from stroke to stroke, are complicated and difficult to determine. However, in chapter 4 we found that the amplitude of VLF waves at frequencies below about 5 kHz had a

positive linear correlation with the lightning current recorded by the SUNYA network. In order to reduce these source effects, the lightning current recorded by the SUNYA network was used to normalize the wave amplitude for frequencies below 5 kHz.

In Chapter 4, we obtained the spectra of a large number of lightning-generated VLF wave packets from sources A and B received by the WIPP and the Thunderstorm II rockets at altitudes ranging from 150 to 412 km. Analyzing the selected spectra, the changes of wave amplitude at different frequencies with altitude were investigated. The spectra of waves received by the WIPP rocket were analyzed in 128 frequency components ranging from 0.25kHz to 32kHz. We found that the amplitudes of most of these frequency components clearly had significant peaks and troughs at altitudes above 150 km.

For examples, Figure 6.2 shows the amplitude variations for waves at frequencies of 1.0, 3.0, 7.0 and 10.0 kHz. Each point in this figure represents a lightning-generated VLF wave packet measured by the WIPP rocket. The altitude range from 100 to 420 km were divided into 16 layers, each with a thickness of 20 km. An average value of the wave amplitude within each layer was calculated and is shown by the dashed line in the figure. All of these wave packets, a total of 47 in this figure, were received during the upleg phase of the rocket flight. These lighting strokes occurred randomly, over a time interval of several seconds or less. Because the rocket passed through higher altitudes with decreasing vertical velocity, more VLF waves were received at the higher altitudes.

As seen in Figure 6.2, the normalized amplitudes of waves from different lightning strokes had a strong residual scatter. This could be attributed to, as mentioned earlier, the source or propagational effects which could not be determined in our study. Despite the divergence of the data points, we can still see that waves at all of the frequencies have statistically greater amplitudes at certain altitude ranges, and smaller amplitudes at other altitude ranges. For example, for the profile at 3 kHz on both up and downleg, most of the wave packets received at altitudes between 250

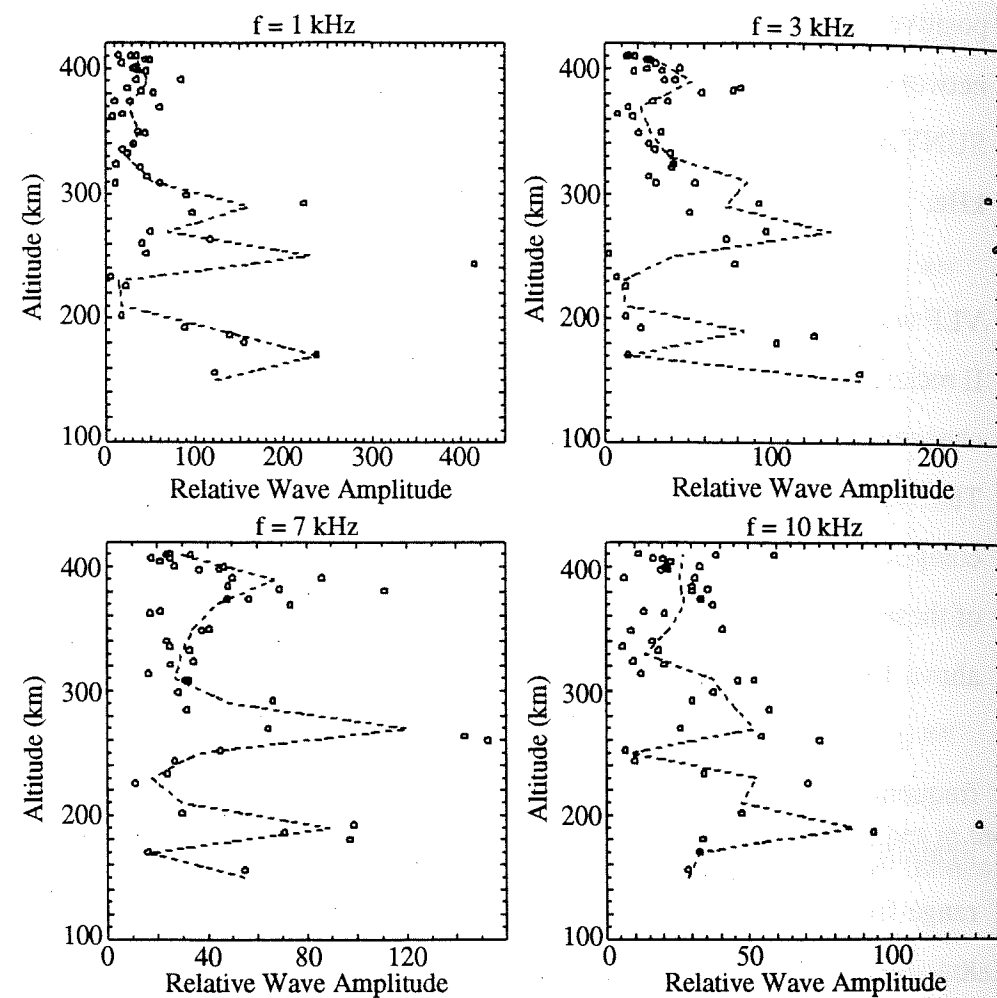f = 1 kHz

f = 3 kHz

f = 7 kHz

f = 10 kHz

Figure 6.2: Variations of VLF wave amplitude observed during the upleg of the WIPP rocket. The dots show the amplitude of waves generated by different lightning strokes and received at different altitudes. The amplitude at four frequencies, 1.0, 3.0, 7.0 and 10.0 kHz, are shown. The dashed lines show the average values of the wave amplitude within each layer with a thickness of 20 km.

km and 300 km were significantly stronger than those received at lower altitudes. Above 300 km, the wave amplitudes were relatively smaller until they reached another peak at 390 km. Differences can also be seen between the various profiles in Figure 6.2 and 6.3. For example, a trough at an altitude of 220 km occurred in the profiles at 1.0, 3.0 and 7 kHz, but did not occur in the profile at 10 kHz. It can be shown that the differences seen in the other frequency components may be significant.
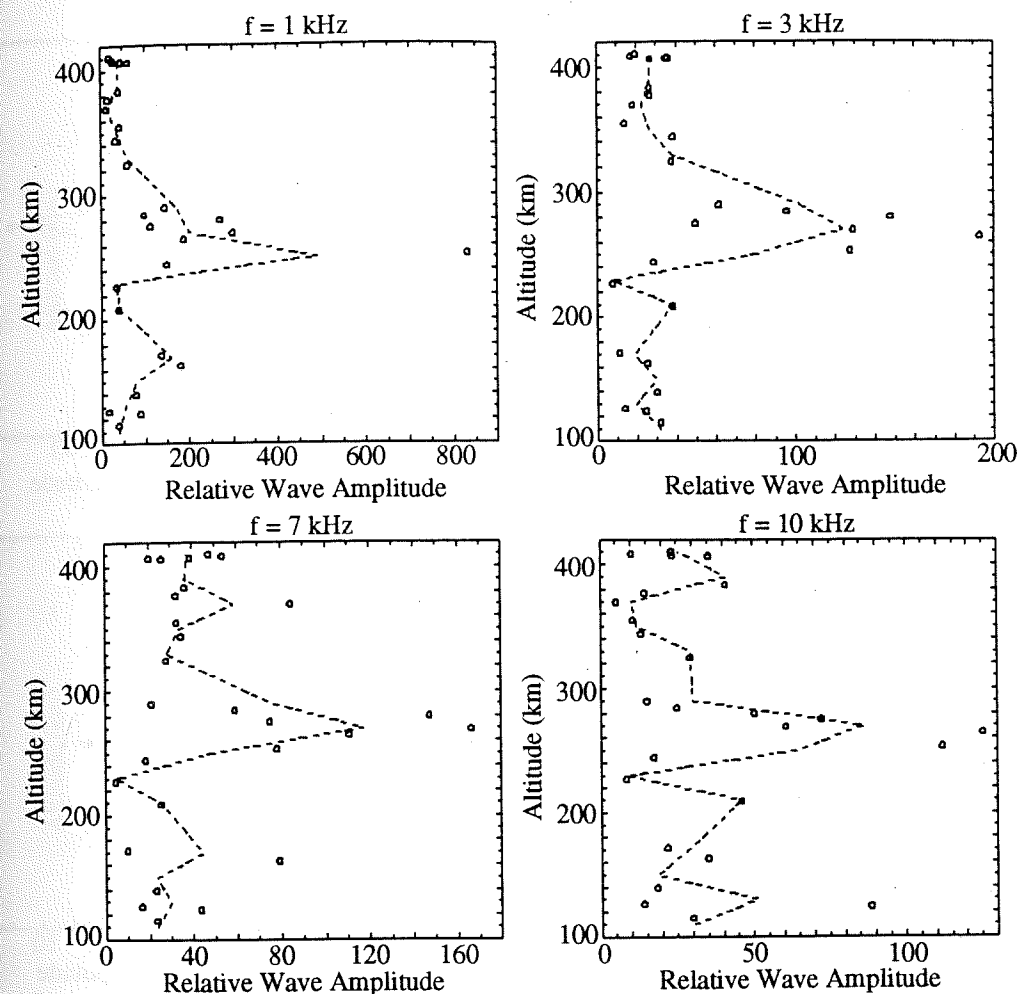
f = 1 kHz

f = 3 kHz

f = 7 kHz

f = 10 kHz

Figure 6.3: Variation of VLF wave amplitude observed during the downleg of the WIPP rocket. These waves are from the same area as those shown in Figure 6.2. The dashed lines are the average value of the wave amplitude within each layer with a thickness of 20 km.

Figure 6.3 shows the waves received during the descent phase (downleg) of the WIPP rocket. In this figure, 28 lightning events located within the same area as those in Figure 6.2 are shown in this figure. The changes of wave amplitude with altitude measured during the downleg of the rocket flight were very similar to those measured during the upleg flight. At 3 kHz, for example, a significant peak at an altitude of 280 km was also observed. Above 280 km, the amplitude of these waves statistically decreased, and again appears to reach a peak around 390 km. These general features are the same as those observed during the upleg of the flight.
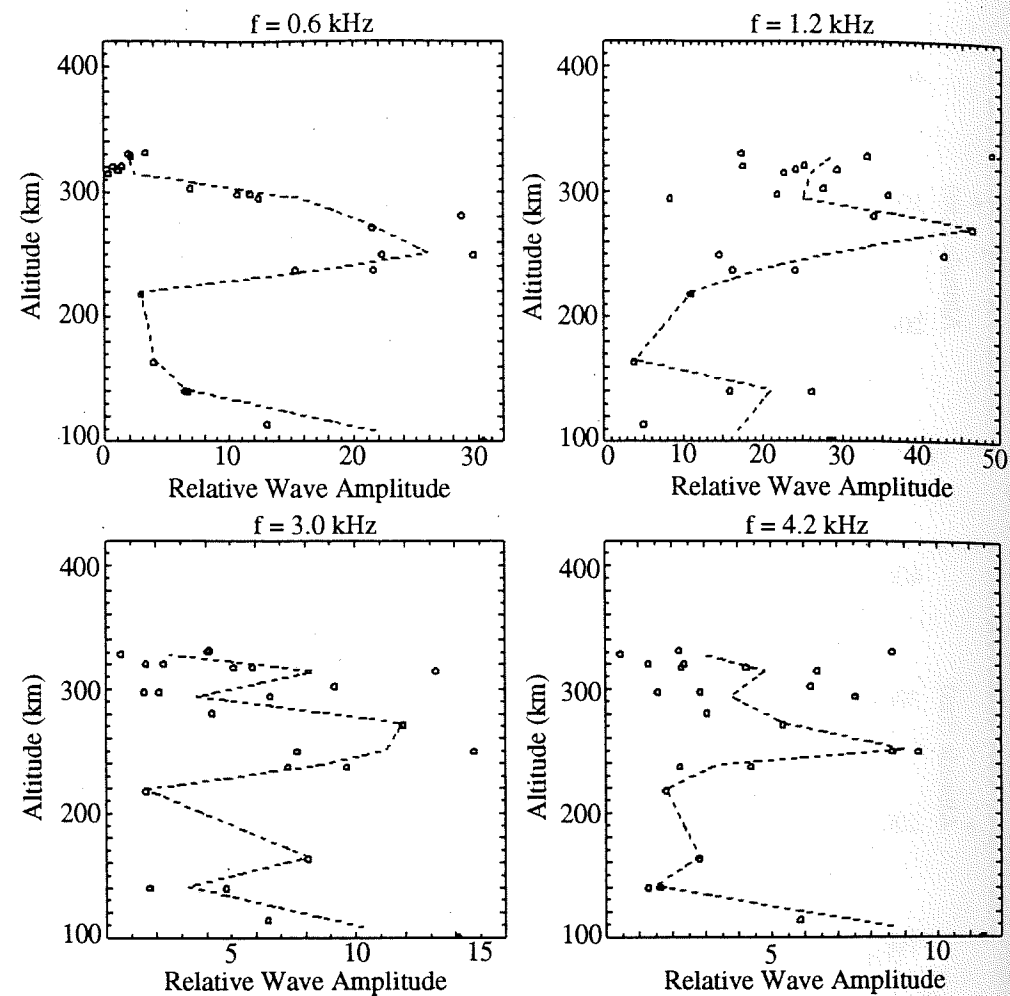
Figure 6.4: Variations of VLF wave amplitude with altitude observed during the upleg of the Thunderstorm II rocket. The amplitude change at frequencies of 0.6, 1.2, 3.0 and 4.2 are shown. The dashed lines show the average value of wave amplitude in each 20-km layer

The wave spectra obtained from the Thunderstorm II data contained 100 frequency components between 0.05 kHz and 5 kHz. Analyzing the selected wave spectra, we found the Thunderstorm II rocket also observed significant changes in the VLF wave amplitude with altitude. The variation of wave amplitude at four frequencies is shown in Figure 6.4 with the same configuration as that of Figures 6.2 and 6.3. A total of 24 wave packets were selected during the upleg of this rocket flight. The apogee of the Thunderstorm II rocket was about 333 km, therefore no wave structures were measured above 330 km. However, this rocket also recorded a
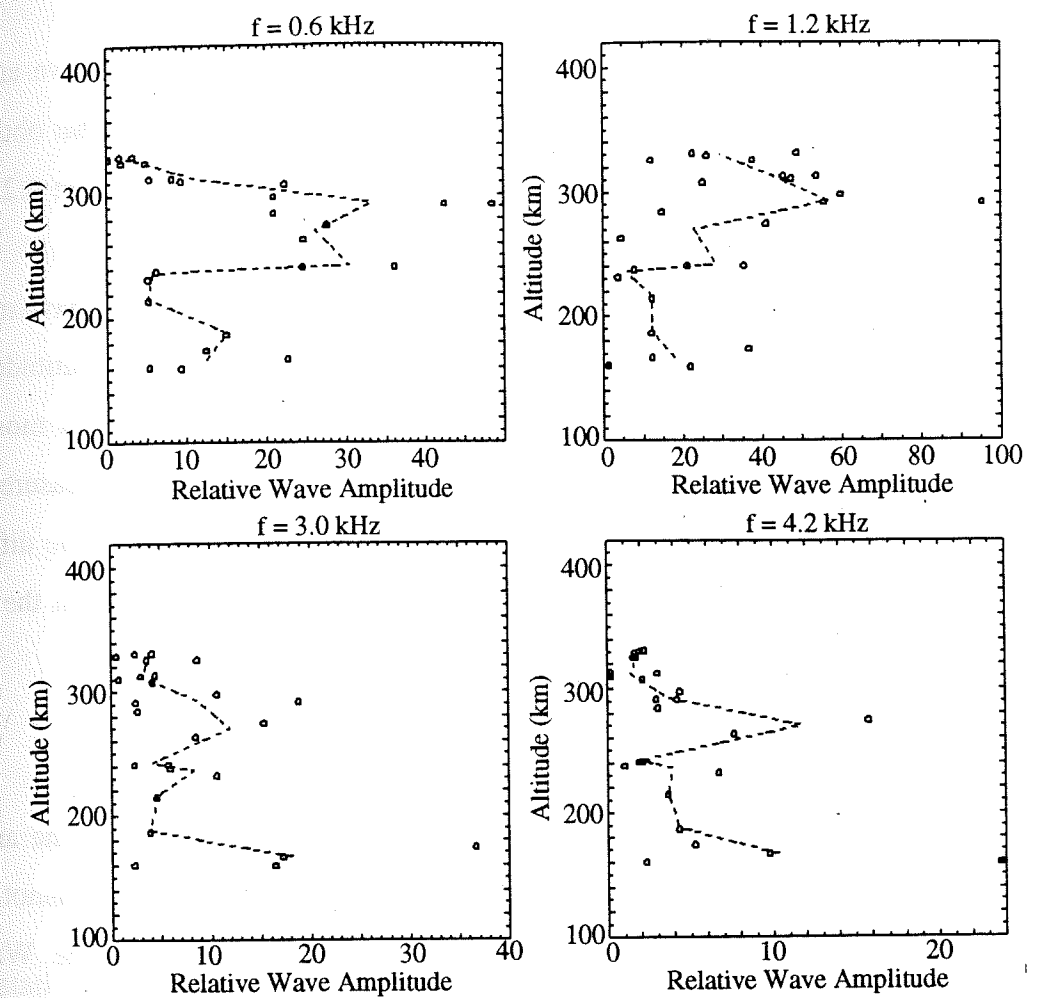

Figure 6.5: Variation of the amplitude of VLF waves with altitude observed during the downleg of the Thunderstorm II rocket. These waves were from the same area as those shown in Figure 6.4. The dashed lines show the average wave amplitude within each 20 km layer.

peak in wave amplitude at an altitude of around 280 km. This can be clearly seen in the data at frequencies of 0.6, 1.2 and 4.2 kHz, in which the waves received at altitudes of 280 km were mostly stronger than those received at lower altitudes. This observation from the Thunderstorm II rocket was consistent with that of the WIPP rocket. Figure 6.5 shows 25 wave packets which were generated by lightning in the same area (area B in Figure 6.1) but received during the downleg of the Thunderstorm II rocket flight. It is seen that the amplitude variation of these waves with altitude measured during the downleg of the flight were basically similar to those measured

during the upleg of the flight.

For the same frequency component, the altitude profile of wave amplitude obtained by the Thunderstorm II rocket seems to be different from that obtained by the WIPP rocket. For example, the profiles at 3 kHz shown in Figure 6.2 and 6.3 appears to be different from those in Figure 6.4 and 6.5.

In summary, both the WIPP and the Thunderstorm II rockets have measured significant amplitude variations in lighting-generated VLF waves at altitudes above 150 km. Peaks and troughs were present in these altitude profiles of most of the frequency components between 0 and 32 kHz. The altitude profiles measured during the upleg and downleg flight of the rockets had similar features. Some differences were seen between the profiles at different frequencies, and between the profiles observed by the WIPP and the Thunderstorm II rockets.

6.5. DISCUSSION

As we mentioned earlier, one of the difficulties of studying the amplitude variation of lightning-generated VLF waves is that the measurements cannot be made continuously with altitude. We have seen that even though the WIPP and Thunderstorm II rockets were flown near very active thunderstorms, there were still not enough measured events to cover all of the altitudes. This is especially true for altitudes below 250 km. We calculated the average wave amplitude within each of the 20-km layers for the waves received during the entire flight of the WIPP rocket. The circles in Figure 6.6 show the average wave amplitude ($\overline{E}$) at 3 kHz. The bars indicate the standard deviation of wave amplitude ($\overline{E} \pm \sigma$) in each layer. It is seen that the average wave amplitudes within the layers at altitudes from 240 to 320 km are more than twice as great as those within the layers from 200 to 240 km and from 320 to 380 km. The minimum wave amplitudes within the two layers from 260 to 300 km are comparable or greater than the maximum amplitude in these layers from 200 to 240 km and from 320 to 380 km. Considering that all of these waves were generated by randomly occurring lighting strokes, the peak at a altitude of 280 km is clearly
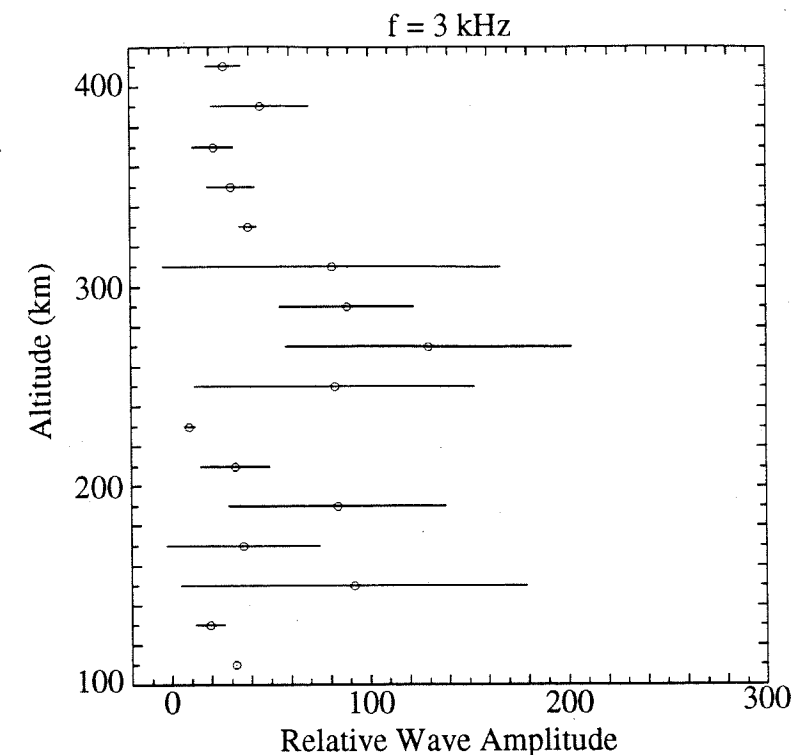
Figure 6.6: Average wave amplitude at 3 kHz within each 20-km layer calculated from the waves received during the entire flight of the WIPP rocket. The circles show the average wave amplitude. The bars indicate the standard deviations of the wave amplitude within each layer.

statistically significant.

It is very unlikely that these features in the wave altitude profiles were generated by any malfunction of the instruments. The VLF wave receiver on the WIPP rocket has an automatic gain control circuit. We have carefully examined the recorded gain changes during the rocket flight, and could not find any association between the gain levels and the statistical changes in the VLF wave amplitudes. The VLF receiver on the Thunderstorm II rocket did not change its gain at all during the flight, yet it measured a peak at the same altitude. This evidence suggests that the peaks and troughs in the wave altitude profiles were not caused by gain changes during the rocket flight. The systematic errors in the rocket measurements were estimated to be less than 20%. Even applying error bars of 20% to the amplitude profiles shown above, we still see significant peaks and troughs.

The wave amplitude peaks and troughs in the altitude profiles were not caused by systematic changes of the lightning sources with time. The current intensities of the lightning flashes used in our study were recorded by the SUNYA lightning network. Examining the current intensities of these lightning flashes, we saw no apparent statistical changes during either the WIPP or Thunderstorm II rocket flights. The profiles obtained during the rocket upleg and downleg both have similar features, even though the waves were from random lightning strokes. It would be extremely difficult to explain this similarity by systematic temporal changes of the sources or by other wave propagation factors.The changes in wave amplitude measured by the two rockets are, therefore, most likely due to spatial changes in the wave amplitude over the flight paths.

If VLF waves encounter a substantial change in the wave refractive index over a distance comparable to the local wavelength, significant wave reflection occurs.The incident waves and the reflected waves form a standing wave pattern. This phenomenon has been observed in VLF hiss between 1.5 - 3.0 kHz (Brittain, et al., 1983) and in transmitter signals at 17.8 kHz (Siefering and Kelley, 1991). A feature of the standing wave pattern is that the distances between the peaks or troughs (fringe distance) are equal to half of the local wavelength. In the profiles observed by the WIPP and Thunderstorm II rockets, the apparent fringe distances were typically on the order of several tens of kilometers. However, such a standing wave pattern of VLF waves for such large fringe distances cannot occur at altitudes above 200 km because the VLF wavelengths in that region are typically shorter than a few kilometers. We conclude that the amplitude variations of lightning-generated VLF waves measured by the WIPP and Thunderstorm II rockets was not due to standing wave patterns.

The measured wave amplitudes are related to the wave refractive index in the local medium. It has been shown in Chapter 4 that if there is no wave energy loss, we have

$$E(z) = \left(\frac{A\omega B(z)}{n_e(z)}\right)^{\frac{1}{4}}, \qquad (6.1)$$

where n_e is the electron density, B is the geomagnetic field and A can be considered approximately constant with altitude (see equations 4.1 - 4.5). Assuming that the altitude profiles of wave amplitude were caused solely by changes in the refractive index, we can roughly calculate an electron density profile from the measured wave amplitudes using equation (6.1). It can be shown that the electron density profile would have large troughs and peaks below 350 km which are significantly different from normal electron density profiles.

It is known that large scale irregularities can occur in the mid-latitude nighttime ionosphere. For example, layers with peak densities at least an order of magnitude greater than the background level are frequently observed to peel off the bottom side of the F region of the ionosphere and descend toward the sporadic E layers below (Shen et al., 1976). Such layers, called "intermediate layers", are primarily due to the oscillatory behavior of the neutral atmosphere (Kelley, 1989). There is evidence indicating that large scale irregularities, such as these intermediate layers, are not the cause of the amplitude change of VLF waves with altitude. During the thunderstorm II campaign, the electron density was measured at altitudes from 240 km to 450 km by another rocket flown almost simultaneously with the Thunderstorm II rocket (Kelley et al., 1990). The measured electron density profile was similar to the IRI altitude profile shown in Figure 1.2 and did not have significant peaks or troughs at altitudes from 200 km to 350 km. Therefore, the profiles of VLF wave amplitude were not produced simply by the changes in the electron density with altitude.

The amplitude variation of lightning-generated VLF waves with the altitude observed by the WIPP and the Thunderstorm II rockets has not been previously reported. This phenomenon is of interest regarding the generation and the propagation of VLF waves in the ionosphere. In an effort to determine its cause, we

investigated the possible effects of wave interference.

As suggested in the "leaky waveguide" mechanism, lightning-generated VLF radiation can couple into whistler waves at any point at the base of the ionosphere. These waves once launched into the ionosphere will presumably have a variety of normal directions. Therefore, waves launched at different locations with different normal directions may be simultaneously received by the rocket. However, in Chapter 5, we have shown that VLF waves injected into the ionosphere with different wave normal directions were generally confined to small regions of the ionosphere due to refraction. This means that only waves injected from a limited region at the base of the ionosphere below the rocket can be received.

The above situation is illustrated in Figure 6.7. As shown in this figure, VLF waves are launched into the ionosphere at different points (A, B, C and D) with different wave normal directions. Due to wave refraction in the ionosphere, the rocket can only receive waves injected at the points between B and C. Waves launched at other points, such as A and D can not reach the rocket. The region between B and C, therefore, serves as a wave aperture. Only waves passing through this aperture will be received by the rocket. Assuming that the wave field measured by the rockets is the coherent superposition of all the possible waves from such "apertures" below the rockets, we made a preliminary calculation to investigate the
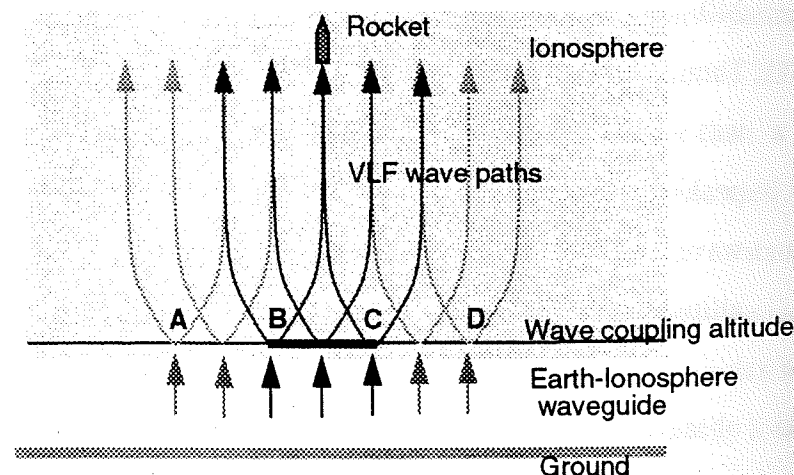

Figure 6.7: The "aperture" of VLF waves received in the ionosphere

interference effects of these waves.

Figure 6.8 shows the model we used in the calculation. In this model, we assumed that every point within the aperture region is an isotropic wave source. We also assumed that the initial phases of all the injected waves were identical and that there was no wave energy loss in propagation. For simplicity, the geomagnetic field was assumed to be in the vertical direction and the wave propagation paths were assumed to be straight lines. The aperture is assumed to be a circular region.

For parallel propagation, we have (see detail in Chapter 7)

$$-\frac{\partial^2 E_x}{\partial z^2} = \frac{\omega^2}{c^2}\varepsilon(z)E_x \tag{6.2}$$

$$-\frac{\partial^2 E_y}{\partial z^2} = \frac{\omega^2}{c^2}\varepsilon(z)E_y \tag{6.3}$$

where E_x and E_y are the two perpendicular electric field components of the wave, ω is the wave frequency and c is the speed of light. ε is the relative electric permittivity given by $\varepsilon = 1 - X/(1 - Y - iZ)$, where X, Y and Z have been defined in Chapter 1. For waves propagating with a small angle to the magnetic field, equations (6.2) and (6.3) are still approximately valid. In a slowly-varying medium, they can be solved
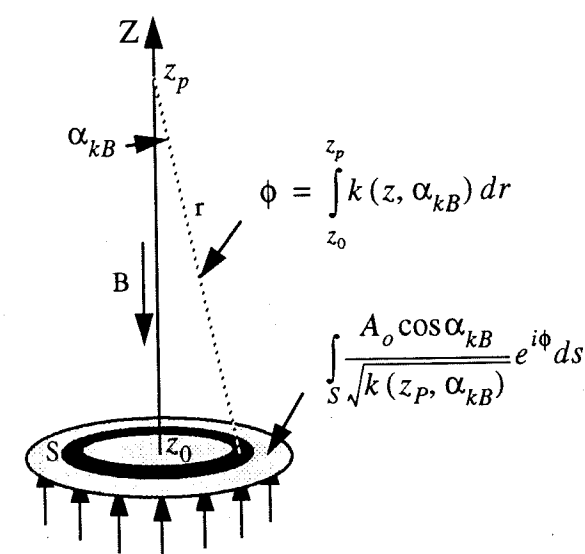

Figure 6.8: A preliminary calculation of wave interference

using the WKB method (Budden, 1985).

For a preliminary calculation, we simply used the WKB solutions of equations (6.2) and (6.3) to calculate the amplitude and the phase of waves. The wave electric field at an altitude of z_p was calculated using

$$E(z_p) = \int_S \frac{A_o \cos\alpha_{kB}}{\sqrt{k(z_P, \alpha_{kB})}} exp\left(i\int_{z_0}^{z_P} k(z, \alpha_{kB})\, dr\right) ds \quad , \qquad (6.4)$$

where A_0 is a constant related to the wave amplitude at the injection altitude, α_{kB} is the angle between the wave normal and the magnetic field, and the wave number

$$k(z, \alpha_{kB}) = \frac{\omega}{c} n_r(z, \alpha_{kB}) \quad .$$

The real refractive index n_r was calculated using the full expression of the Appleton-Hartree equation and the IRI electron density and the effective collision frequency profiles shown in Chapter 1. The wave fields at each point on the axis of the aperture were then calculated by integrating the contribution of all the points over the aperture region.

From the calculation, we found that the interference of waves from an aperture at the base of the ionosphere could generate significant troughs and peaks in the altitude profiles of VLF wave amplitude in the ionosphere. The changes in the altitude profiles depends on the wave frequency, the altitude and the dimension of the aperture. By adjusting these parameters profiles with similar features as those observed by the rockets can be produced.

Examples of the calculated profiles are shown in Figure 6.9. The two profiles, solid lines, in the figure were calculated for waves at 3 kHz and 7 kHz respectively. In this calculation, the altitude and the radius of the aperture were assumed to be 80 km and 60 km respectively, consistent with the previously calculated results for the wave paths (see Chapter 5). For comparison, the wave amplitude profiles received by the WIPP rocket during the entire flight are also shown in this figure.
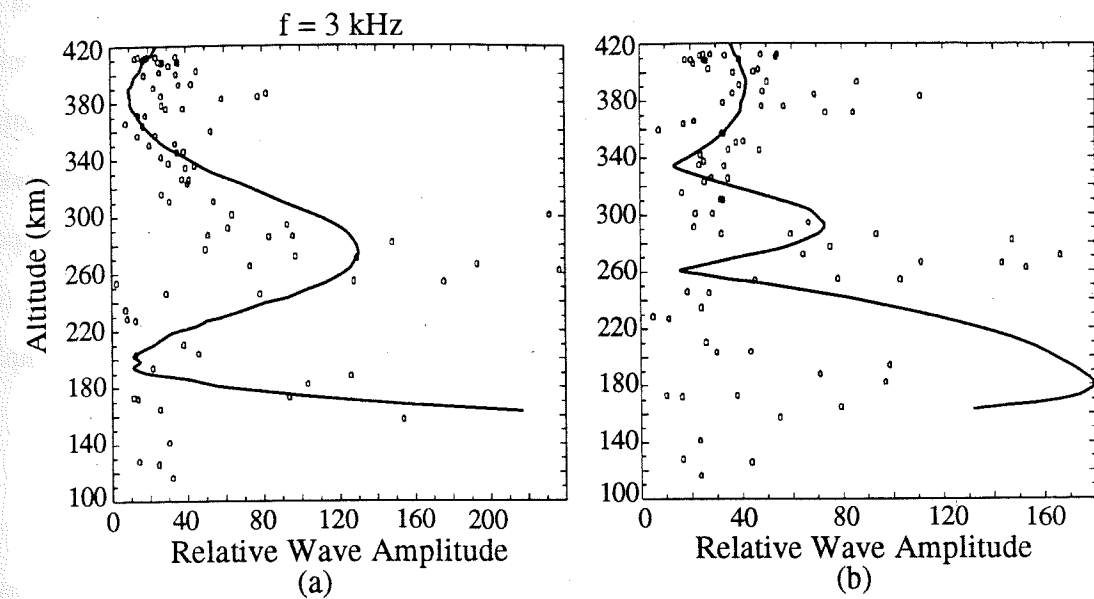
Figure 6.9: Examples of the calculated altitude profiles of VLF wave amplitude. The profiles (the solid curves) shown in (a) and (b) were calculated for waves at 3 kHz and 7 kHz respectively. The dots in the figure are the relative wave amplitude of lightning-generated VLF waves measured by the WIPP rocket during its entire flight.

It is seen in Figure 6.9 (a) that the calculated profile has a significant peak at an altitude of 280 km, which is in good agreement with the rocket data. The calculated profile has a trough at an altitude of 200 km, which can relate to a trough seen at an altitude around 210 km by the rocket. The rocket observed a trough at an altitude around 370 km and the calculated profile also shows a trough at an altitude of 390 km. The calculated profile for 7 kHz waves shown in Figure 6.9 (b) is different from that for 3 kHz waves. In this profile, three peaks occur at altitudes of 180 km, 290 km and 380 km. Examining the observed data, three peaks can also be found, which occur at altitudes of 180 km, 270 km and 390 km. The two troughs shown in the calculated profile at altitudes of 260 km and 330 km may relate to the troughs observed by the rocket at altitudes of 230 km and 320 km.

To calculate the effects of wave interference accurately, the electron density gradient in the lower ionosphere must be considered. The actual wave paths also need to be taken into account. Because of the simplifications in the approximations used in

our preliminary calculation, we do not intend to completely explain the data using these calculated results. In the above, we have pointed out similar features between the calculated profiles and the rocket data. There are apparently some significant differences between the calculated profiles and the data. Nevertheless, our preliminary calculations show that the interference of VLF waves from an aperture located below the rocket could produce features similar to those observed by the rocket. This suggests that the effects of VLF wave interference on the wave amplitude in the ionosphere may be significant.

6.4 CONCLUSION

Significant amplitude changes of lightning-generated VLF waves at altitudes above 150 km have been observed by both the WIPP and the Thunderstorm II rockets. These changes were most likely produced by the spatial structure of the VLF wave amplitude profile, rather than by temporal changes of the lightning sources or other wave propagation factors.

The observed variations in the VLF wave amplitude are not likely to be due to the standing wave pattern produced by wave reflections from different ionospheric layers. The variation did not correlate with changes in the electron density profile and thus cannot be explained simply by changes in the wave refractive index.

This phenomenon has not been reported previously and is of interest regarding the generation and the propagation of VLF waves in the ionosphere. Results from a preliminary calculation indicate that the interference of waves from an aperture region located below the rocket could produce altitude profiles of wave amplitude having features similar to those observed by the rockets. This supports that waves received by rockets in the ionosphere are the coherent superposition of waves from a small aperture region located below the rockets. Each point in this aperture region may be viewed as a source which generates VLF waves at a variety of wave normal angles. The interference of these waves significantly affects the VLF wave amplitude measured in the ionosphere.

CHAPTER 7

THE ABSORPTION OF LIGHTNING-GENERATED
VLF WAVES IN THE LOWER IONOSPHERE

7.1 INTRODUCTION

As we have described earlier, lightning strokes generate strong electromagnetic radiation in the Very Low Frequency (VLF) range. Part of this radiation can couple into whistler mode waves which propagate through the ionosphere and interact with particles in the magnetosphere, producing particle precipitation and other phenomena in the earth's atmosphere and ionosphere (Rosenberg, et al., 1971; Carpenter and LaBelle, 1982; Inan and Carpenter, 1987).

As the whistler waves propagate in the ionosphere, they are subject to absorption due to the collisions between electrons and neutral particles. In this process, electrons acquire energy from the electric field of the wave. After the electrons collide with neutral particles, their direction is changed and the ordered energy imparted by the wave is converted to disordered energy. The average thermal energy of the electrons is thereby increased.

The heating of the ionosphere by radio waves has been well studied (Maslin, 1974). Radio waves have been used as heating sources in some active ionospheric experiments. However, the heating of the ionosphere by very-low-frequency (VLF) waves has not drawn much attention until recent years. One of the observations which generated interest in VLF heating was the "Fast (or Early) trimpi" events (Armstrong, 1983; Inan et al., 1988).

"Trimpi" events are characteristic perturbations in the phase or amplitude of VLF transmitter signals which propagate in the earth-ionosphere waveguide as recorded by VLF receivers on the ground (Carpenter and LaBelle, 1982; Inan and Carpenter, 1987, Inan et al. 1991). It has been suggested that most trimpi events are caused by particle precipitation induced by lightning-generated VLF waves. These precipitating particles enhance the ionization at the base of the ionosphere in a

localized region near the propagation path of the VLF transmitter signal, altering the signal propagation conditions. Normal trimpi events usually occur 0.3-1.5 seconds after the causative lightning, because resonant wave and particle interaction occurs near the magnetic equator and thus the radiation belt particles must travel a large distance before the precipitation can occur. In comparison with normal trimpi events, "Fast (or early) Trimpi" events are VLF signal perturbations which have similar characteristics but occur almost instantaneously (<50 ms) after the causative lightning (Armstrong, 1983; Inan et al., 1988). Such events apparently cannot be explained by the current wave-induced particle precipitation mechanism. One possible explanation for such fast trimpi events is direct heating of the ionosphere by lightning-generated VLF waves. It has been suggested that heating by very strong lightning-generated VLF waves would be enough to produce significant ionization in a local area in the lower ionosphere. This increased ionization could then disturb the sub-ionospheric VLF signals (Inan et al., 1991; Inan, 1990).

As mentioned above, the heating process originates with the absorption of wave energy. Therefore, the calculation of the wave absorption rate is important in the investigation of heating effects in the ionosphere. The ionospheric absorption of radio waves is usually calculated using the WKB approximation, and the wave refractive index given by the Appleton-Hartree equation (Budden, 1985). But since the change of the electric permittivity is so large within a wavelength, the conditions for the WKB approximation may not be satisfied for VLF waves. This is especially true in the lower ionosphere where the largest gradient in permittivity occurs. Generally, the WKB solution and the Appleton-Hartree equation are not appropriate for VLF waves in the lower ionosphere.

In this paper, instead of applying the Appleton-Hartree equation and the WKB approximation, we calculated the absorption of VLF waves at the bottom of the ionosphere numerically for the case of vertical wave injection with a vertical geomagnetic field. The gradient of the permittivity of the ionospheric media was taken into account. First, we compared the WKB results with our numerically

calculated results, and evaluated the deviation of the WKB solution. Then we compared the calculated results with lightning VLF electric field data obtained by a rocket. We found that the lightning VLF spectra recorded by the rocket suggest that there is significant heating of the ionosphere by VLF waves in the lower ionosphere.

7.2 EQUATIONS

Ignoring the effects of ions, we consider the ionospheric media as an electron plasma. For linear waves in the plasma, we then have:

$$\vec{D} = \varepsilon_0 \hat{\varepsilon} \bullet \vec{E}, \tag{7.1}$$

where $\vec{D}$ is the electric displacement, $\vec{E}$ is the electric field and $\hat{\varepsilon}$ is the relative electric permittivity tensor, which can be derived from the momentum equation for electrons. Using Eq. (7.1) in Maxwell's equations, we get

$$\nabla (\nabla \bullet \vec{E}) - \nabla^2 \vec{E} = \frac{\omega^2}{c^2} \hat{\varepsilon} \bullet \vec{E}, \tag{7.2}$$

where c is the speed of light and ω is the frequency of the wave. Here we have assumed that the wave is harmonic.

To simplify the problem, we consider the case for waves that are vertically injected into the ionosphere with the geomagnetic field in the vertical direction. Choosing z to be in the vertical direction, and x and y the two horizontal directions, we have $\partial/\partial x = \partial/\partial y = 0$ and $\partial/\partial z \neq 0$. In this system, the relative permittivity tensor has the form of

$$\varepsilon = \begin{bmatrix} \frac{1}{2}(\varepsilon_1 + \varepsilon_2) & \frac{1}{2}i(\varepsilon_1 - \varepsilon_2) & 0 \\ -\frac{1}{2}i(\varepsilon_1 - \varepsilon_2) & \frac{1}{2}(\varepsilon_1 + \varepsilon_2) & 0 \\ 0 & 0 & \varepsilon_3 \end{bmatrix}, \tag{7.3}$$

where

$$\varepsilon_1 = 1 - X/(1 + Y - iZ), \quad \varepsilon_2 = 1 - X/(1 - Y - iZ), \quad \varepsilon_3 = 1 - X/(1 - iZ) \quad (7.4)$$

and

$$X = \omega_{pe}/\omega, \quad Y = \omega_{ce}/\omega, \quad Z = \upsilon/\omega.$$

In the above equations, ω_{pe} is the plasma frequency, ω_{ce} is the electron gyrofrequency, and υ is the effective collision frequency between electrons and neutral particles. Then Eq. (7.2) gives

$$-\left(\frac{\partial^2 E_x}{\partial z^2}\right) = \frac{1}{2}\frac{\omega^2}{c^2}((\varepsilon_1 + \varepsilon_2) E_x + i(\varepsilon_1 - \varepsilon_2) E_y) \qquad (7.5)$$

$$-\left(\frac{\partial^2 E_y}{\partial z^2}\right) = \frac{1}{2}\frac{\omega^2}{c^2}(-i(\varepsilon_1 - \varepsilon_2) E_x + (\varepsilon_1 + \varepsilon_2) E_y) . \qquad (7.6)$$

For a whistler mode wave in parallel propagation, $E_y = -iE_x$. Then Eq. (7.5) and Eq.(7.6) give

$$-\frac{\partial^2 E_x}{\partial z^2} = \frac{\omega^2}{c^2}\varepsilon_2(z) E_x \quad \text{and} \quad \frac{\partial^2 E_y}{\partial z^2} = \frac{\omega^2}{c^2}\varepsilon_2(z) E_y . \qquad (7.7)$$

As given by Eq. (7.4), $\varepsilon_2(z)$ is related to the electron density profile, the effective collision profile, and the model of the geomagnetic field. If the change in $\varepsilon_2(z)$ is not significant within a wavelength, a W.K.B solution of Eq. (7.7) can be obtained, which is

$$E = \frac{A}{\sqrt{k}}exp(i\int k(z) dz) \qquad (7.8)$$

where $k = \frac{\omega}{c}\sqrt{\varepsilon_2}$, and A is a constant. Here the subscript on E is omitted. The attenuation or absorption of waves can then be calculated from a given permittivity profile by using Eq. (7.8). For the non-parallel propagation case, k is determined by the Appleton-Hartree equation (Budden, 1985).

The WKB approximation does not account for the reflected waves. For radio

waves, the change of permittivity in a wavelength is relatively small and the reflection caused by the permittivity gradient is not significant, so the WKB solution can be a good approximation at high frequency. However, the permittivity gradient in the lower ionosphere is so large for these VLF waves that the reflection of these waves cannot be ignored. Therefore, the WKB solution generally cannot be applied in the bottom region of the ionosphere.

7.3 NUMERICAL SOLUTION

We consider a wave which is vertically injected into a horizontally stratified ionosphere at an altitude of z_0 with an amplitude of E_0. The wave is subject to partial reflections with altitude in the non-uniform media, so that the wave field at each layer is the superposition of the transmitted and reflected wave fields. Because both the permittivity gradient of the ionosphere and the wavelength of the waves decreases with altitude, we can assume the WKB solution becomes approximately valid at a certain altitude z_1 on the upper boundary. Then, Eq. (7.7) can be solved as a boundary value problem:

$$\frac{\partial^2 E}{\partial z^2} = \frac{\omega^2}{c^2}\varepsilon E ; \qquad (7.9)$$

$$E = E_0, \qquad z = z_0 ; \qquad (7.10)$$

$$\frac{\partial E}{\partial z} - i\sqrt{\varepsilon(z)} E \approx 0 , \qquad z = z_1 . \qquad (7.11)$$

The region from z_0 to z_1 is divided into N horizontal layers, each with a thickness of Δz. In the ith layer, Eq. (7.9) can be written as

$$E_{k-1} - b_k E_k + E_{k+1} = 0 , k = 1,2,..., N \qquad (7.12)$$

where $b_k = 2 - \frac{\omega^2}{c^2}\varepsilon_k\Delta z^2 .$

The above N equations can be solved using the boundary conditions from Eq.

(7.10) and Eq. (7.11). Let $E = E_r + iE_i$ and $\varepsilon = \varepsilon_r + i\varepsilon_i$. Then for intermediate layers, we get

$$E_{r_k} = \beta_{r_k}E_{r_{k+1}} - \beta_{i_k}E_{i_{k+1}} + v_{r_k} ,$$

$$E_{i_k} = \beta_{i_k}E_{r_{k+1}} + \beta_{r_k}E_{i_{k+1}} + v_{i_k} , \quad k = 1, 2, ..., N-1 ;$$

where

$$\beta_{r_k} = \frac{a_{r_k}}{a_{r_k}^2 + a_{i_k}^2} , \quad \beta_{i_k} = -\frac{a_{i_k}}{a_{r_k}^2 + a_{i_k}^2} , \quad k \neq 1 ;$$

$$v_{r_k} = \frac{a_{r_k}v_{r_{k-1}} + a_{i_k}v_{i_{k-1}}}{a_{r_k}^2 + a_{i_k}^2} , \quad v_{i_k} = \frac{a_{r_k}v_{i_{k-1}} - a_{i_k}v_{r_{k-1}}}{a_{r_k}^2 + a_{i_k}^2} , \quad k \neq 1;$$

$$a_{r_k} = b_{r_k} - \beta_{r_{k-1}} , \quad a_{r_k} = b_{i_k} - \beta_{i_{k-1}} ;$$

$$b_{r_k} = 2 - \frac{\omega^2}{c^2}\varepsilon_{r_k}\Delta z^2 , \quad b_{i_k} = -\frac{\omega^2}{c^2}\varepsilon_{i_k}\Delta z^2 .$$

At the lower boundary, we have

$$\beta_{r_1} = -\frac{b_{r_1}}{b_{r_1}^2 + b_{i_1}^2} , \quad \beta_{i_1} = -\frac{b_{i_1}}{b_{r_1}^2 + b_{i_1}^2} ;$$

$$v_{r_1} = \frac{b_{r_1}E_o + b_{i_1}E_{i_0}}{b_{r_1}^2 + b_{i_1}^2} , \quad v_{r_1} = \frac{b_{r_1}E_{i_o} - b_{i_1}E_{r_0}}{b_{r_1}^2 + b_{i_1}^2}$$

At the top boundary, E_N is determined by

$$E_{r_N} = \frac{av_{r_N} + bv_{i_N}}{a^2 + b^2} \quad \text{and} \quad E_{i_N} = \frac{av_{i_N} - bv_{r_N}}{a^2 + b^2} ,$$

where

$$a = 1 - (1 + k_i\Delta z)\beta_{r_N} - k_r\Delta z\beta_{i_N} ,$$

$$b = k_r\Delta z\beta_{r_N} - (1 + k_i\Delta z)\beta_{i_N} .$$

In the above equations, k_{i_N} and k_{r_N} are the imaginary and real wave numbers at $z = z_1$. They are calculated by

$$k_{r_N} = \frac{\omega}{c}(\varepsilon_r(z1)^2 + \varepsilon_i(z1)^2)^{1/4}\cos\frac{\varphi}{2} ,$$

$$k_{i_N} = \frac{\omega}{c}(\varepsilon_r(z1)^2 + \varepsilon_i(z1)^2)^{1/4}\sin\frac{\varphi}{2} ,$$

where $\varphi = \text{atan}(\varepsilon_i/\varepsilon_r)$.

The wave amplitude is given by $E = \sqrt{E_r^2 + E_i^2}$. The average Poynting flux of the wave is calculated using

$$S_i = \frac{1}{2\mu\omega\Delta z}[E_{i_k}(E_{r_{k+1}} - E_{r_k}) - E_{r_k}(E_{i_{k+1}} - E_{i_k})], \quad k = 1, 2, ..., N-1$$

The profiles of night-time electron density and the effective collision frequency of electrons and neutral particles used in our calculations were given in Chapter 1. Based on the profiles, the lower and upper boundaries were chosen to be at 80 km and 100 km respectively. The profiles of the electron density and the collision frequency in the altitude range are shown in detail in Figure 7.1. The geomagnetic field was taken as a dipole field with an intensity of 0.38 Gauss at the earth surface.

At the upper boundary, it was assumed that the only wave was the upward transmitted wave which can be approximated using the WKB solution. This assumption was used for two reasons: 1) Our concern is the absorption in the region below 90 km. In this region, the dominant downward waves are the reflected waves from the region around 93 km where a peak of permittivity gradient exists. Above 100 km, the transmitted wave has been strongly attenuated, and the ionospheric permittivity gradient becomes relatively smaller. So the reflected waves from above 100 km are not significant in the region below 93 km. 2) Since the change in electron density at an altitude of 100 km is small, the gradient of permittivity around this altitude is not significant.
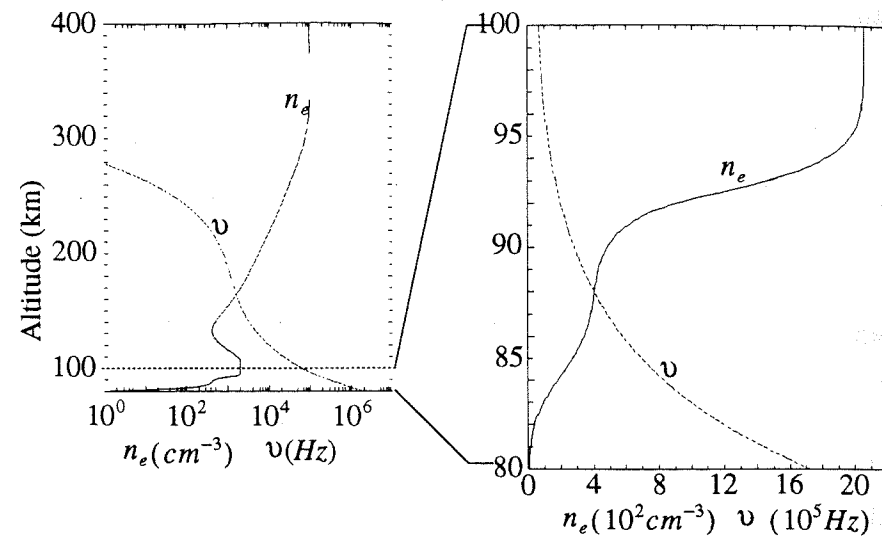
Figure 7.1: The profiles of electron density and the effective collision frequency used in the calculations

In these calculations, the region from 80 km to 100 km was divided into 200 layers (N=200). The thickness of each layer was much smaller than the wavelengths being considered.

7.4. NUMERICAL RESULTS AND WKB RESULTS

As an example, Figure 7.2 shows the calculated results of the electric field Er, Ei, E, and Poynting flux S of a 10 kHz wave. The electric field, Er_0 and Ei_0, were set to 1 and 0 V/m respectively. The changes of Er and Ei with altitude include the changes of the wave phase, the wave refractive index and the wave energy. The wave amplitude E, calculated from Er and Ei, decreased by 70% from 80 km to 100 km. At an altitude of 87 km, there is an increase in wave amplitude. This increase is caused by the interference between the up-going and down-going waves, and it may also appear at other altitudes and at other frequencies. However, even though the wave amplitude increases at certain altitudes, the Poynting flux of the wave decreases monotonically with altitude. This was expected since the waves should not gain any energy in this region. The Poynting flux decreases from 1 erg $\cdot$ cm^{-2} $\cdot$ s^{-1} at 80 km to

0.65 erg $\cdot$ cm^{-2} $\cdot$ s^{-1} at 100 km. This is equivalent to a 3.7 dB attenuation in the wave intensity.
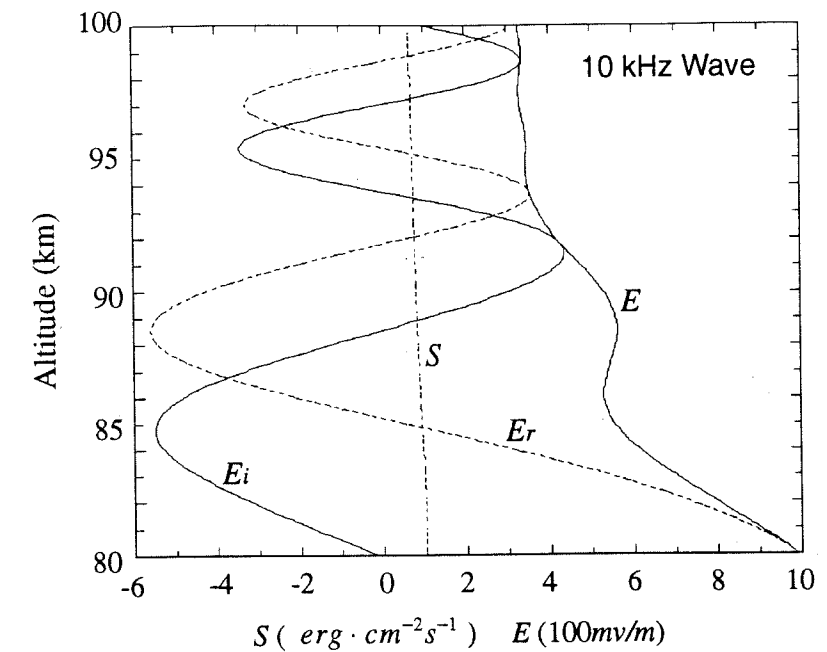

Figure 7.2: Changes of the electric field and energy flux of a 10 kHz wave along the altitude from numerical calculation

With the numerically calculated results, we can evaluate the WKB approximation for VLF waves in the lower ionosphere. Figure 7.3(a) and 7.3(b) show the amplitudes and the energy fluxes calculated by both numerical and WKB methods for 10 kHz and 5 kHz waves in parallel propagation with vertical injection conditions. In Figure 7.3(a), the wave energy flux at the injection point in the numerical result is smaller than that in the WKB result. This is because the transmitted and reflected waves at 10 kHz interfere constructively at 80 km, so that the wave amplitude of E_0 at the lower boundary actually represents a transmitted wave with a smaller amplitude. This effect is reversed at some of the other frequencies, and it does not affect the calculation of the wave absorption rate.

It is shown in Figure 7.3 that the wave amplitude of the WKB results decreases throughout the altitudes from 80 km to 100 km, and does not show the structure caused by the interference of transmitted and reflected waves. From the numerical
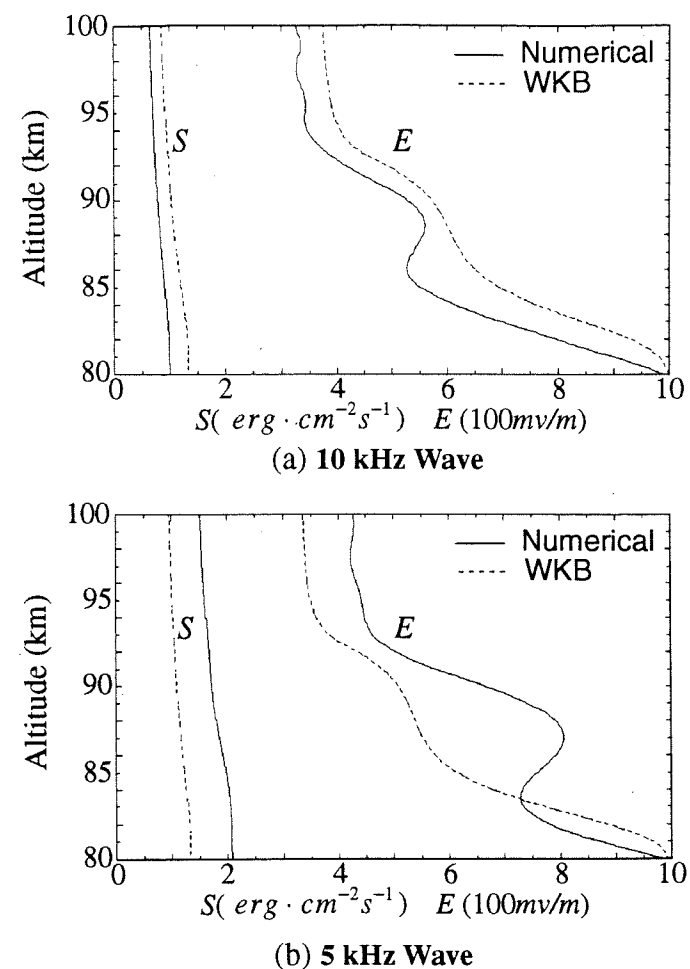
$$\sum_f \frac{1}{S_0}\frac{dS}{dz} \quad (1/1000)$$

Figure 7.5.: Total absorption rates of waves from 0.5 kHz to 10 kHz

contributions by all of the frequencies generated by lightning strokes. The dominant VLF radiation from a lightning stroke is normally in the range of 1-10 kHz (Alpert, et al., 1967).   Using both the numerical and the WKB methods, we calculated the total absorption rate of waves from 0.5 kHz to 10 kHz. Calculations were made every 0.25 kHz, and the absorption rates were then integrated in a flat spectrum from 0.5 kHz to 10 kHz. The result is shown in Figure 7.5. It is seen in this figure that the altitude of the absorption peak calculated using the numerical method is slightly higher than that using the WKB method.   Except for this, the integral absorption rates calculated by the two methods are nearly identical.
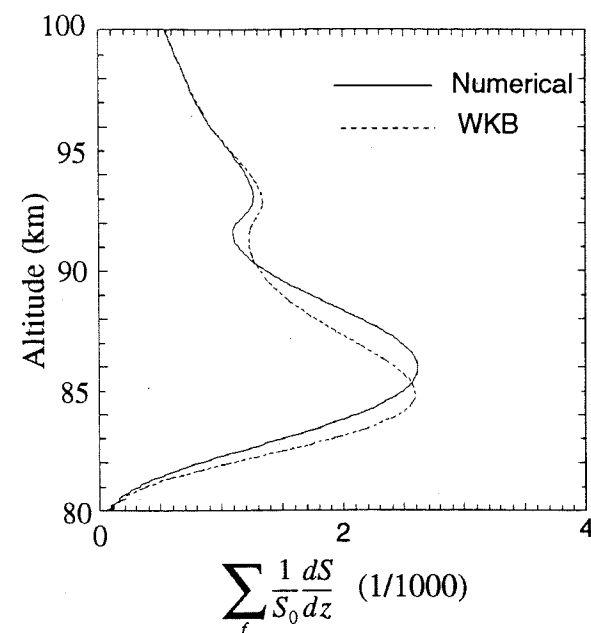
7.5 COMPARISON OF CALCULATIONS AND MEASUREMENTS

As shown above, the absorption of VLF waves in the lower ionosphere increases at higher frequencies.   As the lightning-generated VLF waves propagate through the lower ionosphere, the wave components at higher frequencies are subject to greater energy losses. This filter effect can be investigated by comparing the lightning spectra obtained on the ground and in the ionosphere.

The VLF radiation produced by cloud-ground lightning strokes have been

measured on the ground in previous experiments (Watt and Maxwill, 1957; Taylor, 1963 and Alpert et al., 1967). Typically, the energy peaks of the lightning VLF spectrum range from 5 kHz to higher frequencies.   Some experiments have shown that a peak at 5 kHz is a common feature in the VLF spectrum of whistler-producing lightning strokes measured on the ground (Helliwell, 1965).

The lightning-generated VLF waves in the ionosphere were measured by the WIPP and Thunderstorm rockets.   Figure 7.6 shows the average power spectra of 42 lightning-generated whistler wave packets measured by the WIPP rocket at altitudes from 200 km to 400 km. The sources of the 42 wave packets were all cloud-ground lightning strokes located within several hundred kilometers of the rocket. It is seen in Figure 7.6 that the peak energy intensity of these VLF waves in the ionosphere was at approximately 1kHz. Above 1 kHz, the energy decreased sharply with frequency. Up to 5 kHz, the energy was reduced to less than 10% of the peak value.   This spectra is different from the lightning spectrum measured on the ground which would typically have much higher energy densities at 5 kHz
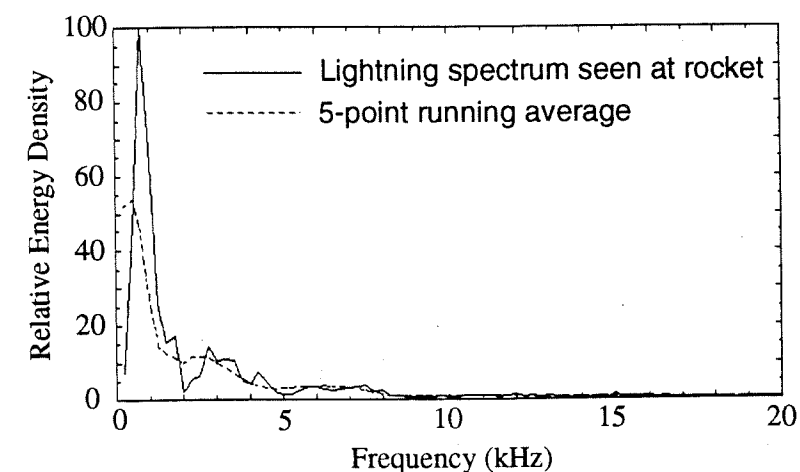

Figure 7.6: Average spectrum of 42 lightning-generated wave packets recorded by the WIPP rocket at altitudes from 200km to 400km

The difference between the spectra measured on the ground and at the rocket is very likely produced by the filtering effect of ionospheric absorption. As we have shown above, the peak absorption of VLF waves in the ionosphere occurs at an

altitude between 80 km and 90 km. Above 100 km, the wave absorption rate is greatly reduced due to the decrease in collision frequency between electrons and neutral particles. The wave energy lost in the region between 80 km and 100 km is much larger than the energy lost at higher altitudes. So the difference between the spectra should be produced mainly by the absorption at altitudes between 80 km and 100 km. However, having calculated the ionospheric absorption using the standard collision frequency profile shown in Figure 7.1, we concluded that the absorption could not change the wave spectrum this much unless a collision frequency profile with much higher values was used.

We noticed that the frequency dependence of the ionospheric absorption at VLF frequencies became more significant as the effective collision frequency increases in a certain range. To show this, we increased the collision profile in Figure 7.1 by factors of 10, 100, 300, and 500, and then calculated the change in the energy flux ratio between 80 and 100 km with frequency for each case. The results are shown in Figure 7.7. It is apparent that wave absorption at all frequencies is greatly increased as a result of increasing the collision frequency. But the increase at higher
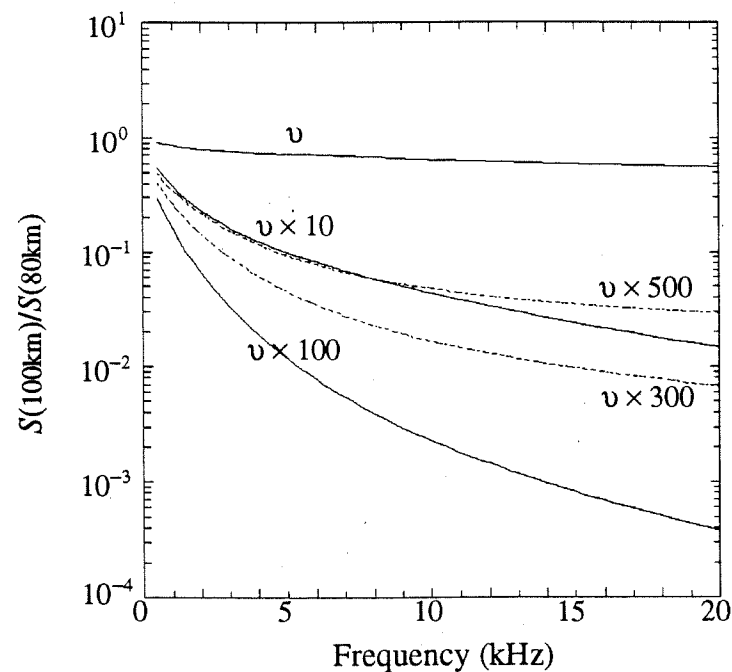

Figure7. 7: Wave attenuation rates calculated from the different profiles of effective collision frequency

frequencies was much higher than those at lower frequencies. For example, as the collision frequency was increased by a factor of 10, the attenuation rate at 1 kHz increased (the Poynting flux decreased as in Figure 7.7) approximately 10 dB while the attenuation rate at 20 kHz increased 40 dB (the Poynting flux decreased by a factor of 100). This effect is more pronounced when the collision frequency is increased by a factor of 100. The frequency dependence of ionospheric absorption is decreased as the collision frequency is further increased, which is shown in Figure 7.6. In this case, the motions of electrons start to be dominated by collisions, and the energy the electrons gain from the waves is mainly determined by the collision frequency instead of the wave frequency.

We calculated the possible changes in an average cloud-ground lightning spectrum using ionospheric absorptions with different collision frequency profiles. Three collision frequency profiles were used, the standard one in Figure 7.1 and the two increased by factors of 10 and 100. The calculated results are shown in Figure 7.8. In the figure, the solid line is a average VLF spectrum of cloud-ground lightning measured on the ground within a distance of 100km from the lightning strokes (Alpert et al, 1967). The dashed lines show the spectrum if an absorption effect, such as that of Figure 7.7, is applied. The spectra have been normalized to their peak value. It is seen from this figure that the absorption calculated using the standard collision
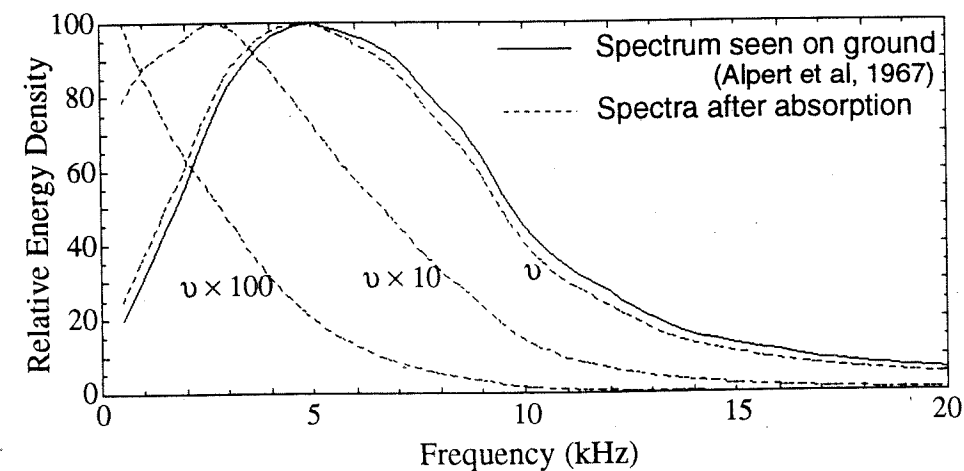

Figure.7. 8: Spectrum changes caused by the absorption of the ionosphere

frequency profile does not significantly change the wave spectra. In comparison with the data in Figure 7.6, it is apparent that the absorption calculated using the highest collision frequency profile, which is 100 times greater than the standard profile, can best explain the observed data.

The profile of effective collision frequency shown in Figure 7.1 is based on many measurements and has been widely used (Budden, 1985), however, it is very unlikely to be the actual profile in our situation. The profile of collision frequency does change slightly with time of day and with seasons. It also depends on latitude. But these changes are very small and can be generally ignored (Budden, 1985). A plausible explanation for an actual higher collision frequency profile could be due to the self-modulation effect of the lightning-generated VLF waves.

As the wave energy is absorbed in a region of the ionosphere, the local electron temperature is increased. The increase in electron temperature will then lead to an increase in the collision frequency, which, in turn, will cause stronger absorption. Such a self-modulation effect has been observed and studied at radio frequencies (Maslin, 1974). It has been suggested that it plays a critical role in the heating of the ionosphere by lightning-generated VLF waves (Inan et al., 1991). But so far there has not been any reported evidence of the self-modulation effect on lightning-generated VLF waves. The spectrum of VLF waves measured in the ionosphere appears to be the first evidence for significant self-modulation of lightning-generated VLF waves in the lower ionosphere.

7.6 SUMMARY

Numerical calculations were made for VLF waves propagating upward in the lower ionosphere. The WKB approximation was evaluated using numerically calculated results. It was shown that the WKB method is not appropriate for calculating the amplitude of VLF waves in the lower ionosphere. For an individual wave, such as from a transmitter, the wave absorption rates and the maximum absorption layer calculated from the WKB method could have significant differences

from the real case. For lightning-generated VLF waves, which approximately cover a spectra from 1 kHz - 10 kHz, the total absorption calculated by WKB method seems to be a good approximation.

Both the calculations and the wave spectra recorded by a rocket show the frequency dependence of ionospheric absorption at VLF frequencies. The spectrum of lightning-generated VLF waves received at the rocket suggests that the actual effective collision frequency profile might be much larger than the standard profile being widely used. This appears to be the first observational evidence that the self-modulation effect is significant for lightning-generated VLF waves in the lower ionosphere. This also implies that there is significant heating of the lower ionosphere by lightning-generated VLF waves.

The frequency dependence of ionospheric absorption at VLF frequencies changes with the effective collision frequency. By simultaneously measuring the amplitudes of VLF waves at different frequencies on the ground and in the ionosphere we may be able to investigate the heating effects in the lower ionosphere.

CHAPTER 8

CONCLUSIONS

8.1 SUMMARY

In this dissertation, we studied lightning-generated VLF waves in the ionosphere using the data from the Wave Induced Particle Precipitation (WIPP) and the Thunderstorm II campaigns. We have observed some phenomena which have not been previously reported. We have also obtained some model results regarding the propagation and absorption of VLF waves in the ionosphere. The main points of this dissertation are summarized as follows:

a) Our down-looking optical lightning detector on the WIPP rocket detected some Anomalous Optical Events (AOEs) which do not resemble any other known phenomena in the earth's atmosphere and ionosphere. These optical events were normally accompanied with weak VLF sferics clusters and were associated with the "fast trimpi" events. These events occurred at altitudes above 30 km and might have been caused by high-altitude electrical discharges.

b) We investigated the relation between the amplitude of lightning-generated VLF waves measured in the ionosphere by the rockets and the intensity of lightning currents measured on the ground by the SUNYA lightning network. It was found that at frequencies below 5 kHz the amplitude of VLF waves in the ionosphere had positive linear responses to the lightning current intensity. At frequencies above 5 kHz, the linear correlation between the wave amplitude and the SUNYA current intensity was poor. This indicated that lightning strokes with stronger SUNYA currents did not necessarily launch stronger VLF waves into the ionosphere at frequencies above 5 kHz.

c) Using the data from the optical lightning detector, we have been able to determine the propagation times of lightning-generated VLF waves received by the rockets. From their propagation times, we determined that these waves were coupled into the ionosphere from a localized area directly below the rockets. This indicates

that VLF waves generated by lightning with a horizontal range further than several hundred kilometers are injected into the ionosphere by the "leaky waveguide" mechanism, instead of the "aperture antenna" mechanism.

d) We found that the amplitude of lightning-generated VLF waves did not monotonically decrease with altitude in the ionosphere as normally expected; it instead had significant peaks and troughs at altitudes above 150 km. Such altitude profiles of VLF wave amplitude cannot be explained by standing wave patterns or by variations in the ionospheric electron density.

e) In an effort to interpret the altitude profile of VLF wave amplitude, we synthesized a model to investigate the possible effects of VLF wave interferences. In this model, VLF waves received at the rocket were regarded as the coherent superposition of waves from an "aperture" area below the rocket. Preliminary calculations show that this model could produce altitude profiles of VLF wave amplitudes similar to those observed by the WIPP and Thunderstorm II rockets.

f) The direct heating of the lower ionosphere by lightning-generated VLF waves has evoked interest in recent years. This heating is caused by wave absorption in the lower ionosphere, which is normally calculated using the WKB approximation. However, due to the sharp electron density gradient, the conditions for the WKB approximation are generally not valid for VLF waves in the lower ionosphere. We performed a numerical calculation to investigate the absorption of VLF waves in the lower ionosphere, in which the electron density gradient was taken into account. The WKB approximation was evaluated using the numerical results.

g) Our calculations showed that the frequency dependence of the VLF wave absorptions in the lower ionosphere became more significant as a result of increasing the collision frequency between the electrons and neutral particles. We found that the peak frequency in the average spectra of lightning-generated waves received by rockets was generally lower than that in the spectra received on the ground. We also found that the difference between the spectra received by the rockets and on the ground supported the hypothesis of a significant enhancement of the collision

frequency in the lower ionosphere. This is the first direct evidence for the significant "self-modulation" effects of lightning-generated VLF waves in the lower ionosphere and also an evidence of heating of the lower ionosphere by the lightning-generated VLF waves.

8.2 FUTURE STUDIES

Our studies have improved our knowledge of the lightning-generated VLF waves in the ionosphere, but many questions still remain. A summary of suggested future studies follows:

a) The Anomalous Optical Events (AOEs) detected by the WIPP rocket have not yet been well understood. Further observations by rockets and balloons are required to study the causes and effects of this phenomenon. Since the AOE is usually accompanied by characteristic VLF signals, it is also possible to investigate this phenomenon using the ground-based VLF receivers. If AOE's are caused by high altitude discharges, they may turn out to be extremely important to heating and dynamics in the ionospheric D region.

b) We have determined that the typical lightning-generated VLF packets received by rockets at a horizontal range farther than several hundred kilometers from the sources were coupled into the ionosphere in the "leaky waveguide" mechanism. We have not been able to observe any effects generated by the "aperture antenna" mechanism (Kelley, et al, 1985). The wave spectra and power generated by the aperture antenna may be different from that generated by lightning return strokes. The Thunderstorm II rocket has detected strong electric field pulses shortly before receiving the typical lighting-generated VLF packets (Kelley et al., 1990). These pulses were suggested to be caused by whistler waves at frequencies above 60 kHz. It would be of our interests to investigate if these high frequency waves were generated in the ionospheric media by an "aperture antenna" or launched into the ionosphere from the earth-ionosphere waveguide.

c) We have proposed a new wave interference model to explain the altitude

profiles of the amplitude of lightning-generated VLF waves observed by the WIPP and the Thunderstorm II rockets. Our preliminary calculations of the model have shown some promising results. But more accurate calculations are necessary in order to evaluate the model. The gradient of electron density and real wave paths should be taken into account in the further calculation. The possible effects of the altitude profiles of VLF waves on ionospheric processes relevant to the VLF waves also need to be studied.

d) The absorption of VLF waves in the lower ionosphere in known to increase with frequency. Our calculation shows that this frequency dependence of the absorption is enhanced as a result of increasing the collision frequency between the electron and neutral particles. Therefore, measuring the relative amplitudes of VLF waves at two frequencies in the ionosphere may be a method in future experiment to detect the collision frequency changes (or heating effects) in the lower ionosphere.

e) From the data of the WIPP and Thunderstorm II campaigns, it is possible to estimate the total VLF energy injected into the ionosphere by an average lightning stroke. From our calculations of VLF wave absorptions, the energy deposition by lightning-generated VLF waves at each altitude in the lower ionosphere can be estimated. It thus appears possible to evaluate from the data both the large-scale and the small-scale effects of lightning-generated VLF energy in the lower ionosphere in comparison with other energy sources in the region, such as solar radiations and precipitating particles.

BIBLIOGRAPHY

Alpert, J. L., D. S. Fligel, and G. A. Michailova, The propagation of atmospherics in the earth-ionosphere waveguide, *J. Atmos. Terr. Phys., 29*, 29, 1967

Armstrong, W. C., Radio propagation evidence suggesting discharge and other coupling to the ionosphere (and possible triggered lightning), *EOS, 68*, No. 44, 1222, 1987

Armstrong, W. C., A Gas-discharge trigger experiment which might account for the synchronization of some lightning by whistlers, *EOS, 69*, No. 16, 445, 1988

Armstrong, W. C., Observed frequency anomalies in atmospheric VLF radio impulses: their predominance in clusters associated with possible coupling between lightning discharges and the ionosphere, *EOS, 70*, No. 15, 292, 1989

Arnoldy, R. L., P. M. Kintner, Rocket observations of the precipitation of electrons by ground VLF transmitters, *J. Geophys. Res., 94*, 6825, 1989

Boulch, M. L. and C. Weidman, UHF-VHF radiation from lightning, Lightning Electromagnetics, Hemisphere Publishing Corporation, p211, 1990

Bell, T. F., U. S. Inan, V. S. Sonwalkar, and R. A. Helliwell, DE-1 observations of lower hybrid waves excited by VLF whistler mode waves, *Geophys. Res. lett., 18*, 393, 1991a

Bell, T. F., R. A. Helliwell, and M. K. Hudson, Lower hybrid waves excited through linear mode coupling and the heating of ions in the auroral and subauroral magnetosphere, *J. Geophys. Res., 96,* 11,379, 1991b

Berger, K., The Earth flash, Lightning, vol. 1, 119, Academic press, London, 1977

Boys, C. V., Progressive lightning, *Nature, 118,* 749, 1926

Brault, J. W. and O. R. White, The analysis and restoration of astronomical data via the fast fourier transform, *Astron. & Astrophys. 13,* 169, 1971

Brittain, R., P. M. Kintner, and M. C. Kelley, Standing wave patterns in VLF hiss, *J. Geophys. Res., 88,* 7059, 1983

Brook, M. and T. Ogawa, The Cloud Discharge, Lightning, Vol. 1, 191, Academic press, London, 1977

Burton, E. T. and E. M. Boardman, Audio-frequency atmospherics, *Proc. I. R. E., 21,* 1476, 1933

Carpenter, D. L., and J. W. LaBelle, A study of whistlers correlated with bursts of electron precipitation near L = 2, *J. Geophys. Res., 87,* 4427, 1982

Carpenter, D. L., U. S. Inan, M. L. Trimpi, R. A. Helliwell, and J. P. Katsufrakis, Perturbations of subionospheric LF and MF signals due to whistler-induced electron precipitation bursts, *J. Geophys. Res., 89,* 4427, 1984

Carpenter, D. L. and R. E. Orville, The excitation of active whistler mode signal paths in the magnetosphere by lightning, *J. Geophys. Res., 94,*8886, 1989

Chalmers, J. A., Atmospheric Electricity, Clarendon Press, Oxford, 151, 1949

Christian, H. J., R. L. Frost and S. J. Goodman, The optical characteristics as measured from above cloud tops, *VII International Conference on Atmospheric Electricity*, American Meteorological Society, 1984

Etcheto, J., R. Gendrin, J. Solomon and A. Roux, A self-consistent theory of magnetospheric ELF hiss, *J. Geophys. Res., 78,* 8150, 1973

Franz, R. C., R. J. Nemzek and J. R. Winckler, Television image of a huge cloud-to-space discharge above a thunderstorm system, *Science*, 249, 48, 1990.

Goldberg, R. A., S. A. Curtis, and J. R. Barcus, Direct observation of magnetospheric electron precipitation by lightning, *J. Atmos. Terr. Phys. 48*, 293, 1986

Hargreaves, J. K., The upper atmosphere and solar-terrestrial relations: an introduction to the aerospace environment, Van Nostrand Reinhold Co. Ltd., 1979

Hale, L. C., The coupling of ELF/ULF energy from lightning and MEV particles to the middle atmosphere, ionosphere and global circuit, submitted to *J. Geophys. Res.*, 1992

Hale, L. C., and M. E. Baginski, Current to the ionosphere following a lightning stroke, *Nature, 329,* 814, 1987

Heide, F., Meteorites, the University of Chicago press, 1964

Helliwell, R. A., Whistlers and related ionospheric phenomena, Stanford university press, Stanford, Calif., 1965

Helliwell, R.A., J. P. Katsufrakis and M. L. Trimpi, Whistler-induced amplitude perturbation in VLF propagation, *J. Geophys. Res., 78,* 4679, 1973

Helliwell, R. A., A. G. Jean and W. L. Taylor, 1958. Some properties of lightning impulses which produce whistlers. *Proc. IRE, 46*(10), 1760-62. P.121 (ch 4.)

Henderson, R. W., R. E. Orville, and V. P. Idone, An independent check of the peak current estimates from magnetic direction finding systems, *EOS, Trans. AGU., 69,* 1988

Holzworth, R. H., M. C. Kelley, C. L. Siefring, L. C. Hale and J. D. Mitchell, Electrical measurements in the atmosphere and the ionosphere over an active thunderstorm, 2. Direct current electric fields and conductivity, *J. Geophys. Res., 90,* 9824, 1985

Holzworth, R. H., K. W. Norville, P. M. Kintner and S. P. Powell, Stratospheric conductivity variations over thunderstorms, *J. Geophys. Res., 91,* 13257, 1986

Hu, H., R. H. Holzworth and Y. Q. Li, Thunderstorm related variations in stratospheric conductivity measurements, *J. Geophys. Res., 94,* 16429, 1989

Inan, U. S. and D. L. Carpenter, Lightning-induced electron precipitation events observed at L ~ 2.4 and phase and amplitude perturbations on subionospheric VLF signals, *J. Geophys. Res., 92,* 3293,1987

Inan, U. S. T. F. Bell and J. V. Rodriguez, Heating and ionization of the lower ionosphere by lightning, *Geophys. Res. Lett., 18,* 705, 1991

Ishikawa, H. and A. Kimpara, Lightning mechanism and atmospheric radiation, Recent Advances in Atmospheric Electricity, 583,Pergamon press, London, 1958

Jacchia, L. G., Photographic meteor phenomena and theory, Harvard College Observatory and Center of Analysis of M. I.T., Technical report number 3, Cambridge, 1949

Jackson, J. D., Classical electrodynamics, second edition, John Willey & Sons, New York, 1975

Kelley, M. C., C. L. Siefring, R. F. Pfaff, P. M. Kintner, M. Larsen, R. Green, R. H. Holzworth, L. C. Hale, J. D.Mitchell and D. Le Vine, Electrical measurements in the atmosphere and the ionosphere over an active thunderstorm,1. Campaign overview and initial ionospheric results, *J.Geophys. Res., 90,* 9815, 1985

Kelley, M. C., J. G. Ding, G. Berg, R. H. Holzworth, K. D.Baker and R. B. Torbert,

Lightning effects in the ionosphere above 400 km: The thunderstorm II campaign, *EOS, 69,*No. 44, 1063, 1988

Kelley, M. C., J. G. Ding and R. H. Holzworth, Intense ionospheric electric field pulses generated by lightning, *Geophys. Res. lett. 17,* 2221, 1990

Kennel, C. F., and H. E. Petschek, Limit on stably trapped particle fluxes, *J. Geophys. Res., 71,* 1, 1966

Kimpara, K. Electromagnetic energy radiated from lightning, Problems of Atmospheric and Space Electricity, Elsevier Publishing Company, page 352, 1965

Kintner, P. M., R. Arnoldy, M. McCarthy, R. Holzworth, D. Massey, G. Parks and U. Inan, A sounding rocket investigation of lightning induced wave particle precipitation, *EOS, 68,* No. 44, 1987

Kintner, P. M., R. Brittain, M. C. Kelley, D. L. Carpenter and M. J. Rycroft, In situ measurements of transionospheric VLF wave injection, *J. Geophys. Res., 88,* 7065, 1983

Kitagawa, N. and M. Kobayashi, Field-changes and variations of luminosity due to lightning flashes, Recent Advances in Atmospheric Electricity, 445, Pergamon press, London, 1958

Kitagawa, N., M. Brook and E. J. Workman, Continuing currents in cloud-to-ground lightning discharges, *J. Geophys. Res., 67,* 637, 1962

Li, Y. Q., R. H. Holzworth, H. Hua, M. McCarthy, R. D. Massey, P. M. Kintner, J. V. Rodriguez, U. S. Inan and W. C. Armstrong, Anomalous optical events detected by rocket-borne sensor in the WIPP campaign, *J. Geophys. Res., 96,* 1315, 1991

Lin, Y. T., M. A. Uman and R. B. Standler, Lightning return stroke models, *J. Geophys. Rev., 85,* 1571, 1980

Lin, Y. T., M. A. Uman, J. A. Tiller, R. D. Brantley, W. H. Beasley, E. P. Krider, and C. D. Weidman, Characterization of lightning return stroke electric and magnetic fields from simultaneous two-station measurements, *J. Geophys. Rev.,84,* 6307, 1979

Lohrey, B. and A. B. Kaiser, Whistler-induced anomalies in VLF propagation, *J.*

Geophys. Res., 84, 5121, 1979

Master, M. J., M. A. Uman, Y. T. Lin, and R. B. Standler, Calculations of lightning return stroke electric and magnetic fields above ground, *J. Geophys. Res., 86,* 12, 127, 1981

Mackerras, D. A., Comparison of discharge processes in cloud and ground lightning flashes, *J. Geophys. Res., 73,* 1175, 1968

Massey, R. D., M. McCarthy and G. Parks, An upper limit on lightning-induced electron precipitation at mid-latitudes, in press *Geophys. Res., Letters,* 1990

Malan, D., Sur les decharges orageuses dans la haute atmosphere, *Compte Rendus Acad. Sci. Paris 205,* 812, 1937.

Maynard, N. C., T. L. Aggson, and J. P. Heppner, Electric field observations of ionospheric whistlers, *Radio Science 5,* No. 7, 1049, 1970.

McCartney, E. J., Optics of the Atmosphere, 97, John Wiley & Sons, New York, 1976

Mogono, Choji, Thunderstorm, Developments in Atmospheric Science, 12, Elsevier Scientific Publishing Company, 1980

Nanevicz, J. E., E. F. Vance, and J. M. Jamm, Observation of lightning in the frequency and time domains, Lightning Electromagnetics, Hemisphere Publishing Corporation, p. 191,1990

Nemzek, R. J. and J. R. Winckler, Observation and interpretation of fast sub-visual light pulses from the night sky, *Geophys. Res. Letters, 16,* 1015, 1989

Newman, M. M., Lightning discharge channel characteristics and related atmospherics, Recent Advances in Atmospheric Electricity, Proceedings of the second conference on atmospheric electricity, Pergamon Press, page 475, 1958

Norinder, H.,m and E. Knudsen, The relation between lightning discharges and whistlers. *Planet. Space Sci.,1,* 173, 1959

Ogawa, T. and M. Brook, The mechanism of the intracloud lightning discharge, *J. Geophys. Res, 69,* 5141,1964

Ögelman, H., Millisecond time scale atmospheric light pulses associated with solar and magnetospheric activity, *J. Geophys. Res., 78,* 3033, 1973

Orville, R. E., R. W. Henderson, and L. F. Bosart, An east coast lightning detection network, *Bull. Am. Meteorol. Soc., 64,* 1029, 1983

Orville, R. E., R. A. Weisman, R. B. Pyle, R. W. Henderson, and R. E. Orville, Jr., Cloud-to-ground flash characteristics from June 1984 through May 1985, *J. Geophys. Res., 92,* 5640, 1987

Omholt, A., The optical aurora, Springer, Berlin, 1971

Press, W. H., B. P. Flannery, S. A. Teukolsky, and W. T. Vetterling, Numerical Recipes (FORTRAN version), Cambridge Univ. Press, 1990

Pierce, E. T., Very-low-frequency atmospherics due to lightning flashes. Prepared under Air Force Contract No. AF 33(657)-7009 by Stanford Research Institute, Menlo Park, Calif. p.121, 1962

Pierce, E. T., Atmospherics and radio noise, Lightning, Vol. 1, New York: Academic Press, p 351-384, 1977

Ratcliffe, J. A., The Magneto-ionic theory and its applications to the ionosphere, Cambridge, Eng.: Cambridge Univ. Press. p 16, 23, 27, 61, 1959

Rawer, K., D. Bilitza and S. Ramakrishnan, Goals and status of the IRI, *Rev. Geophys. Space Phys. 16,* 177, 1978

Robinson, N., Solar Radiation, Elsevier publishing company, Amsterdam, 1966

Rodriquez, J. V., U. S. Inan, W. C. Armstrong, Y. Q. Li, R. H. Holzworth, A. J. Smith, R. E. Orville, and T. J. Rosenberg, Unusual trimpi events observed during a particle injection event, to be submitted to *J. Geophys. Res.,*1990

Rodriquez, J. V., U. S. Inan, Y. Q. Li, R. H. Holzworth, A. J. Smith, R. E. Orville and T. J. Rosenberg, A case study of lightning, whistlers, and associated ionospheric effects during a substorm particle injection event, *J. Geophys. Res.,* 97, 65, 1992

Rosenberg, T. J., R. A. Helliwell, and J. P. Katsufrakis; Electron precipitation associated with discrete very-low-frequency emissions, *J. Geophys. Res., 76,* 8445, 1971

Rumi, G. C., VHF radar echoes associated with atmospheric phenomena, *J. Geophys. Res., 62,* 547, 1957

Shen, J. S., W. E. Swartz, D. T. Farley and R. M. Harper, Ionization layer in the nighttime E region valley above Arecibo, *J. Geophys. Res., 81,* 5517, 1976

Schonland, B. F. J., The lightning discharge, Handb.,Phys., 22, 576, 1984

Siefering, C. L, Upward propagating electric fields from thunderstorm and VLF

transmitters, Ph.D dissertation, 1987

Siefering, C. L., M. C. Kelley, Analysis of standing wave patterns in VLF transmitter signals: effects of sporadic E layers and in situ measurements of low electron densities, *J. Geophys. Res., 96*, No. 10, 17814, 1991

Taylor, W. L., Lightning characteristics as derived from sferics, Problems of Atmospheric and Space Electricity, Elsevier Publishing Company, p 388, 1965

Thomson, D., J., Spectrum estimation technique for characterization and development of WT4 waveguide, I, *Bell Syst. Tech. J., 56*, 1769, 1977

Thomson, E. M., M. A. Calib, M. A. Uman, W. H. Beasley, and M. M. Master, Some features of stroke occurrence in Florida lightning flashes, *J. Geophys. Res., 89*, 4919, 1984

Tümer, O.T., Further evidence for the dependence of Fast Atmospheric Light Pulsations on solar activity, *J.Geophys. Res., 87*, 2569, 1982

Turman, B. N., Detection of lightning superbolts, *J.Geophys. Res., 82*, 2566, 1977

Turman, B. N. and B. C. Edgar, Global lightning distributions at dawn and dusk, *J. Geophys. Res.*, 87, 1191, 1982

Turtle, J. P., E. C. Field, Jr., C. R. Warber, and P. R. McGill, Low-frequency transverse electric atmospheric noise: measurement and theory, *Radio Science, 24*, No. 3, 325, 1989.

Uman, M. A., The lightning discharge, Academic Press,1987

Uman, M. A., R.D. Brantley, J. A. Tiller, Y. T. Lin, E. P. Krider, and D. K. McLain, Correlated electric and magnetic fields from lightning return strokes, *J. Geophys. Res., 80*, 373, 1975

Vampola, A. L. and D. J. Gorney, Electron energy deposition in the middle atmosphere, *J. Geophys. Res., 88*, 6267, 1983

Vaughan, O. H. and B. Vonnegut, Recent observations of lightning discharges from the top of a thundercloud into the clear air above, *J. Geophys. Res., 94*, 13179, 1989

Voss, H. D., W. L. Imhof, M. Walt, J. Mobilia, E. Gaines, J. B. Reagan, U. S. Inan, R. A. Helliwell, D. L. Carpenter, J. P. Katsufrakis and H. C. Chang, Lightning-induced electron precipitation, *Nature, 312*, Dec., 1984

Wait, J. R., Propagation effects for EM pulse transmission, *Proc. IEEE 74*, 9, 1173, 1986

Weidman, C. D., E. P. Krider, C. G. Park, and B. Blockley, Correlated measurements of lightning radiation fields and whistlers in Proceedings in Atmospheric Electricity, edited by L. H. Ruhnke and J. Latham, A. Deepak, Hampton, Va.,1983

Wilson, C. T. R., A theory of thundercloud electricity, *Proc. Phys. Soc., 37*, 32D, 1925

Woodman, R. F. and E. Kudeki, A causal relationship between lightning and explosive spread F, *Geophys. Res. Lett. 11*, 1165, 1984
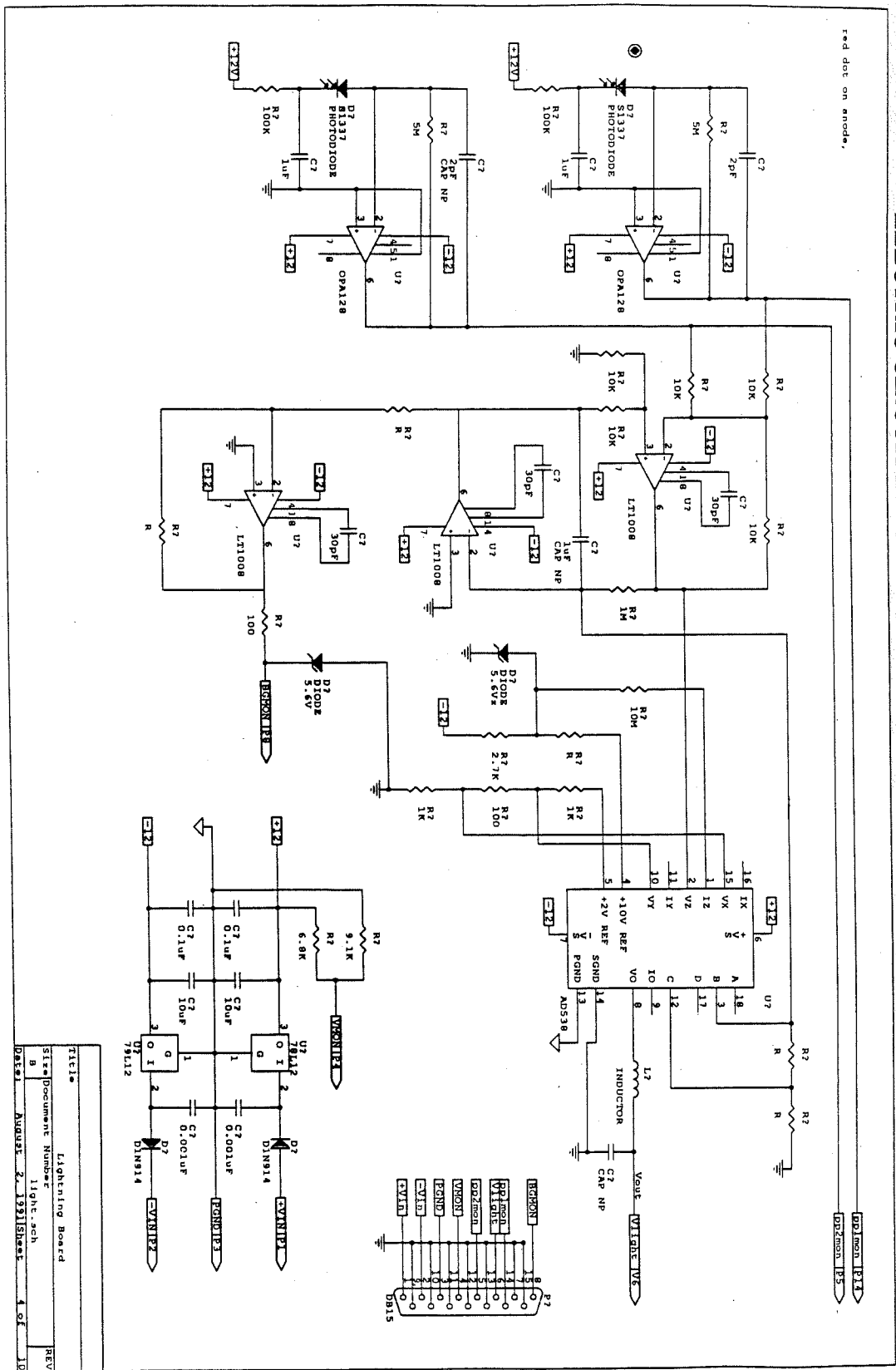
APENDIX B

COMPENSATION FACTOR FOR FFT

In Chapter 4, we padded the data sequence with constants to a standard length before performing the FFT. The addition of padding constants affects the spectrum amplitude from the FFT as would any filters. To compare different spectra, an amplitude compensation factor, which is related to the length of the padded sequence, must be applied to the FFT output. This is needed to compare frequency components from the less dispersed and shorter lightning wave packet below 200 km with those at higher altitudes which are longer because of dispersion.

The Fourier transform of a data sequence $F(t_j)$ is (Brault et. al, 1971)

$$\tilde{F}(f) = \frac{1}{N} \sum_{j=1}^{N} F(t_j) e^{-i2\pi ft_j} \, , \tag{1}$$

where $t_j = (j-1)\Delta t$, Δt is the sampling interval, N is the number of data points, and f is the frequency. If the data sequence $F(t_j)$ is padded with M zeros, the Fourier transform of the padded sequence with length $M+N$ would be

$$\tilde{F}'(f) = \frac{1}{N+M} \sum_{j=1}^{N+M} F(t_j) e^{-i2\pi ft_j} = \frac{1}{N+M} \sum_{j=1}^{N} F(t_j) e^{-i2\pi ft_j} \, . \tag{2}$$

Here we have used $F(t_j) = 0$ when $j > N$. Therefore, the compensation factor is (Brault et. al, 1971)

$$\frac{\tilde{F}(f)}{\tilde{F}'(f)} = \frac{N+M}{N} \, . \tag{3}$$

Because the data sequence is sampled for a limited time, using equation (1) is equivalent to windowing the data with a rectangular window function. This rectangular window function may generate many false frequency components. To reduce these false frequencies, a variety of window functions can be chosen (Press et. al, 1990). Assuming a window function $w_N(t_j)$ (which may depend on the data sequence length) is applied to the FFT, then the Fourier transform of a data sequence $F(t_j)$ is

$$\tilde{F}(f) = \frac{1}{N} \sum_{j=1}^{N} w_N(t_j) F(t_j) e^{-i2\pi f t_j} \quad . \tag{4}$$

It can be seen from equations (1) - (4) that when the window function is related to the data length, the compensation factor for padded data sequence cannot be $(N+M)/N$, because this factor does not account for the effect of the data length on the window function. In our case, a numerical 4π prolate window (Thomson, 1977) is applied in FFT transformation. This numerical window function is related to the data length, but the effect of the data length on this window function is difficult to obtain analytically. Therefore, we took the window function and the FFT as a "black box" and calculated the compensation factor using a calibration method. Figure 9.1 is a diagram of our calibration method. We performed the FFT with the numerical window on simulated data sequences with different padded lengths. Comparing the output of the FFT, the compensation factor ($\tilde{F}(f) / \tilde{F}'(f)$) was obtained.
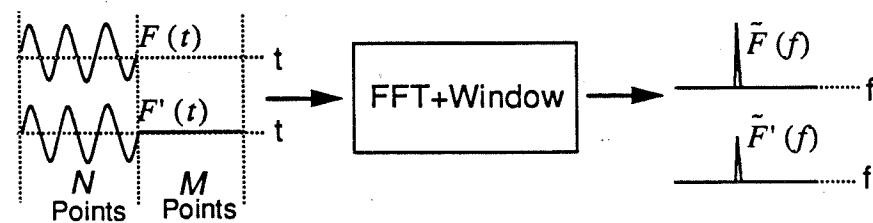

Figure 9.1: Calculation of the compensation factor for the FFT

The solid line in Figure 9.2 shows the calculated compensation factors as a function of the ratio between the original data length and the data length with padded constants The N and M are the numbers of the original data points and the padded points respectively. The dashed line in Figure 9.2 shows the result calculated from $(N+M)/N$. It can be seen from the figure that the two calculation results are close when the original data length is longer than 40% of the entire data length, which was the case for more than 50% of our data. When the data length is shorter than 40% of the entire data length, the calibration results is significantly greater than the result calculated from $(N+M)/N$.

We have calculated the compensation factors using simulated waves at different frequencies and found that the results were approximately the same.
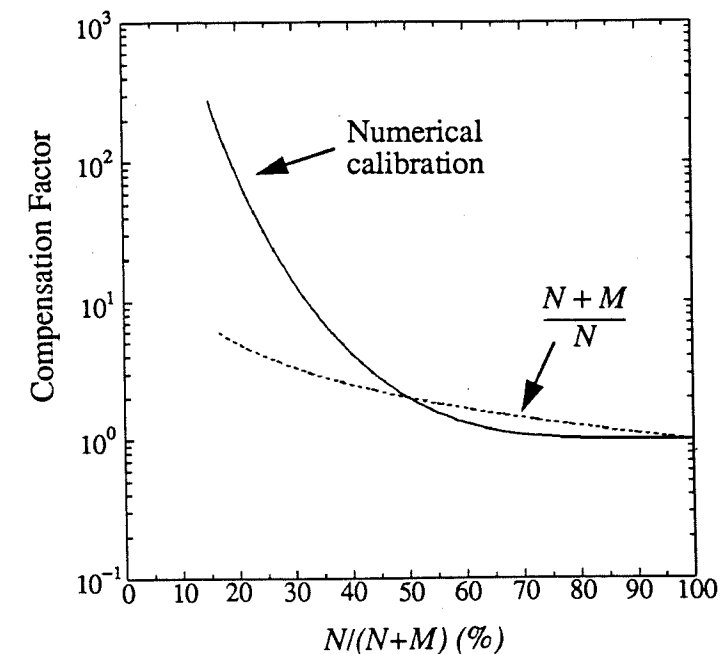

Figure 9.2: Compensation factors for the padded data sequences used when performing FFT on the VLF data. The N and M are the numbers of the original data points and the padded points

VITA

Ya Qi Li was born May 23, 1955, in Sichuang, People's Republic of China. He received his BS degree in Physics at the Beijing University, Beijing, P. R. China and his MS degree in Space Sciences at the Graduate School of Chinese Academy of Sciences, Beijing, P. R. China.